UNIVERSITY OF BIRMINGHAM

Investigations into Parthenolide and Boronic Acid Oxidation towards Prodrug Development

By

Alexander S. Quy

A thesis submitted to University of Birmingham for a degree of

DOCTOR OF PHILOSOPHY

School of Chemistry

College of Engineering and Physical Sciences

University of Birmingham

February 2023

UNIVERSITY OF
BIRMINGHAM

University of Birmingham Research Archive

e-theses repository

This unpublished thesis/dissertation is copyright of the author and/or third parties. The intellectual property rights of the author or third parties in respect of this work are as defined by The Copyright Designs and Patents Act 1988 or as modified by any successor legislation.

Any use made of information contained in this thesis/dissertation must be in accordance with that legislation and must be properly acknowledged. Further distribution or reproduction in any format is prohibited without the permission of the copyright holder.

Contents

Abbreviations

5-FU	5-fluorouracil
ADP	Adenosine diphosphate
ALL	Acute lymphocytic leukaemia
AML	Acute myeloid leukaemia
Ar	Aryl
ARS	Alizarin Red S
ATP	Adenosine triphosphate
AUC	Area under the curve
BA	Boronic acid
Bn	Benzyl
Boc	*tert*-Butyloxycarbonyl
Boc_2O	Di-*tert*-butyl dicarbonate
CAPS	N-cyclohexyl-3-aminopropanesulfonic acid
CE	Common era
CLL	Chronic lymphocytic leukaemia
CML	Chronic myeloid leukaemia
DCC	N,N'-Dicyclohexylcarbodiimide
DCM	Dichloromethane
DIPEA	Diisopropylethylamine (Hünig’s base)
DMAP	4-Dimethylaminopyridine

DMAPT	Dimethylaminoparthenolide
DMPK	Drug metabolism and pharmacokinetics
DMSO	Dimethylsulfoxide
DNA	Deoxyribonucleic acid
EC_{50}	Half maximal effective concentration
ESCs	Embryonic stem cells
Et	Ethyl
Et al.	Et alia (and others)
Et_3N	Triethylamine
EtOH	Ethanol
FDA	Food and drug agency
FOLFORINOX	Folinic acid, fluorouracil, irinotecan, oxaliplatin
GSH	Glutathione
h	hours
H_2O	Water
H_2O_2	Hydrogen peroxide
HRMS	High resolution mass spectrometry
HSCs	Haematopoietic stem cells
HTS	High throughput screening
IC_{50}	Half maximal inhibitory concentration
IR	Infrared
ITC	Isothermal titration calorimetry
IV	Intravenous

K_2CO_3	Potassium carbonate
MeCN	Acetonitrile
MeOH	Methanol
$MgSO_4$	Magnesium sulfate
µM	Micromolar
NADH	Nicotinamide adenine dinucleotide
NADPH	Nicotinamide adenine dinucleotide phosphate
NF-κB	Nuclear factor kappa B
NMR	Nuclear magnetic resonance
PBS	Phosphate buffered saline
Ph	Phenyl
pK_a	Acid dissociation constant
PTL	Parthenolide
RFU	Relative fluorescence units
RNS	Reactive nitrogen species
ROS	Reactive oxygen species
RT	Room temperature
SAR	Structure-activity relationship
TFA	Trifluoroacetic acid
THF	Tetrahydrofuran
TLC	Thin layer chromatography
UV	Ultraviolet
UV-Vis	Ultraviolet – visible light

Acknowledgments

First and foremost, I would like to thank my supervisor Professor John S. Fossey for his support throughout this PhD and for allowing me to undertake a PhD in his group. None of this thesis would be possible without you, with our “brief chats” that lasted into the evening and all the experiences you helped me fulfil. You mentored me through my masters and PhD and have made me the scientist I am today. I would also like to thank Dr Angelo Agathanggelou for your support with the biology side of the project, as well as a significant amount of emotional support. To my new supervisor Dr Paul Davies, thank you for taking me under your wing and helping me through what has been a tough time for us all. Dr Andrew Leach and Professor Eric V. Anslyn, I’d like to thank you for all the scientific contributions you have both made to this project and for helping with many suggestions as to how to proceed.

All the past members of the Fossey group that I had the pleasure of working with have proven invaluable with their shared knowledge and experience, and I hope that we all keep in touch. I started this journey with Orla and Harry, and you have both been amazing friends and sounding boards for when everything was going awry. Xingjian, you helped me as a master’s student and gave me a boost for when I started my PhD, helping me to wrap up your work. Huy and Fernanda, you coached me through the first two years of the PhD and Holly, you helped me through that last stretch of the PhD and beyond into the real world, and for that I am ever grateful to you all. Finally, Dr George Williams, I think you know as well as I do that this wouldn’t have all been possible without you, and I’m forever grateful we never played chicken. You make a great academic and an even better friend. Never change.

A PhD isn’t possible without people outside your discipline. I’d like to thank all the members of Birmingham Panthers Korfball club for keeping me sane and in vaguely good physical health during the PhD. I’d like to thank Josh, Ben R and Ben J for always being on hand if I needed to vent or just go for a pint.

I would like to thank my family who have helped me throughout the process and supported my life decisions, no matter how crazy. Above all, I would like to thank my incredible partner, Louise. We’ve been together for the whole PhD, and I don’t know how you have put up with me for all that time. Thank you for always being there and comforting me, even after the difficult days you’ve always stood by me. I know that you always will be by my side, and I by yours.

I would like to dedicate this thesis to John, my supervisor, mentor, and friend. I will be forever grateful for how much you have shaped my life. I miss you, and I hope I've made you proud.

1 Introduction and literature review

Cancer is one of the leading causes of death worldwide. Current chemotherapy treatments display off-target effects leading to side effects. Through exploiting the intrinsic differences between healthy cells and cancerous cells, more targeted therapies can be developed using boronic ester oxidation chemistry. Examined in this work are the efforts made into understanding the fundamentals of boronic ester oxidation chemistry, ultimately to inform design of cancer therapy prodrugs. For a starting lead compound, as many drugs on the market are derived from natural products, this work also discusses the scope for using parthenolide as a leukaemia therapy.

1.1 Cancer

1.1.1 General background

Cancer accounted for close to 10 million deaths in 2020 worldwide.[1] In the UK alone, over 137,000 people died from cancer in 2020.[2] It is a disease that develops over time, thus is more prevalent in the older population, with over 50% of cancer diagnoses made in people over the age of 70.[2] Cancer is a group of non-communicable diseases that involves the uncontrollable division of cells in the body.[3] Healthy cells in the body are constantly subjected to events that could damage DNA, for example ionising radiation such as UV [4, 5], poor diet (e.g. salted fish and processed meats),[6-8] inhalation of tobacco,[9] consumption of alcohol,[10] and some viral diseases such as human papilloma virus.[11]

Deoxyribonucleic acid (DNA) is made up of a double strand of nucleotides that consist of a phosphate group, deoxyribose sugar and a base. There are four bases, adenine (A), cytosine (C), guanine (G) and thymine (T), and the order in which these bases appear in DNA provides the DNA sequence. This sequence makes up the genetic code, whereby the sections of that code, genes, provide the instructions for the biosynthesis of proteins. Each group of three bases codes for one amino acid.[12, 13] Proteins consist of a chain of amino acids and are made up of four sub-types of structure. Primary protein structure is the order of the amino acids in the polypeptide chain. The amide bonds of the amino acid chain enable hydrogen bonding within the protein, giving it its secondary structure where α-helices and β-pleated sheets are seen. The overall three-dimensional structure of the protein as a result of the interactions between the R groups of the amino acids is known as its tertiary structure. Finally, quaternary structure describes how different polypeptide chains interact to form the whole protein.[14] All proteins bind to other molecules[15] and are important a range of biological processes. For example, enzymes are proteins that are required for functions such as digestion, DNA replication, respiration, nerve function and more.[16] Disruption to these functions can be catastrophic for the cell, and when occurring on a large scale, the individual. Damage to DNA can lead to mutations in genes, causing a disorder in the genetic sequence, therefore a disturbance in the synthesis of proteins. When mutations occur in genes that code for oncogenes or tumour-suppressor genes, the cell can become cancerous.[17] Rapid proliferation of these cells then causes tumour growth.[18]

1.1.2 White blood cells

White blood cells are produced in bone marrow through haematopoiesis, a process by which haematopoietic stem cells (HSCs) differentiate into all human blood cells.[19] Stem cells are unspecialised cells and are able to become other cells through a process called differentiation.[20] HSCs are a type of tissue-specific stem cell found in the bone marrow and are pluripotent, meaning they are capable of differentiating into multiple different cell types.[21] HSCs initially split into either myeloid or lymphoid progenitor cells (**Figure 1.1**). Myeloid progenitor cells differentiate into red blood cells that carry oxygen round the body, platelets that clot and prevent bleeds, and myeloid white blood cells, including neutrophils and macrophages, that seek microorganisms and kill them to prevent infection.[22] Lymphoid progenitor cells differentiate into B-cells and T-cells, which produce our immune response. Every day, up to a trillion new blood cells are produced from HSCs to maintain healthy blood and in order to sustain this level of proliferation, HSCs self-renew.[23, 24] Bone marrow transplants consist of infusing healthy HSCs within your bone marrow to boost production of blood cells and can be crucial in the treatment of several blood disorders, including blood cancers such as leukaemia and lymphoma,[25] and sickle cell anaemia, a disease that causes production of abnormal, sickle shaped red blood cells.[26]

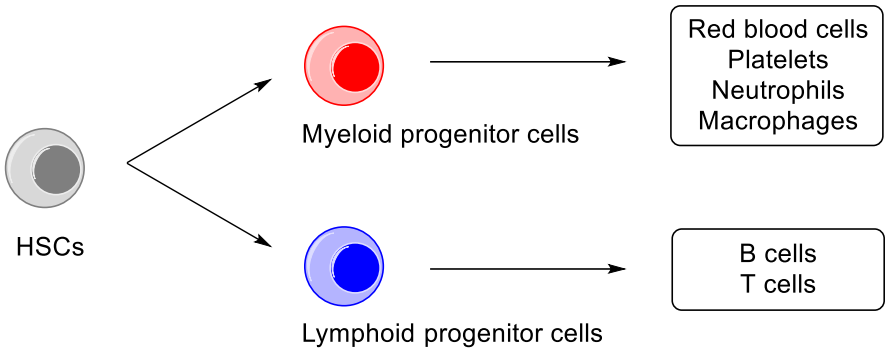

Figure 1.1 *– Proliferation of haematopoietic stem cells into myeloid and lymphoid progenitor cells, then onwards to the cells found in blood serum, i.e. red blood cells, platelets, neutrophils, macrophages, B cells and T cells.*

1.1.3 Leukaemia overview

Leukaemia is cancer of the blood cells, caused by an increase in leucocyte numbers either in the bone marrow or blood.[27] It is the 12th most common cancer in the UK, with 3% of all new cancer referrals being due to leukaemia.[28] There are different types, categorised depending on the type of blood cell that is affected. Chronic and acute myeloid leukaemia (CML and AML) affect the myeloid cells,[29] whereas chronic and acute lymphocytic leukaemia (CLL and ALL) affect the lymphoblasts.[30] One difference between acute leukaemia and chronic leukaemia is the speed of onset, where the percentage change in blast cells in the bone marrow from healthy marrow to cancerous marrow is different. Healthy bone marrow cells are made up of between 1% and 5% blast cells, whereas in acute leukaemias, this figure is greater than 20% and in chronic cases, between 10% and 20%.[31, 32] This increase can be quantified and is used to classify the type of leukaemia. Additionally, chronic leukaemias occur almost exclusively in adults, with the majority of patients being asymptomatic when diagnosed, whereas acute leukaemias occur in all ages with common symptoms including shortness of breath, fever, and bleeding.[33]

1.1.4 Chronic lymphocytic leukaemia

CLL is caused by the rapid proliferation of B-cells in the body, occurring when the cells are in their HSC stage.[34] It is a disease primarily diagnosed in the older population, with a median diagnosis age of 70, and more commonly occurs in men.[35-37]

Diagnosis of CLL is most commonly achieved through routine blood tests carried out for another reason, where an increased presence of lymphocytes is seen. As this could also indicate other diseases such as infection, additional blood tests identify the expression of certain proteins on the B cells allowing a diagnosis to be made.[37-39]

Treatment is only given to patients with CLL that present with symptoms or whose disease is at an advanced stage. Patients who are asymptomatic are monitored until the disease progresses or there is an acceleration in the progression.[40] It has been shown that treatment in patients with early stage CLL have no prognostic advantage to chemotherapy.[41, 42] Patients below the age of 65 suffering with CLL are often given a trio of chemotherapies: fludarabine, cyclophosphamide and rituximab (FCR, **Figure 1.2**, compounds **1**-**3**).[43, 44] It is an effective treatment with complete remission shown in over 70% of patients trialled.[45] However, side effects from this treatment reduce the patient's quality of life, and are considered too harsh to use this treatment on the elderly.[46, 47] For older patients, chlorambucil (**Figure 1.2**, compound **3**) is often used as a treatment, not necessarily to cure the cancer, but to alleviate symptoms.[48]

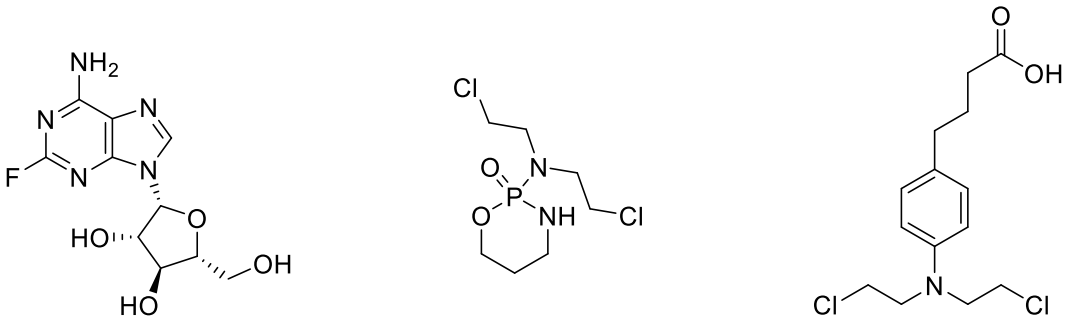

Fludarabine, **1** Cyclophosphamide, **2** Chlorambucil, **3**

***Figure 1.2** – Structures of FCR treatment drugs fludarabine (**1**, left) and cyclophosphamide (**2**, centre), and chlorambucil (**3**, right).*

1.1.5 Oxidative stress in cancer cells

Cells in the body produce reactive oxygen species (ROS) and reactive nitrogen species (RNS) as a result of metabolism, and these species are overexpressed in cancer cells.[49] Antioxidants produced in the body ensure that levels of ROS and RNS remain balanced. An imbalance in this homeostasis can cause damage to cells. Sustained damage over a long period of time can cause mutations within the cell and in some cases, cause cancer.[50, 51]

1.1.5.1 Reactive oxygen species

The term ROS describes multiple oxygen species found in cells, including but not limited to hydrogen peroxide, superoxide anions and the hydroxyl radical, and are split into two groups; free oxygen radicals and non-radicals outlined in **Table 1.1**. They are the products from the reduction of molecular oxygen in the cells, which occurs during normal cell activities, for example respiration.[52, 53]

Table 1.1 *– Non-exhaustive list of ROS species found in cells split between free oxygen radicals and non-radical ROS. Nitric oxide radical is a reactive nitrogen species (RNS)*

Free oxygen radical ROS		Non-radical ROS	
Superoxide anion	$O_2^{\bullet -}$	Hydrogen peroxide	H_2O_2
Hydroxyl radical	$OH^{\bullet}$	Hypochlorite	$HOCl$
Nitric oxide (RNS)	$NO^{\bullet}$	Singlet oxygen	$^1O_2$

The main location for the production of ROS is the mitochondria, where respiration occurs.[54, 55] Mitochondria are the organelles that generate adenosine triphosphate (ATP), the molecular vehicle for energy in cells, from adenosine diphosphate (ADP) through addition of a phosphate group. Through the generation of ATP, superoxide anions are formed that are consequently converted to hydrogen peroxide via superoxide dismutase.[56, 57] The majority of the production of ROS is carried out enzymatically by the mitochondrial electron transport chain.[54, 58]

ROS is involved in some cell signalling pathways.[59-61] Low levels of ROS are required for the regulation of HSC proliferation,[62] and high levels can be toxic, preventing HSCs becoming progenitor cells.[63] During pregnancy, embryonic stem cells (ESCs) can differentiate into every cell of the human body. In order to do this, ESCs must not only differentiate into every cell, but also replicate themselves, known as self-renewal. Bigarella *et al*. showed that the regulation between these two functions is partly regulated by ROS.[64]

1.1.5.2 Oxidative stress in cancer cells

Cancer cells have higher levels of ROS than normal, healthy cells, with 0.1-1 μM in healthy cells and 10-100 μM in cancer cells.[65, 66] When levels of ROS are too high, cell death can occur, known as apoptosis.[67] This occurs with oxidative stress, as the increased levels of oxidants causes lipid, protein and DNA to be oxidised, leading to tissue damage.[68] High levels of ROS in cancer cells is caused by enhanced activity in the mitochondria, resulting in higher metabolism inside the cell. This in turn allows the cell to replicate more readily, leading to an increase in tumour sizes and the spread of the disease to other parts of the body.[66]

1.1.5.3 Antioxidants

To maintain the balance of ROS, cells require antioxidants to counteract any increases in oxidants. They inhibit free radical reactions and reduce cell damage caused by ROS.[69] Vitamin C (**4**) and E (**5**) are examples of antioxidants that are acquired from diet (**Figure 1.3**).[70]

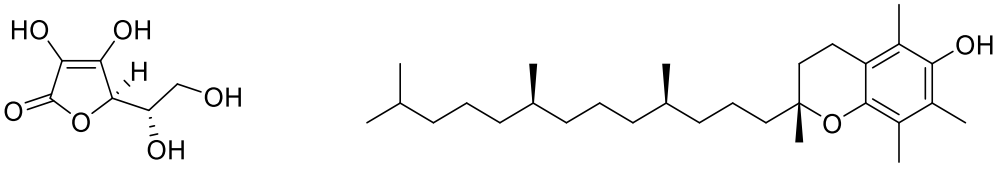

Vitamin C, **4** Vitamin E, **5**

Figure 1.3 *– Structures of vitamin C (left, **4**) and vitamin E (right, **5**), both antioxidants.*

Cells also produce antioxidants, such as glutathione (GSH) and superoxide dismutase.[71] GSH is a thiol-containing peptide produced in the cytosol and exists in two states, reduced (**Scheme 1.1**, compound **6**) and oxidised (**Scheme 1.1**,

compound **7**).[72] GSH acts as a cofactor to the enzyme glutathione peroxidase to reduce hydrogen peroxide to water, forming the oxidised form of GSH.[73] Reduced GSH is reformed via the enzyme glutathione reductase and NADPH, a cofactor and reducing agent found in cells.[74]

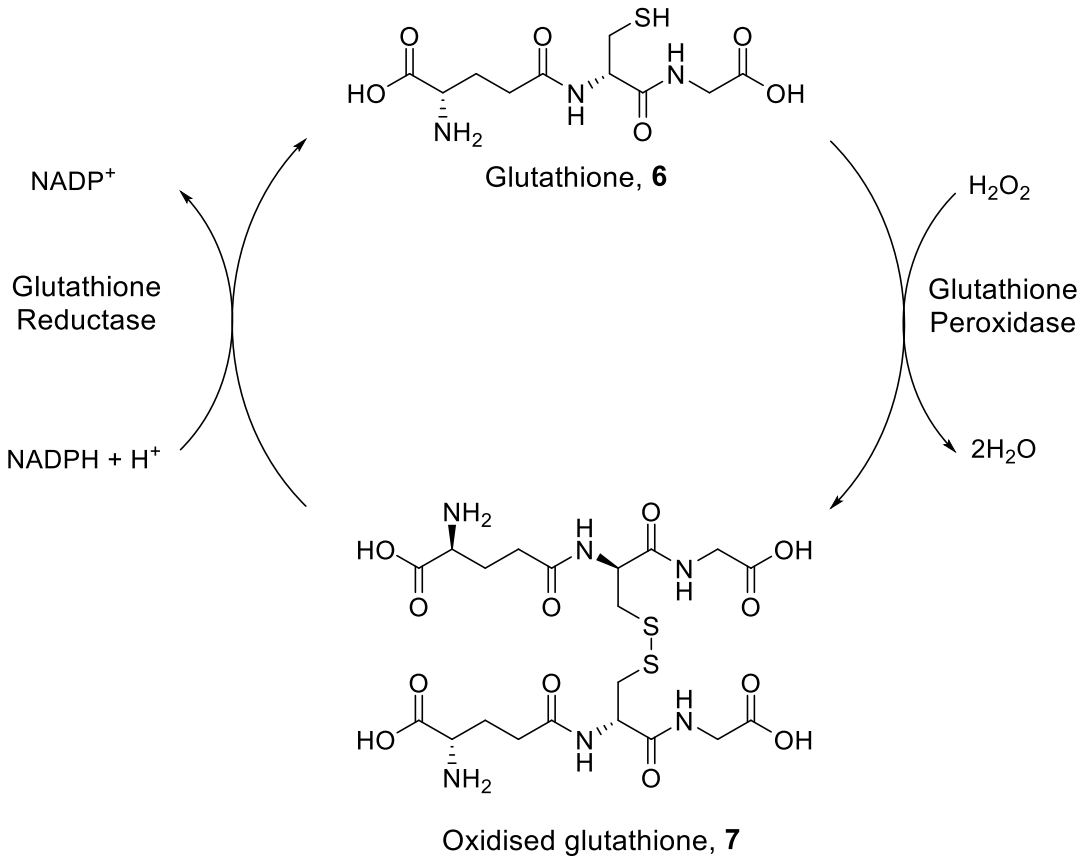

Scheme 1.1 *– Redox loop of glutathione (top,* ***6****), first oxidised by glutathione peroxidase to oxidised glutathione (bottom,* ***7****), followed by reduction back to glutathione via glutathione reductase.*

1.2 Natural products in cancer therapy

1.2.1 Natural products in medicine

Natural products have been used for millennia in medicine, dating back to ancient Egyptian times when roots and plants were used to treat symptoms such as coughs

and inflammation.[75] To this day, some of the most common drugs are directly derived from natural products. It is still an active area of research in pharmaceutical discovery, with up to half of drugs being either directly or indirectly derived from natural products.[76, 77] Natural products tend to feature properties desirable to modern drug discovery. They often have a high sp^3 character, are often 3D in shape, as well as having highly diverse scaffolds, allowing a wider range of proteins to be more specifically targeted.[78-80]

Serendipitous discoveries of blockbuster drugs from natural products are abundant throughout recent history.[81] Penicillin G (**Figure 1.4**, compound **8**), a β-lactam derived from the fungus *Penicillium notatum,* famously discovered by Fleming in 1929, is still used almost 100 years on at the frontline of anti-microbial medicine.[82, 83] Over the years, additional derivatives of penicillin have been synthesised and approved for use, offering a broader range of activity and improved pharmacological properties.[84-86]

Opioids are given as analgesics when non-opioid drugs such as paracetamol and ibuprofen (**Figure 1.4**, compounds **9** and **10** respectively) are not sufficient for pain management, or where their use is contraindicated.[87] They are part of the family of alkaloids derived from the opium poppy and include the common analgesics, codeine and morphine, and narcotic, heroin (**Figure 1.4**, compounds **11**, **12** and **13** respectively).

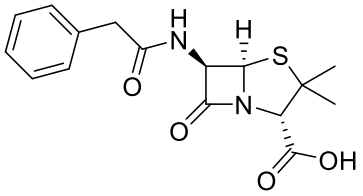

Penicillin G, **8**

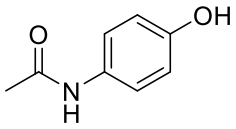

Paracetamol, **9**

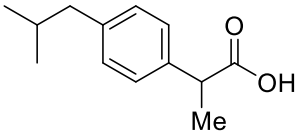

Ibuprofen, **10**

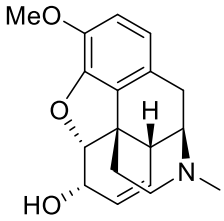

Codeine, **11**

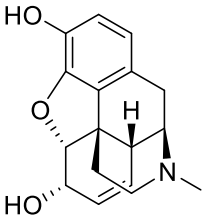

Morphine, **12**

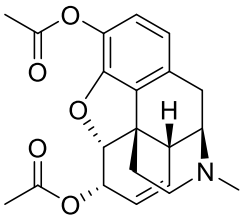

Heroin, **13**

Figure 1.4 *– Structures of Penicillin G (**8**, top left), analgesics paracetamol (**9**, top centre) and ibuprofen (**10**, top right), and opioids codeine (**11**, bottom left), morphine, (**12**, bottom centre), and heroin (**13**, bottom right).*

1.2.2 Cancer drugs

Cancer treatments normally target different steps of cell replication, for example disrupting the DNA replication step.[88] Since cell replication occurs in all cells, healthy and cancerous, the specificity of the drugs is low, meaning they can cause side effects that limit the dose, therefore limiting the efficacy of the drugs.[89]

1.2.2.1 Natural products in cancer therapy

Over 60% of anti-cancer drugs used today are derived in some way from natural products.[90, 91] Anthracyclines are widely used broad spectrum anti-cancer treatments,[92] with doxorubicin (**Figure 1.5**, compound **14**) a front-line drug in an array of cancers including breast,[93] bladder,[94] and some blood cancers.[95] It is derived from the bacteria *Stretomyces peucetius,* and the majority of clinical doxorubicin is produced by the bacteria.[96-98] Wild type and genetically engineered strains of the

bacteria are used for the biosynthesis of the drug as it is far cheaper to produce by bacteria than synthetically due to its large structure and chemical lability.[99, 100]

Enediynes are a class of anti-cancer drugs with high cytotoxicity, made biosynthetically by *Actinomycetes*, a bacteria.[101] The first example of this class of drugs was Neocarzinostatin (**Figure 1.5**, compound **15**), a natural product isolated form the bacteria *Streptomyces carzinostaticus*.[102, 103] Its mechanism of action is through binding to the minor groove of DNA and inducing cleavage of the double strand, leading to apoptosis of the cells. This class of drug can be used as both an antibiotic and an anti-cancer treatment, however the drugs tend to be poor at differentiating between healthy cells and the cancer cells leading to unwanted side effects.[104-106]

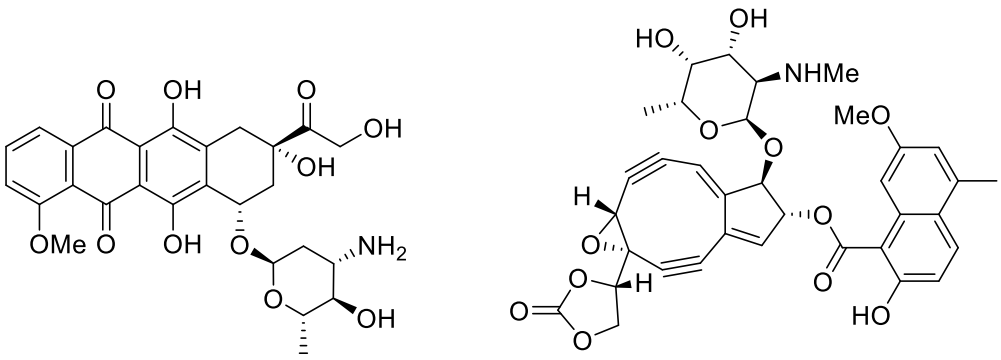

***Figure 1.5** – Structures of doxorubicin (**14**, left) and necarzinostatin (**15**, right).*

Paclitaxel, also known as Taxol (**Figure 1.6**, compound **16**), is an anti-cancer drug discovered in the late 1960s isolated from the bark of the Pacific yew tree, *Taxus brevifolia*. It is an indicated chemotherapy for the treatment of ovarian, breast and some lung cancers.[107-109]

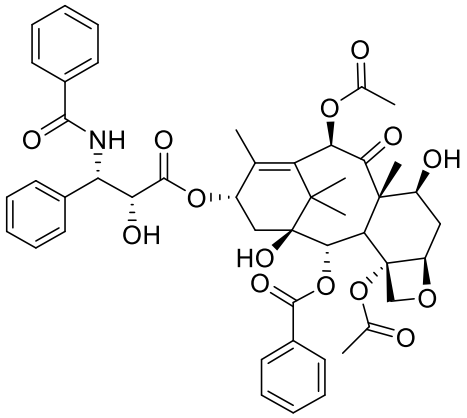

Taxol, **16**

Figure 1.6 *– Structure of Taxol, compound* ***16.***

Extraction of Taxol from the tree bark tends to be low yielding: one kilogram of Taxol requires the bark of 2500 trees. Due to the associated environmental damage with this, a synthetic route was required for this drug to be commercially viable. Holton *et al.* published the first total synthesis of Taxol in 12 steps and a 40% overall yield.[110] In the same year, Nicolaou and co-workers also published a total synthesis of Taxol from commercially available starting materials.[111] Commercially, Taxol is not synthesised in this way, and is instead synthesised via a semi-synthetic route in four steps, starting from 10-deacetylbaccatin III, a compound extracted from the leaves of the European yew tree (**Figure 1.7**, compound **17**), decreasing the number of trees that have to be cut down, therefore reducing the environment impact.[112]

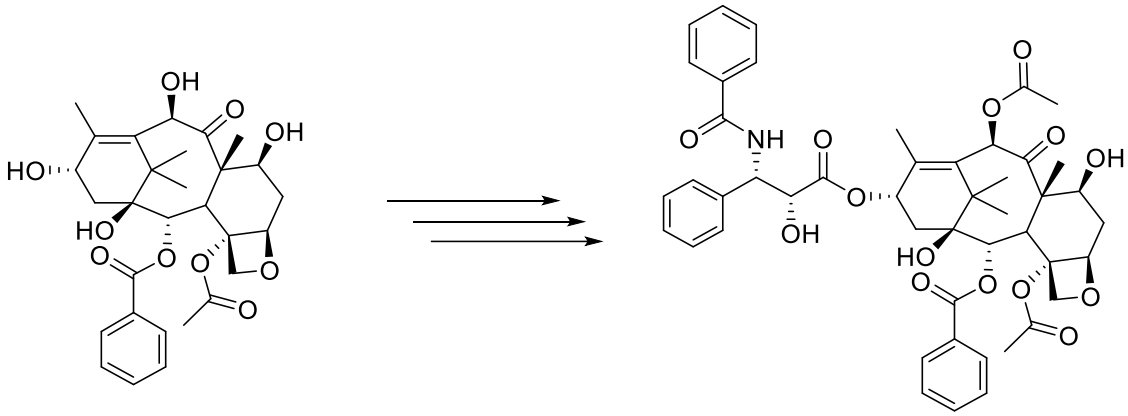

10-deacetylbaccatin III, **17**

Taxol, **16**

Figure 1.7 *– Semisynthesis of Taxol (**16**, right) from 10-deactylbaccatin III (**17**, left).*[113]

1.2.2.2 Early chemotherapies: Nitrogen mustards

The first therapeutic drug to be used as a chemotherapy was a compound originally designed for chemical warfare in the 1940s, nitrogen mustard.[114] Following an accident whereby 100 tonnes of the gas was released resulting in thousands of deaths, nitrogen mustard was found to cause leukopenia, a reduction in the number of white blood cells in the blood.[115] Nitrogen mustards are an alkylating agent and work through a nucleophilic substitution reaction with the nitrogen on guanine in DNA. An initial intramolecular nucleophilic attack forms an aziridinium ion, in turn facilitating *N*-alkylation of guanine (**Scheme 1.2**).[116-118]

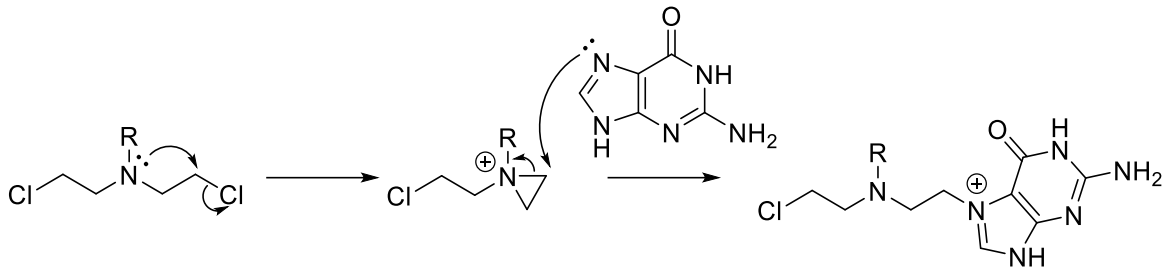

Scheme 1.2 *– Mechanism showing the initial intramolecular nucleophilic attack to form the aziridinium ion, followed by the first alkylation by guanine N7 to nitrogen mustard.*

1.2.2.3 Modern chemotherapy

From 2009 to 2020, the number of anti-cancer drugs approved by United States Food and Drug Administration (FDA) per year has increased, from 8 approvals in 2009 to 57 in 2020. 24 of the 57 new anti-cancer drugs that were approved for clinical use in 2020, exhibited a new mechanism of action.[119] Of those patients where cancer treatment was ineffective, 90% of cases were due to drug resistance,[120] and 90% of the 600,000 people who died from cancer in 2017 died due to drug resistance.[121] To overcome drug resistance, cancer treatment is often given as a cocktail of drugs, such as FOLFIRINOX treatment indicated for advanced pancreatic cancer.[122] The treatment is made up of four drugs: folinic acid (FOL) that increases the effect of 5-fluorouracil;[123] 5-fluorouracil (F) that disrupts DNA synthesis;[124] irinotecan (IRIN) that inhibits DNA replication and transcription;[125] and oxaliplatin that forms inter and intra strand links in DNA, causing an inhibition in DNA replication.[126]

1.3 Parthenolide

1.3.1 Background

Parthenolide (PTL) is a natural product obtained from the feverfew plant.[127] PTL has historically been used as an anti-migraine and anti-inflammatory medicine, and is still used today as a herbal remedy, sold as a dry herb capsule.[128, 129] It has been reported that in the first century CE, Greek doctors prescribed the feverfew plant for inflammation.[130-132] The anti-inflammatory mechanism of action of PTL is the inhibition of NF-κB, a transcription factor that switches on the expression of multiple genes for the inflammatory process through degradation of its inhibitor and subsequent entry into the nucleus.[133, 134]

PTL consists of a fused ten-membered and five-membered lactone ring with a double bond and epoxide on the former and a terminal alkene on the latter. In a number of publications, the structure of PTL has been described unclearly, causing difficulty in assigning the stereochemistry about the epoxide (**Figure 1.8**).[135-137] Throughout this thesis, PTL will be depicted as in **Figure 1.8**, compound **18**.

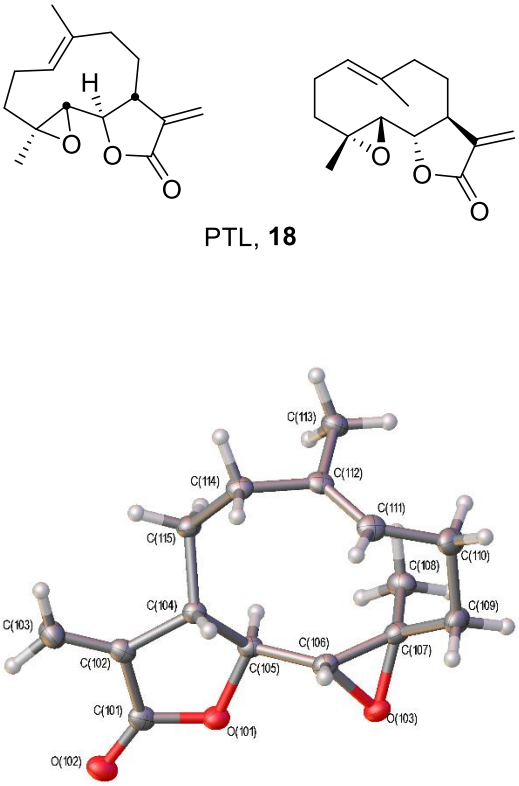

PTL, **18**

Figure 1.8 *– Structural depictions of PTL,* ***18****, with the correct, clearer stereochemistry about the epoxide, left, and the unclear, right. Crystal structure of PTL below.*[127]

Epoxides readily undergo nucleophilic attack, thus have been reported to increase the toxicity of drugs considering the abundance of nucleophiles in a cell. Epoxide containing drugs have shown increased potency for this reason, and have been used as a functional group in anti-cancer agents.[138] Carfilzomib (**Figure 1.9**, compound **19**) is an example of an epoxide containing anti-cancer drug and is an indicated treatment for multiple myeloma, a cancer of the bone marrow.[139] However, the epoxide functionality of PTL is not important in the anti-cancer activity of PTL. Long and co-workers found that in PTL, when the epoxide functional group is swapped for a cyclopropane ring, its anti-cancer activity is retained, *in vitro*, and therefore shows a negligible structure-activity relationship for the epoxide.[140]

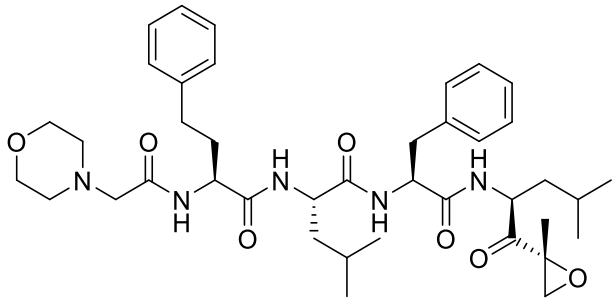

Carfilzomib, **19**

Figure 1.9 *– Structure of carfilzomib,* ***19****.*

1.3.2 Mechanism of action

There are two main mechanisms of action of parthenolide on cancer cells, both involving NF-κB, a transcription factor. NF-κB has two subunits, p50 and p65 and controls DNA transcription.[141] One of the mechanisms by which PTL is thought to work is through inhibition of NF-κB, achieved by PTL binding to the cysteine at the 38 (Cys38) position on the p65 subunit. This was investigated by Merfort and co-workers, where Cys38 was replaced by serine. It was theorised that the thiol of Cys38 reacts with the double bond of the lactone ring of PTL in a nucleophilic attack. By replacing Cys38 with serine replaces the thiol with an alcohol that does not react. When this change was carried out, PTL no longer bound to the DNA, therefore inhibiting its effectiveness as a drug.[142] The second potential mechanism is the inhibition of IκB kinase, the enzyme that breaks down the protein IκBα, a known inhibitor of NF-κB. With reduced IκB kinase activity, the concentration of IκBα increases, leading to the inhibition of NF-κB.[141]

One consideration is that the thiol on Cys38 is potentially alkylated by the double bond on the lactone ring. This calls into question whether the derivatives of PTL with activity

are acting as a drug or a prodrug of PTL, where a retro-aza-Michael reaction returns the terminal double bond making it available for alkylation by the thiol (**Scheme 1.3**). If this were to occur at the binding site, the release of an amine from the molecule would provide a base to aid in deprotonation of the thiol, making it more susceptible to alkylation with the double bond on the lactone ring.[142]

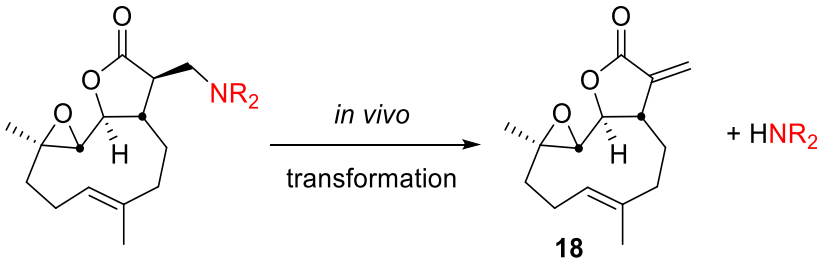

Scheme 1.3 *– Proposed retro-aza-Michael reaction that occurs* in vivo *to form the parent compound PTL (**18**) from the amino derivative.*

1.3.3 Derivatisation of PTL

The water solubility of PTL is poor; the highest serum concentration measured by Sweeney *et al.* was 200 nmol/L, preventing its use as an oral therapeutic.[143] Consequently, its bioavailability is poor, meaning a high oral dose would be required to get to the required serum concentration which from *in vitro* studies was targeted at 5 µmol/L.[143, 144] Derivatisation of PTL has been attempted to try to increase its water solubility as well as to improve its potency against several diseases such as AML and CLL.[127, 145] By adding groups to improve water solubility such as amines,[145] or increasing the polarity and decreasing the logP, the activity of PTL has been dramatically increased against CLL.[127]

1.3.3.1 Lactone ring double bond

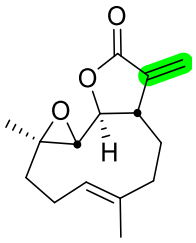

Figure 1.10 *- PTL with the double bond on the lactone ring highlighted. Section 1.3.3.1 summarises some of the transformations carried out on the bond highlighted.*

In pursuit of investigating the structure-activity relationship for an anti-viral drug against hepatitis C, Hwang *et al.* reduced the terminal alkene selectively using palladium on carbon (**Scheme 1.4**). However, the activity of the drug against the target consequently decreased, an expected outcome from the authors.[146] This is indicative of a mechanism of action involving the double bond, where alkylating capabilities give the compound its anti-cancer effect as well as its anti-viral effect.[147]

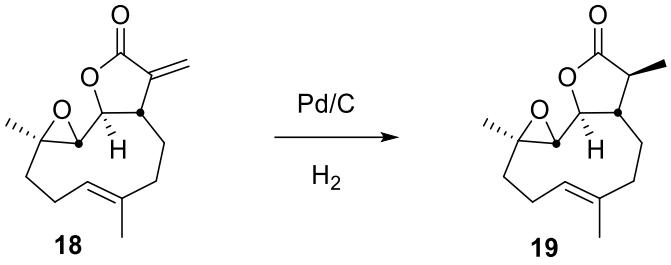

Scheme 1.4 *– Selective reduction of the double bond on the lactone ring of PTL with palladium on carbon and hydrogen.*

The most successful transformation in terms of increasing activity against cancer cell lines was the addition of nucleophiles to the double bond. Specifically, a range of amines have been introduced via an aza-Michael addition. In 2009, Crooks and co-workers described the analogue of PTL with a dimethylamine appended to the lactone

ring, termed DMAPT (dimethylaminoparthenolide, **Scheme 1.5**, compound **20**). By adding this group, the percentage of cell death of AML cells increased, compared to PTL. The water solubility of the drug increased 100-fold, when compared to PTL, as the new analogues are made into water soluble salts.[148]

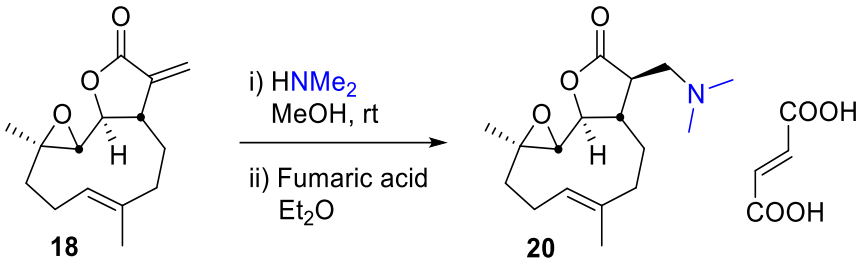

Scheme 1.5 *– Synthesis of DMAPT fumarate salt (**20**) from PTL (**18**) and dimethylamine.*

The largest library of aminoparthenolide derivatives was developed by Fossey and co-workers.[127] The authors synthesised 76 compounds and tested their anticancer efficacy against the MEC-1 cell line to indicate activity against CLL. Of the 76 compounds tested, a short list of the most potent compounds were subjected to *in vitro* DMPK studies and *in vivo* investigation to identify the best candidate for a clinical drug, (**Figure 1.11**, compound **21**).[127] The loss of the double bond in these examples does not cause a reduction in the anti-cancer activity of the drug as the reduction example shown in **Scheme 1.4**. This is because a conversion back to PTL within the cell is likely, which has been proven by LC/MS analysis of the cells by Hwang *et al*.[146]

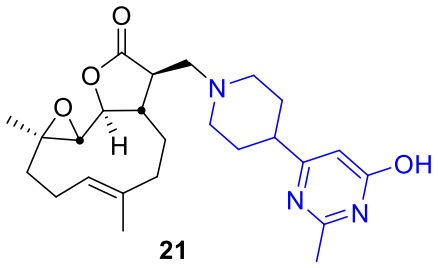

21

Figure 1.11 *– Lead compound known as ALF-01 (**21**) developed by Fossey and coworkers.*

1.3.3.2 Ring double bond

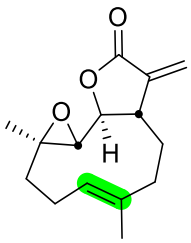

Figure 1.12 *- PTL with the double bond on the lactone ring highlighted. Section 1.3.3.2 summarises some of the transformations carried out on the bond highlighted.*

Harki *et al.* attempted to improve the activity of PTL against acute lymphoblastic leukaemia (ALL) by altering the chemistry around the double bond within the ten-membered ring. Firstly, selective reduction using platinum oxide and hydrogen to form a saturated ten-membered ring had a negligible effect on the activity. Secondly, a Simmons-Smith reaction introducing a cyclopropane ring, followed by a Michael addition to the lactone double bond, had an equally negligible improvement of the activity against ALL (**Scheme 1.6**).[149] This lack of difference in activity against ALL indicates that the double bond on the ten-membered ring is not important in the mechanism of action.

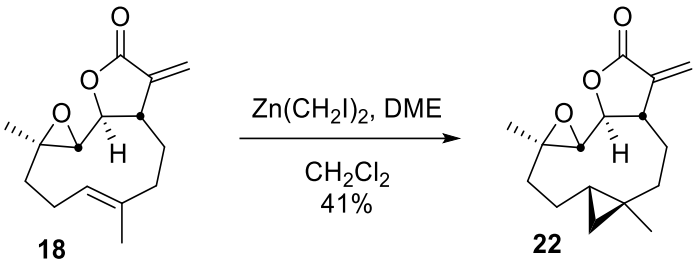

Scheme 1.6 *– Cyclopropanation of the double bond of the ten-membered ring.*

1.3.3.3 Alkenyl methyl

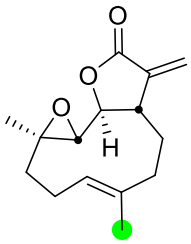

Figure 1.13 *- PTL with the double bond on the lactone ring highlighted. Section 1.3.3.3 summarises some of the transformations carried out on the bond highlighted.*

Enzymatic hydroxylation of the alkenyl methyl group, by Fasan and co-workers, yielded a convenient handle for further functionalisation.[150] Using engineered cytochrome P450 enzymes, hydroxylated PTL was synthesised in a 54% yield on a 400 mg scale. From compound **23**, alkylation to form ethers and acylation to form esters were carried out. The LC_{50} values against acute myeloid leukaemia (AML) cells similar to that of PTL, showing that the methyl group also does not have a role in the mechanism of action of PTL.[135, 150, 151]

5-Fluorouracil (5-FU, **Scheme 1.7**, compound **24**) is a common anti-cancer drug used in clinic for multiple cancers including breast, gastric and as a topical agent in skin cancer.[152] It has previously been reported that PTL and 5-FU give a synergistic anti-cancer effect when co-administered.[153] Ding *et al.* have covalently bound 5-FU to PTL

to form one drug with the same synergistic anti-cancer effect, attaching it via a linker on the alkenyl methyl. First, the hydroxylation is carried out to form the alcohol via an oxidation reaction with selenium oxide and tert-butyl hydroperoxide.[137] Various linkers were then appended on the alcohol, for example a triazole via an azide formation followed by a copper catalysed click reaction, or through acylation to form an ester (**Scheme 1.7**). One of the compounds synthesised showed a greater than five-fold increase in activity against a specific 5-FU resistant liver cancer than PTL.[154]

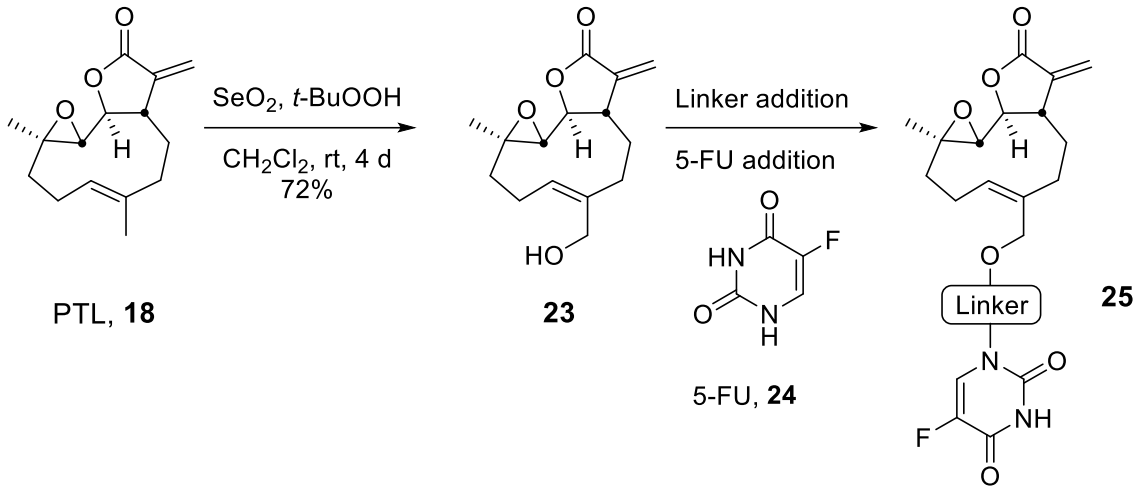

***Scheme 1.7** – Alkyl hydroxylation of PTL followed by the addition of a linker and the cancer drug 5-fluorouracil (5-FU, **24**) to form compound **25**.*

1.4 Boron in medicinal chemistry

1.4.1 Chemistry of boron

Boron is the fifth element in the periodic table and has three outer shell electrons. Neutral boron species adopt an sp^2 trigonal planar geometry with an empty *p*-orbital orthogonal to the plane of the molecule. The characteristics of the reactivity of boron centres are owed in part to the empty *p*-orbital imparting an electron deficient nature to the boron centre.[155]

Boron sp^2 centres are strong Lewis acids and can form covalent bonds to hybridise the centre to sp^3. Lewis acids accept electrons from electron pair donors to form an anionic boronate.[156] This is possible under physiological conditions, so drug development has seen an increase in the number of compounds containing boron to make covalently binding drugs.[157, 158]

1.4.2 Boron in medicine

There are around 60 different detectable chemical elements in the body.[159] Boron is essential for certain bodily functions, including the growth of bones and the healing of wounds.[160-162] Most drugs are made up of traditional elements, i.e. carbon, hydrogen, oxygen, nitrogen, sulfur and halogens. There are very few approved drugs that feature non-traditional elements.[163] Given the enormity of chemical space with just these elements, it has not been considered necessary to explore alternatives. However, considering its unique and interesting chemical properties, boron has started to be introduced in new drugs for various diseases as outlined below.[164]

1.4.2.1 Bortezomib

Bortezomib (**Figure 1.14**, compound **26**) is an approved anti-cancer drug that came to market in 2003 and was the first boron containing drug approved for clinical use.[165] It is a dipeptide that features a boronic acid. The boronic acid binds to the hydroxyl group of a threonine residue in the 26S proteasome, blocking crucial pathways in the cell, leading to apoptosis.[166]

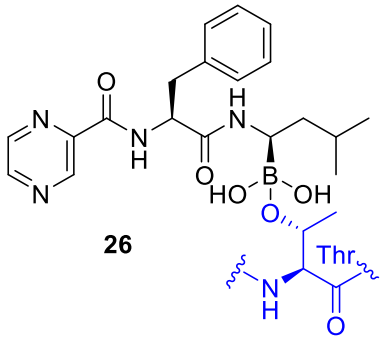

26

Figure 1.14 *– Covalent binding of bortezomib (black,* ***26****) with the hydroxyl of a threonine residue.*

1.4.2.2 Tavaborole

Tavaborole (**Figure 1.15**, compound **27**) was introduced into clinic in 2014 and is indicated for patients with onychomycosis, a type of fungal nail infection.[167] It works through inhibition of transfer RNA (tRNA) synthetase, a class of enzymes involved in RNA replication in microbes. The boron atom hybridises to sp^3 when forming a covalent bond with the ribose sugar on adenosine monophosphate within the tRNA.[168] Structure activity relationship (SAR) studies were carried out, initially by expanding the oxaborole ring, switching to a boronic acid, then removing boron all together. These changes inhibited the effect of the drug on the target, showing the importance of the size of the ring and the presence of the oxaborole ring on the activity.[169]

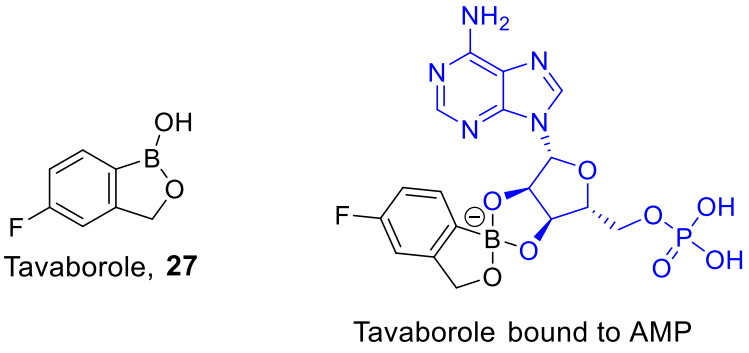

Figure 1.15 *– Structure of Tavaborole (left,* ***27****) and its binding to the diol of the ribose sugar of AMP (right).*

1.4.2.3 Boron neutron capture therapy

Boron neutron capture therapy (BNCT) is an alternative form of treatment to traditional chemotherapies, many of which are becoming less effective due to resistance.[170] BNCT is a form of targeted cancer therapy used on the primary tumour. The initial work to establish its principles was carried out by Locher in 1936.[171] First, the patient is injected with a non-radioactive boron-10 isotope containing drug into the primary tumour.[172] The patient is then subjected to irradiation from a neutron beam, targeted at the tumour site. The neutrons breakdown the boron compounds by adding a neutron to the nucleus, creating boron-11, followed by fission into lithium-7 and an α-particle, or helium-4. This α-particle provides high energy over a short distance (10 μM) and ruptures the cell containing the drug (**Figure 1.16**).[173]

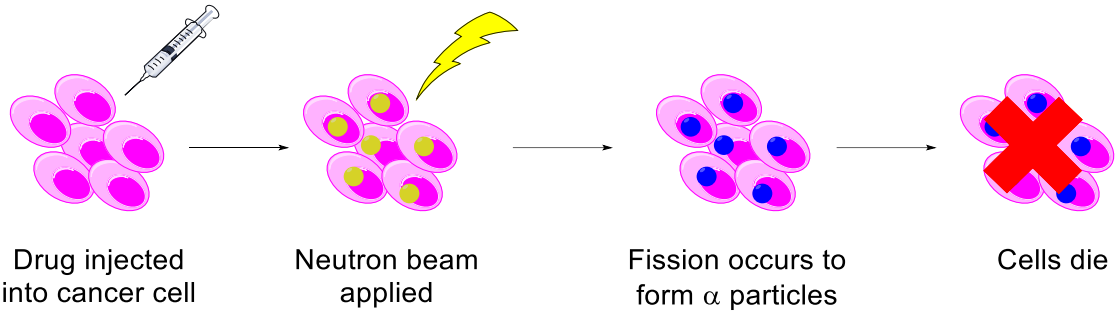

Figure 1.16 *– Graphic to show the basic steps of how boron neutron capture therapy (BNCT) works. A drug is injected into the tumour, followed by a neturon beam that causes nuclear fission to occur and ultimately cell death.*

1.4.3 Prodrug definition

A prodrug is an inactive drug that is converted into an active drug *in vivo*. This is to overcome issues such as solubility, toxicity, and poor specificity. Prodrugs have been used for decades: aspirin, one of the first prodrugs developed in 1899, metabolises to the active form, salicylic acid, in the basic conditions of the intestines. However, it is now known that aspirin is effective without the transformation.[174]

Side effects caused by anti-cancer drugs can be dire, and in some cases life threatening.[175] This is, in part, due to the lack of specificity of cancer drugs, whereby they also attack healthy cells.[176] By masking an anti-cancer drug as a prodrug, it is possible to increase the specificity of the drug and decrease the side effects. ROS levels being higher in cancer cells than healthy cells serve as a point of difference that can be exploited in making prodrugs.[66]

1.4.4 Oxidation of boronic acids

Boronic acids and esters oxidise to the corresponding alcohol under a number of mild conditions, from ROS to microwave assisted air.[177] Therefore, boronic acids and

esters can be used as ROS-activated moieties for use in anti-cancer treatments[178], systems for targeted drug-delivery,[179] and saccharide sensors.[180]

1.4.4.1 Mechanism of oxidation

The current accepted mechanism for the oxidation of boronic acids and esters is outlined in **Scheme 1.8**. There is an initial nucleophilic attack of the peroxide on the empty *p*-orbital of the boron to form the tetrahedral boronate intermediate. This is followed by a migration of the carbon-boron bond to form a carbon-oxygen bond. Finally, water is introduced to form boric acid and the alcohol.[181]

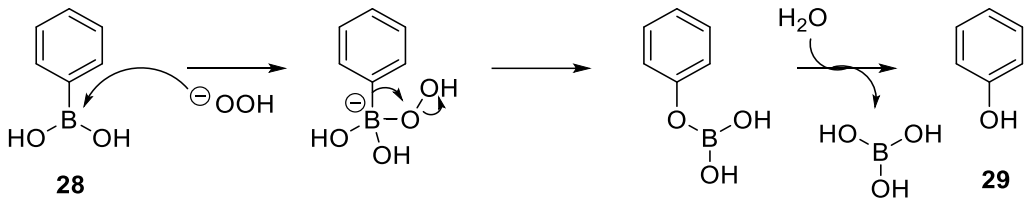

Scheme 1.8 *– Current accepted mechanism for the oxidation of arylboronic acids.*

1.4.4.2 Boron in cancer therapy

Boronic acids and esters can act as a mask for the corresponding alcohol, which can be revealed with the presence of ROS such as hydrogen peroxide (**Figure 1.17**).[182] The higher levels of ROS in cancer cells acts as a useful tool to reduce off target effects and increases the concentration of the active phenol-containing drug within the cancer cells, reducing toxicity.[183]

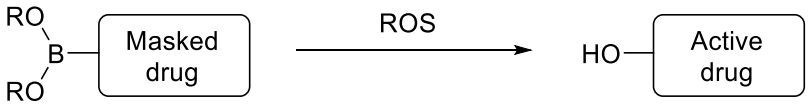

Figure 1.17 *– Generic activation of boron containing prodrugs by ROS to form an alcohol containing active drug.*

Tamoxifen is a common drug used for breast cancer. It is metabolised to its active form, 4-hydroxytamoxifen (**31**), in the body; a phenol containing drug.[184] Jiang *et al.* replaced the alcohol with a boronic acid and the equivalent boronic pinacol ester directly bonded to the aromatic ring (**Scheme 1.9**). They found that the boron-containing drugs did convert to 4-hyroxytamoxifen and were as effective or more effective than 4-hydroxytamoxifen at inhibiting the growth of breast cancer cell. However, these experiments were performed *in vitro*. Further studies *in vivo* are required to test these drugs as potential clinical therapies.[185]

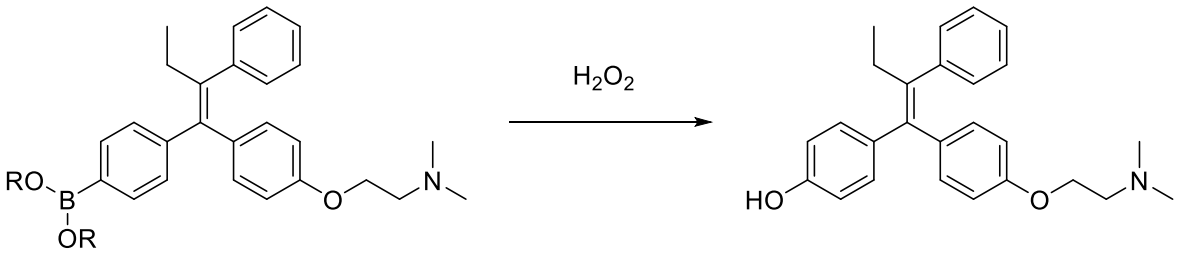

Boron containing bioisosteres of tamoxifen, **30**

4-Hydroxytamoxifen, **31**

Scheme 1.9 *– Simple scheme to show the oxidation of boron containing bioisosteres of Tamoxifen (**30**) to form the active drug 4-hydroxytamoxifen (**31**).*

Camptothecin (**Figure 1.18**, compound **32**) is a natural product anti-cancer drug. Four analogues are used clinically with improved solubility, for example irinotecan (**Figure 1.18**, compound **33**).[125] A boronic acid was added to the molecule to form a prodrug (**35**) by Lu and co-workers to reveal the aryl-alcohol, SN-38 (**34**), in a cancer cell. They

found that the conversion of the boron-containing prodrug to the alcohol was dependent on the concentration of hydrogen peroxide present, showing this to work as a hydrogen peroxide dependent prodrug (**Figure 1.18**). They also demonstrated that there was little loss of activity against the breast cancer cell lines being measured.[186]

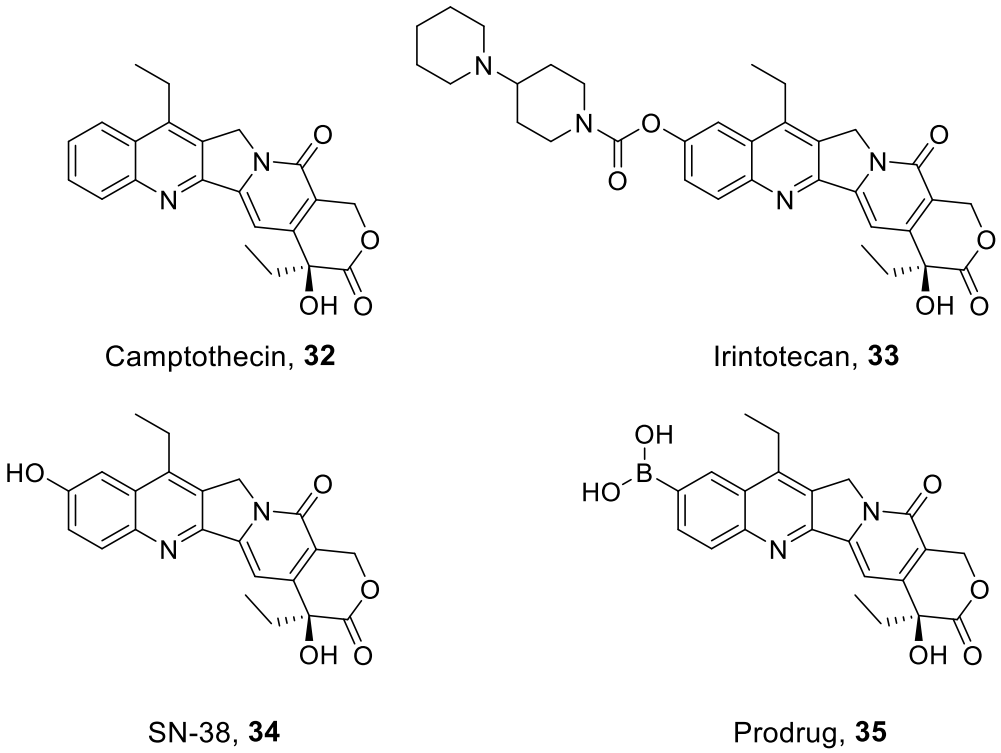

***Figure 1.18** – 4 analogues of camptothecin.*

1.4.4.3 Self-immolative linkers

Jourden and Cohen, in 2010, investigated a self-immolative linker initiated by the oxidation of a boronic ester to release the active drug 1,2-HOPO-2 (**38**). Oxidation of the boronic ester to the alcohol starts an electron cascade to release the active drug. They confirmed the release of the active drug through absorption spectroscopy, finding that when the boronic ester was replaced with hydrogen, the self-immolation did not

occur. This shows the the necessity of the oxidation of the boronic ester to start the cascade (**Scheme 1.10**).[187]

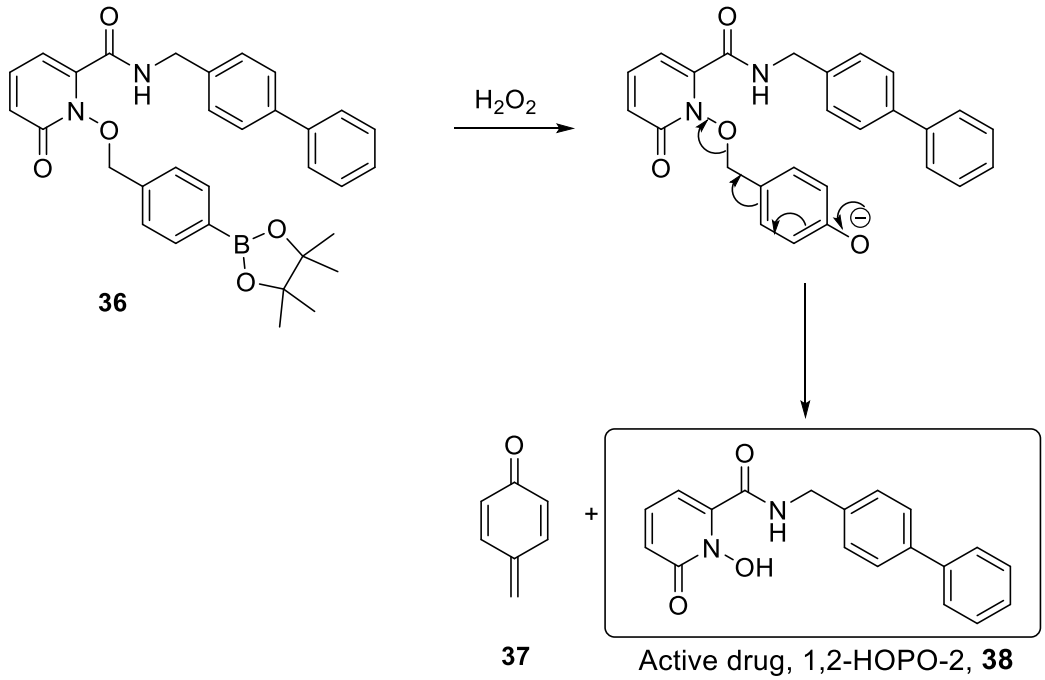

Scheme 1.10 *– Oxidation of boronic ester,* ***36****, causes the start of a self-immolative cascade to reveal the active drug,* ***38****.*

1.4.4.4 Sensors using boronic acids

A molecular sensor is a probe that changes one of its properties when interacting with an analyte.[188] Boronic acids readily bind with 1,2- and 1,3- diols making them the ideal moiety to sense sugars, given this is a common feature of sugars. The inclusion of a fluorescent moiety to the molecule provides the potential for a “switch on or off” sensing system.[189] Shinkai and co-workers developed a boronic acid based probe for sensing sugars that turned fluorescence on when bound (**Figure 1.19**).[190]

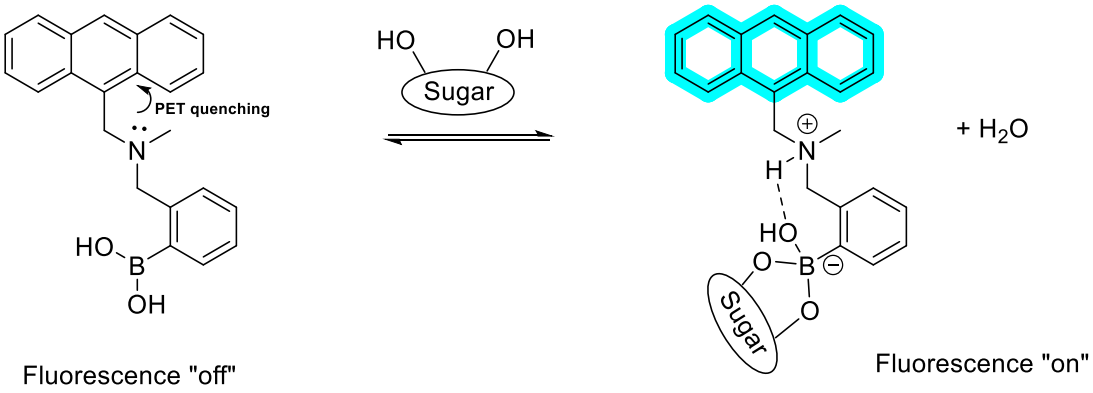

***Figure 1.19** – An early example of a fluorescent sugar sensor, where the unbound boronic acid is not fluorescent and the sugar bound boronic acid is fluorescent.*

In this example, the unbound sensor has fluorescence “switched off” due to quenching from the nitrogen lone pair into the anthracene. This quenching is known as photoinduced electron transfer (PET) which involves a charge transfer between separate parts of a molecule or intermolecularly.[191] When bound to a sugar, this quenching is not present and the molecule fluoresces.[192]

1.5 Aims and objectives

The aims of this work were firstly to develop new analogues of parthenolide and test their potency against chronic lymphocytic leukaemia. Secondly, to develop an experimental protocol to probe the mechanism of boronic acid and ester oxidation.

In the field of parthenolide synthesis, reported methods have not been able to prepare aniline derivatives. As benzylamine and phenethylamine derivatives had shown activity against CLL, we explored whether a new method developed by another member of the Fossey group, Dr Xingjian Li, could be used to access a new class of aniline-containing parthenolide derivatives for testing potency.

By better understanding the mechanism of the oxidation of boron species, boronic ester containing drugs and sensors can be tailored to the need at hand. For example, tailoring a boronic ester to only oxidise under certain conditions and not others, such as the high ROS environment of a cancer cell, will improve targeting of cancer drugs. Understanding whether changing the boronic ester has any impact on the oxidation will also contribute to the knowledge of boronic ester chemistry. To help understand the mechanism of oxidation, an experimental protocol to assess the relative binding strength of boronic acids to various diols needs to be developed, as does a robust methodology for analysing the kinetic components of the oxidation reaction.

2 Parthenolide derivatisation

The work in section 2.1 has been published in Tetrahedron.[193] Aspects of the research in section 2.2 are published in MedChemComm.[127]

2.1 Aniline derivatives

2.1.1 Drug discovery process

Target-based small molecule drug discovery process can be split up into early discovery and late discovery (**Figure 2.1**). In early discovery, the target is first identified, i.e. what protein is a drug going to bind to. Following this, libraries of drug-like compounds are developed and tested through high throughput screening to identify “hit” compounds that have activity against the target. A hit compound is described as a molecule with the desired activity against the target of interest in a screen.[194] Smaller chemical transformations are applied to the basic hit compound to improve its activity and its drug-like properties such as its pharmacokinetic properties (absorption, distribution, metabolism, excretion, and toxicity) to form a lead compound in a stage known as hit-to-lead. Once a lead compound has been found, they can progress further in the drug discovery process with *in vivo* studies and preclinical trials.[194] Getting to this point requires a mammoth effort to develop thousands of novel compounds which comes at a cost of both time and money. To reduce the human effort put into the early stages of drug discovery, academia and industry alike are introducing and improving *in silico* based drug-design to aid researchers in making compounds that are more likely to have activity against the target.[195]

Figure 2.1 *– Flowchart to show an overview of the stages of drug discovery, from identifying a target to clinical trials.*

2.1.1.1 Computational docking

Molecular computational docking is a method used to predict non-covalent binding interactions between a receptor and a small molecule.[196] It is used in drug discovery to give an indication of structure activity relationship (SAR).[197] Chimera is a free open-source software that is used to give an indication of docking poses and binding energy of a compound with a protein target. The use of free-to-use software to guide small research groups in drug design projects has been well documented.[198] While it can be useful to aid in design of small molecules, computational docking is not yet at the point that it can replace traditional *in vitro* testing of biologically relevant assays.

2.1.1.2 Anilines in drug discovery

In large library synthesis, ease of synthesis is important for a high throughput system. Anilines tend to be easy to synthesise, and therefore commonly feature in library generation. In a study on structural alerts in drug discovery, a prominent structure that appeared in 44% of toxic drugs was the aniline, causing DNA mutations.[199, 200]

2.1.2 Parthenolide extraction

PTL was extracted from the feverfew plant grown on the University of Birmingham campus at Winterbourne Gardens. This perennial grows as a small bush, and both the

flower and woody material were both cultivated and dried in a greenhouse to remove as much water as possible. Once dried, the plant material was stored in vacuum bags so they could be processed when required.

Dried plant material was cut up into chunks (no larger than 1 cm) and then warmed in 80 °C water for 10 minutes. The plant material was removed from the resultant “tea”, then reextracted twice more via the same method. The water was allowed to cool to room temperature, then extracted with chloroform three times. The solvent was removed, resulting in a brown sticky oil that was combined and purified by flash column chromatography. Further purification was required through recrystallization in diethyl ether to yield pure PTL.

Figure 2.2 *– Pure PTL crystals (left) and feverfew (right).*

2.1.3 Previous attempts

The double bond on the lactone ring of PTL readily undergoes a Michael addition in protic solvents. Amine derivatisation on the double bond of the lactone ring has been well documented.[148] Amines that have previously been added to PTL are varied, including primary and secondary amines as well as cyclic and acyclic amines. Aniline

compounds have not been added to PTL, perhaps due to the potential toxicity, or possibly due to the difficulty in synthesis.

2.1.4 Synthesis

Previous attempts to synthesise aniline containing PTL derivatives using the published methodology in **Scheme 1.5** yielded no product. This could be down to the poor nucleophilicity of the nitrogen on the aniline ring due to the lone pair of the nitrogen being conjugated with the aromatic ring. The reaction stereoselectivity arises from the stereoselective protonation of the enolate which can only occur readily from the bottom face (**Figure 2.3**). After the initial nucleophilic attack from the amine, the protonation step can only occur from one face of the molecule, hence the high stereoselectivity of this reaction.[136]

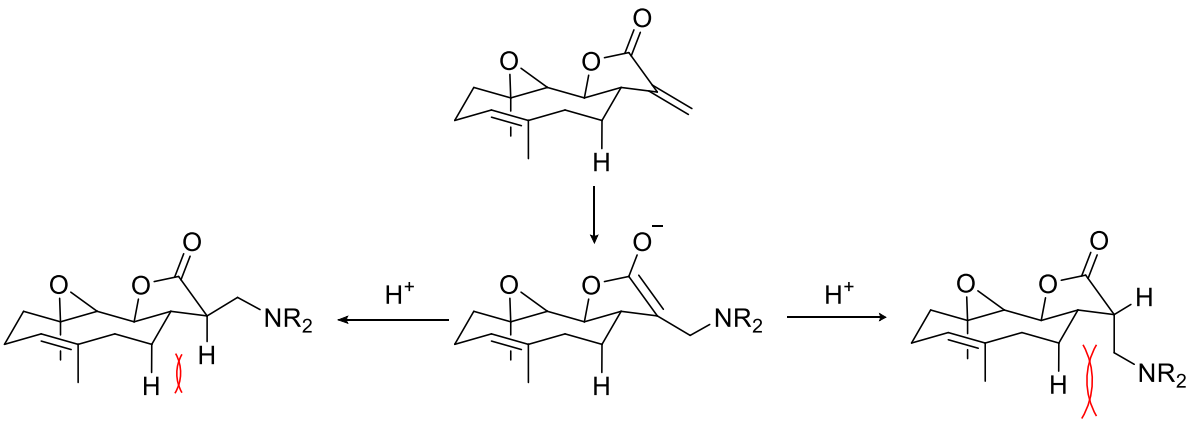

***Figure 2.3** – Stereochemical outcome of a Michael addition with PTL and an amine, potentially due to the thermodynamic stability of the product.*

A method developed by the Fossey group involves the use of squaric acid as a catalyst for PTL derivatisation. A previous student, Dr Xingjian Li, identified conditions for a high yielding synthesis of PTL-aniline derivatives (**Scheme 2.1**) using squaric acid in

catalytic quantities. Inspiration was taken from Azizi *et al.* on the use of squaric acid in Michael additions with poor nucleophiles.[201]

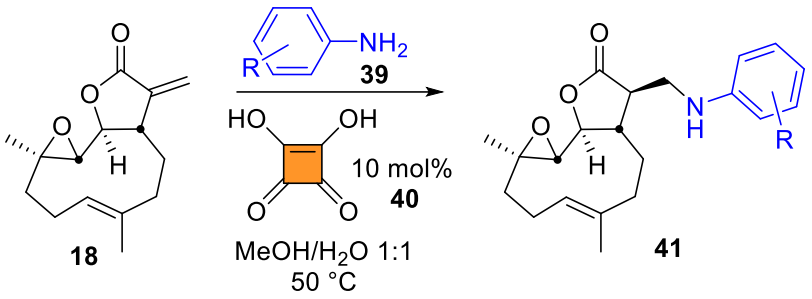

Scheme 2.1 *– Squaric acid catalysed reaction of PTL with anilines.*

Squaric acid has the formula $C_4O_4H_2$ and is structurally comprised of a cyclobutene ring with two carbonyls and two hydroxyl groups, named due to it being an almost perfect square by X-ray crystallography.[202] It was used by Tietze's group as the ester in a double amide coupling, whereby the sequential formation of two different amides could be achieved under aqueous conditions (**Figure 2.4**).[203, 204] Squaric acid is a diprotic acid with a first and second pK_a of around 1.5 and 3.4 respectively.[205]

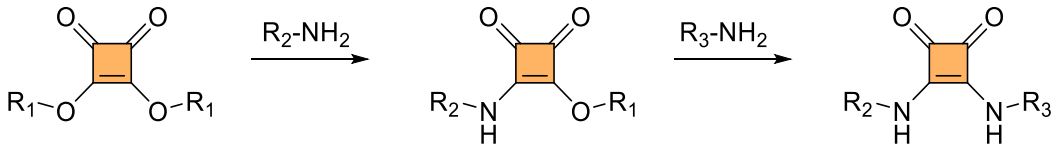

Figure 2.4 *– General scheme for the sequential double amide coupling to squaric acid.*

2.1.4.1 Small library synthesis

With over one gram of PTL in hand, it was decided to make as many aniline derivatives of PTL as possible to study any relationship between the structure and the activity of the compound against CLL. Anilines were selected based on the availability in the lab

with some additional anilines purchased to have a range of electron donating and electron withdrawing groups. Yields for this reaction varied from as low as 8% up to 54% as outlined in **Table 2.1**. In every case, unreacted PTL was recovered through column chromatography.

***Table 2.1** – Aniline containing PTL derivatives synthesised and the yields of the reactions.*

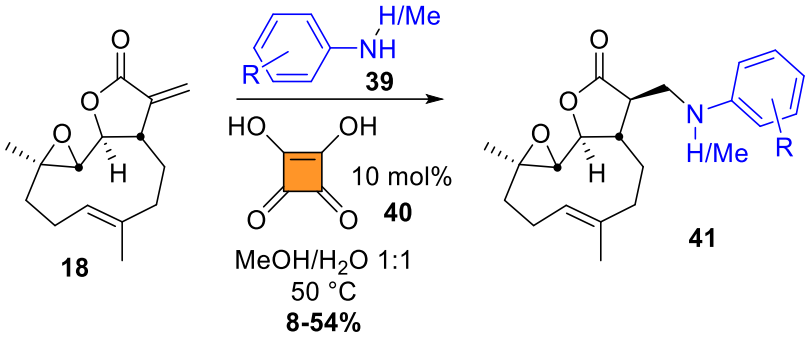

Entry	*Compound number*	*H/Me*	*R*	*Yield, %*
1	**41a**	H	4-Me	51
2	**41b**	H	4-F	35
3	**41c**	H	4-Br	9
4	**41d**	H	4-OMe	54
5	**41e**	H	3,5-OMe	26
6	**41f**	H	3,5-Me	28
7	**41g**	H	3-OMe	24
8	**41h**	H	3-Me	18
9	**41i**	Me	H	8
10	**41j**	Me	4-F	12
11	**41k**	Me	4-OMe	36

While the yield for this reaction was low, some patterns emerged between the nature of the substituent around the ring and the yield. Generally, the more electron donating substituents such as the methoxy gave higher yields (**Table 2.1**, entry 4, compound **41d**, 54%) and the slightly deactivating halogens such as the bromide gave lower

yields (**Table 2.1**, entry 3, compound **41c**, 9%). Secondary anilines (**Table 2.1**, entries 9-11, compounds **41i** to **41k**) gave lower yields than their equivalent primary anilines. **Table 2.2** shows the yield of each reaction, along with the p*K*$_a$s of the corresponding ions to give an indication of why the yields follow this trend.

***Table 2.2** – Comparison of yield of the reaction outlined in **Table 2.1** compared with the p*K*$_a$ of the aniline.*

Entry	*Compound number*	*Aniline*	*Yield*	*p*K$_a$*
1	**41a**	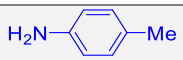	51	10.8
2	**41b**	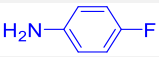	35	10.5
3	**41c**	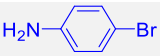	9	10.6
4	**41d**		54	10.9
5	**41e**	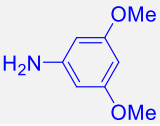	26	10.3
6	**41f**	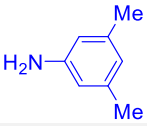	28	10.8
7	**41g**	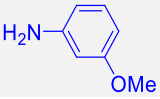	24	10.5
8	**41h**	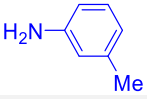	18	10.7
9	**41i**	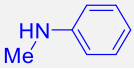	8	10.6
10	**41j**	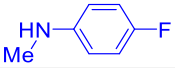	12	10.4
11	**41k**	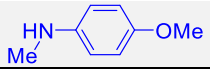	36	10.7

*p*K$_a$s were found using chemdraw and are a prediction of the p*K*$_a$ of the ammonium ion.

There is very little change in the p*K*$_a$ of the anilines and so it is unlikely that this plays a role in the outcome of the reaction.

2.1.5 Anti-CLL activity

A minimum of 95% purity by proton NMR was ensured for all the compounds synthesised. They were then transferred to the Institute for Cancer Research at the University of Birmingham for testing against the MEC1 cell line, a cell line commonly used for CLL testing.[206]

2.1.5.1 Setting up in vitro *testing*

Cell cultures and *in vitro* testing were performed by Dr Agathanggelou in the Institute for Cancer Research at the University of Birmingham. MEC1 cells are first bought and cultured in medium containing fetal bovine serum. Well densities of 25000 cells per well were set up in 96 well plates and the compounds were added in triplicate wells. Resazurin was added to each well (50 µg/mL) and left to incubate at 37 °C for three hours. Resazurin (**Figure 2.5**, compound **42**) is a purple dye that can be reduced to resorufin, a pink dye that is highly fluorescent (**Figure 2.5**, compound **43**). Reduction occurs enzymatically by mitochondrial reductase that are present in live cells. The level of resorufin in the well gives an indication of how many cells are alive and metabolising. Cell viability was measured by fluorescence intensity at 590 nm after excitation at 540 nm.

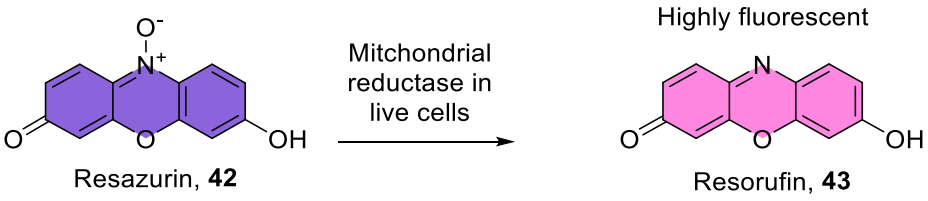

***Figure 2.5** – Reduction of non-fluorescent resazurin (**42**) by mitochondrial reductase in live cells to the formation of highly fluorescent resorufin (**43**) which can be used to give an indication of cell viability.*

2.1.5.2 Anti-CLL activity

The anti-CLL activity of all the aniline containing parthenolide derivates are outlined in **Table 2.3** and are compared with the activity of PTL. Unfortunately, the EC_{50}, a measure of drug potency whereby half of the targeted biological function is inhibited, of most of the compounds (entries 1-10, compounds **41a** to 41j) were above the highest concentration of drug used (100 μM). Compound **41k** (**Table 2.3**, entry 11) showed slightly better activity against the cell line, however at 76.2 μM, it is not an improvement on the parent compound PTL.

Table 2.3 *– Anti-CLL activity of aniline containing parthenolide derivatives compared with PTL.*

Entry	*Compound number*	*EC_{50}, μM*
1	**41a**	>100
2	**41b**	>100
3	**41c**	>100
4	**41d**	>100
5	**41e**	>100
6	**41f**	>100
7	**41g**	>100
8	**41h**	>100
9	**41i**	>100
10	**41j**	>100
11	**41k**	76.2 ± 0.3
12	PTL, **18**	4.6 ± 0.9

From the data given, it can be seen that adding an aniline to PTL does not improve its anti-leukaemic activity, however the development of the synthesis of the compounds was an important aspect to this work to access the new class of PTL derivatives, and the synthesis outlined can be transferred to other Michael addition reactions with poor nucleophiles.

2.1.6 Computational docking

As previously discussed in section 1.3.2, the potential for a retro-aza Michael reaction to occur *in vivo* as a prodrug mechanism for PTL derivatives means that the results from computational docking on these molecules may not be indicative of their activity or the true binding event that occurs. Nevertheless, the docking poses of the derivatives of PTL to NF-κB were also investigated to see if there was any correlation between the docking score and activity, as well as to gain knowledge of the way in which computational docking is undertaken.

Each compound made in this section was subjected to the molecular docking protocol outlined in the experimental section and their lowest energy docking score is presented in **Table 2.4**. In simple terms, the docking score provided by the Autodock Vina code combines the intramolecular and intermolecular contributions to the free energy of binding.[207] The docking scores do not vary by much as compared to PTL and the poses in which they sit in their lowest energy conformation is the same for all the anilines. The only compound to have a lower docking score (therefore better binding) than PTL was the *meta*-methyl compound (compound **41h**, entry 8, **Table 2.4**), however it did not show increased activity (**Table 2.3**). The individual docking scores are all close together, and with the error associated with the method, it would be difficult to draw absolute conclusions from these data. It can therefore be concluded that while molecular docking has been shown to be useful in drug discovery projects in the past, in this particular case the compounds of interest do not have good enough activity against the target for this to be a useful tool, or the binding site of the drug is different to the binding site described by Merfort and co-workers.[142]

***Table 2.4** – Docking scores between the aniline containing derivatives of PTL and the NF-κB protein using the open-source Chimera software.*

Entry	*Compound number*	*Docking Score*
1	**41a**	-5.2
2	**41b**	-5.2
3	**41c**	-5.1
4	**41d**	-5.1
5	**41e**	-5.1
6	**41f**	-5.3
7	**41g**	-5.3
8	**41h**	-5.4
9	**41i**	-5.0
10	**41j**	-5.0
11	**41k**	-4.9
12	PTL, **18**	-5.3

2.2 ALF01

In collaboration with Sygnature Discovery, a previous member of the Fossey group at the University of Birmingham, Dr Xingjian Li, synthesised a library of amine containing PTL derivatives and tested against CLL. A total of 120 amines were used to make a library of aminoparthenolide derivatives with a total of 76 successful products. They were all subjected to biological testing against CLL with a range of activities, with 12 having sub 20 μM activity. Previously investigated PTL and DMAPT were used as reference compounds in this study, with EC_{50} values of 3.4 and 2.8 respectively. Additional DMPK studies were carried out on the ten most active compounds all with an EC_{50} value of less than 15 μM, and following *in vitro* and *in vivo* studies, compound **21** (termed ALF01) was selected as the lead compound. The synthesis of ALF01 is outlined in **Scheme 2.2**.

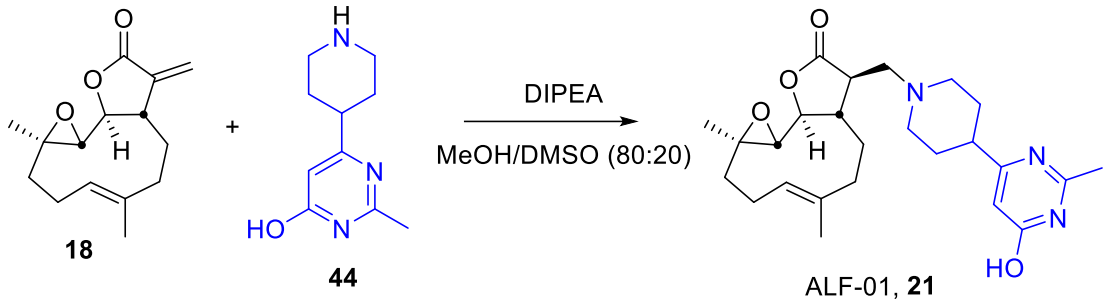

Scheme 2.2 *– Synthesis of ALF01, compound* ***21****.*

2.2.1 Synthesis of ALF amine[*]

The amine required to make ALF01 was not commercially available when required, and so a synthetic method was sought. The following retrosynthetic analysis of amine **44** was used (**Scheme 2.3**).

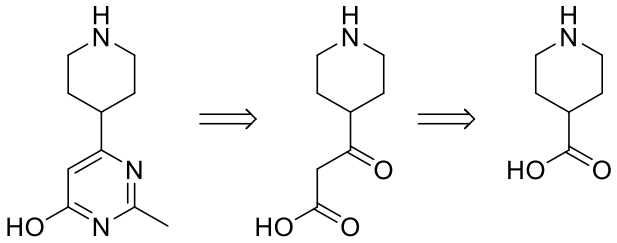

Scheme 2.3 *– Retrosynthetic analysis of ALF amine,* ***44****, from isonipecotic acid,* ***46****.*

2.2.1.1 Synthesis of ester

Isonipecotic acid (**46**) was *N*-Boc protected initially to form *N*-Boc isonipecotic acid (**47**). Initial reactions were carried out using sodium hydroxide (1 M) in THF, however yields of this reaction were below 50%. Increasing the concentration of sodium hydroxide (2 M) improved the yield to 92%. Potassium ethyl malonate (**49**) was

[*] All experimental work in section 2.2.1.1 was carried out by the author of this doctoral thesis in a previous master's thesis and is included here for continuity.

commercially available, however its synthesis from diethyl malonate is facile and overall more cost-effective. This was thus synthesised through the dropwise addition of potassium hydroxide in ethanol to a solution of diethyl malonate (**48**) in ethanol with rapid stirring produced the malonate (**49**) in an 84% yield, which was collected by filtration.

The reaction of potassium ethyl malonate with *N*-Boc isonipecotic acid to form compound **50** was carried out under conditions that were adapted from work by Masamune and co-workers (**Scheme 2.4**).[208] Magnesium complexed ethyl malonate was added to the synthesised imidazolide congener in the other. Upon mixing of the two separate reactions and stirring overnight, the product was obtained in a 24% yield following purification. This was deemed too low for efficient synthesis of the ester **50**. On addition of triethylamine, the yield increased to 67%.

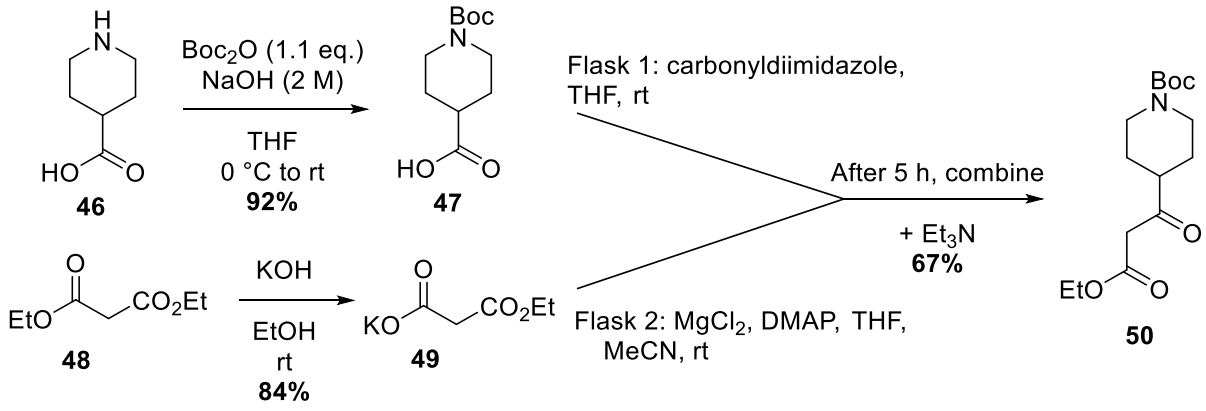

Scheme 2.4 *– Convergent synthesis of ester **50** from isonipecotic acid and diethyl malonate.*

2.2.1.2 Synthesis of ester - PhD

The reaction to form the ethyl β-keto ester via the method outlined in section 2.2.1.1 requires multiple reactions and careful transfers to increase the yield, and the

maximum yield achieved for this reaction is 67%. An alternative method was found in which ester **50** could be synthesised by treatment of *N*-Boc isonipecotic acid with Meldrum's acid to form acetal **51**. Ethanolysis of the intermediate acetal, which was not isolated, forms ethyl β-keto ester **50** through reflux in ethanol with an overall yield of 82%.

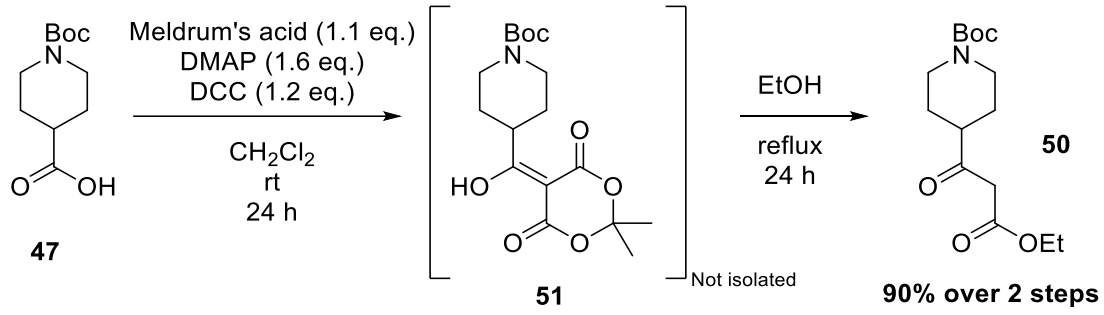

Scheme 2.5 *– 2 step synthesis of compound* ***50*** *via intermediate* ***51****.*

2.2.1.3 Pyrimidine formation

Vidal *et al.* described a method of forming pyrimidines from ethyl β-keto esters and amidine hydrochlorides using ultrasound, a base, and water as the solvent.[209] Inspiration was taken from this study to use in the pyrimidine formation, however initial reactions using the exact conditions described did not form any of the required pyrimidine (**Scheme 2.6**, compound **53**). After 15 minutes of sonication, the reaction was still not a homogenous solution, with the ethyl β-keto ester **50** an insoluble oil.

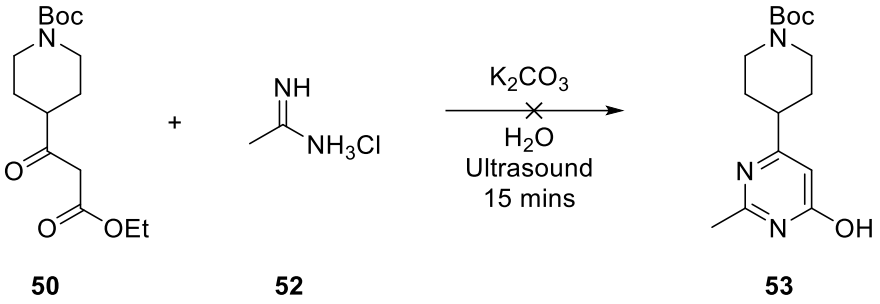

50 **52** **53**

Scheme 2.6 *– Failed attempt at pyrimidine formation using the exact conditions described by Vidal* et al*.*

A second attempt was made using a half and half mix of water and methanol to completely dissolve the reaction mixture. The exact conditions were met using a sonicator bath, however no reaction occurred following an hour of sonication, despite all reactants being in solution. A third attempt was made using the same conditions as the second attempt but this time heating to 70 °C. Under these conditions (**Scheme 2.7**), a yield of 77% was achieved.

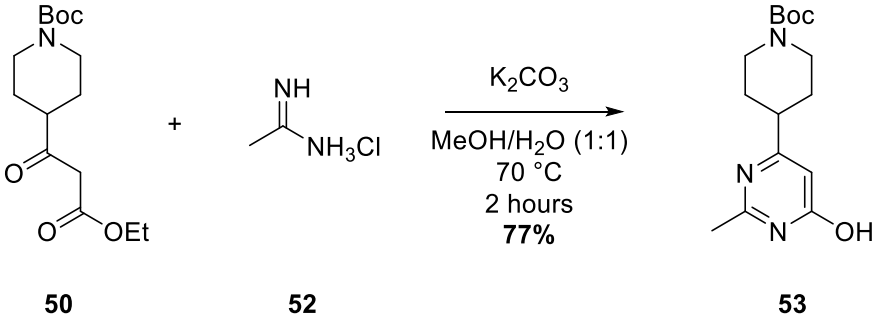

50 **52** **53**

Scheme 2.7 *– Method used for the formation of the pyrimidinol* ***53****.*

2.2.1.4 Boc deprotection

The final step to making amine **44** was a deprotection of the Boc group. A common method of achieving this in high yields is with the use of trifluoro acetic acid (TFA) in

dichloromethane.[210] This was carried out on compound **53** to form the target amine **44** in 83% yield (**Scheme 2.8**).

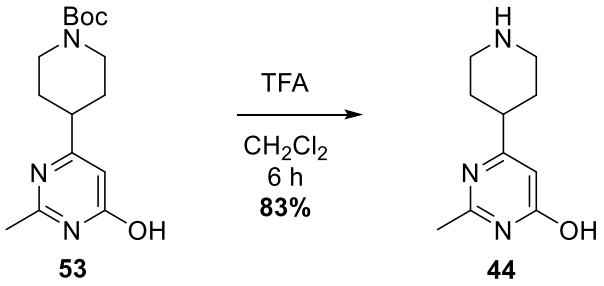

Scheme 2.8 *– Boc-deprotection of compound* ***53*** *to form the target amine* ***44****.*

2.2.2 Biological activity

Compound **21** was submitted for biological testing in the same manner as outlined in section 2.1.5.1. The results obtained from this experiment showed that compound **21** had an EC_{50} of 10.6 ± 2.0 μM, compared with PTL which has an EC_{50} of 6.2 ± 2.0 μM in that particular assay. Given experimental errors, the change in activity between PTL and the compound **21** is minimal, however it was shown in drug metabolism and pharmacokinetic (DMPK) studies† that the "drug-like" properties of compound **21** were superior to that of PTL as well as the other drugs tested in the study.

2.3 Conclusion and future work

11 aniline containing derivatives of PTL were synthesised and tested for their potency against a chronic lymphocytic leukaemia cell line. The compounds synthesised did not show any improvement in the potency against CLL, however the work has helped develop a synthetic method for carrying out Michael additions with poor nucleophiles.

† DMPK studies carried out by an external company.

A synthetic route to compound **21**, ALF01, has been developed from commercially available starting materials. Compound **21** exhibits similar potency to PTL, but with superior drug-like properties. The micromolar potency against the MEC1 cell line is still relatively high compared to already marketed cancer therapies, and therefore any future work in this field should focus on reducing the potency as much as possible, whilst still improving the drug-like properties of the compound.

Other work in the group to synthesise phenol-containing PTL derivatives that showed similar potency to PTL led us to consider forming prodrugs using boronic esters to target cancer cells, exploiting their intrinsically higher ROS levels.

3 Oxidation of phenylboronic acids

3.1 Background

3.1.1 Accepted putative mechanism of boronic acid oxidation

Phenylboronic acids and esters undergo oxidation to the corresponding phenol in the presence of reactive oxygen species, for example hydrogen peroxide. The general putative mechanism for the oxidation of arylboronic acid by hydrogen peroxide is shown in **Scheme 3.1**. There is an initial attack of the peroxide anion on the trigonal boron centre invoking a configuration change to the tetrahedral boronate anion. Following this, a 1,2-shift of the carbon to form a carbon-oxygen bond, and subsequent rapid hydrolysis forms the phenol and boric acid.

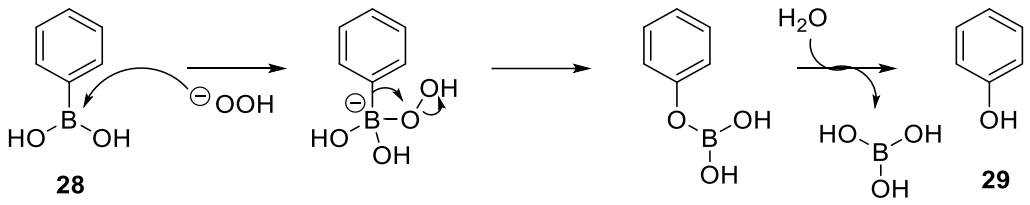

Scheme 3.1 *- Currently accepted mechanism for the oxidation of arylboronic acids by hydrogen peroxide to the corresponding phenol and boric acid.*[211]

The mechanism in **Scheme 3.1** has three steps, any of which could be the rate-limiting step. It is likely in this mechanism that the rate-limiting step is the 1,2-shift where the carbon-boron bond breaks and the carbon-oxygen bond is formed, causing the boron to become more electron deficient owing to the increased electronegativity of the oxygen compared to carbon.[211] If this were true, then only the intermediate boronate complex would feature in the rate equation, hence the order of the reaction would be first order overall with respect to the intermediate boronate. Computational

calculations of the mechanism of the oxidation of boronic acids provided an alternative story, with a concerted process theorised in **Scheme 3.2**.

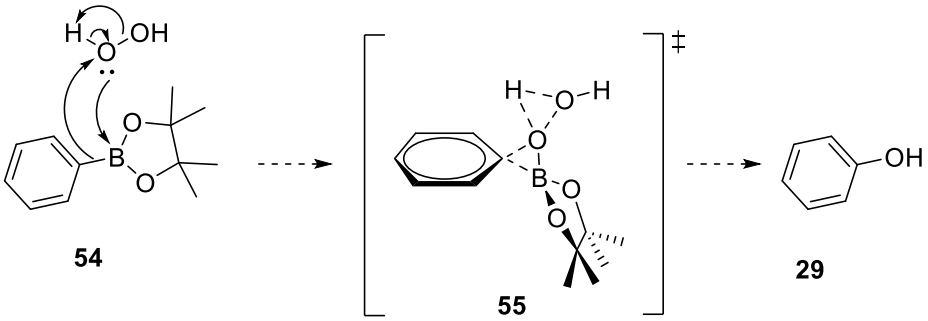

Scheme 3.2 *– Computationally theorised mechanism for the oxidation of phenylboronic acids and esters whereby a concerted attack of the peroxide to boron and 1,2-shift creates the transition state.*

In the newly hypothesised mechanism, the rate-limiting step would be the concerted attack of peroxide and boronic acid, forming transition state **55**, and therefore it would be expected that the rate of the reaction would be first order with respect to both peroxide and boronic ester, making the overall reaction rate second order. It would be difficult to measure the difference in rate orders between the two mechanisms as only the concentrations of the boronic acid and peroxide can be controlled, and not the concentration of the intermediate boronate complex. Nevertheless, the reaction order gave an idea of the reliability of the following results.

3.1.2 Boronic ester dependency

A previous study by Lloyd-Jones and co-workers on the mechanism of protodeboronation found that the structure of the boronic ester changed the rate of the reaction. For example, under the conditions they described, an arylboronic pinacol

ester underwent protodeboronation 220 times slower than the equivalent arylboronic acid as shown in **Scheme 3.3**.[212]

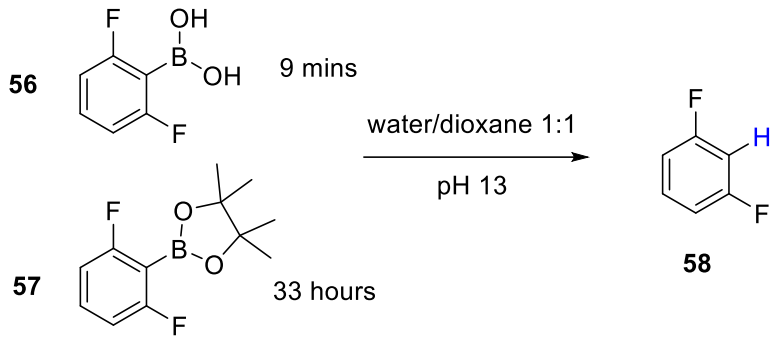

Scheme 3.3 *– Protodeboronation of an arylboronic acid and the corresponding pinacol ester in the same conditions at vastly different rates.*[212]

Controlling the rate of oxidation of boronic esters has potential advantages when using boron in sensing or drug delivery. For example, in prodrug development, fine-tuning the propensity of a drug to oxidation could mean that only within cells with high enough levels of reactive oxygen species would a boronic ester oxidise into the target phenolic drug. Formation of the active drug can therefore be localised at the tumour site where ROS levels are higher, reducing off-target effects and increasing the efficacy of the drug.[66] This same principle could be applied to ROS sensing where different boronic esters on the same structure could oxidise at different concentrations of ROS, giving multiple colour and fluorescence changes.

Chapter 3 outlines the experiments undertaken to attempt to prove the new theoretical mechanism and how the nature of the boronic ester can change the rates of oxidation.

3.1.3 Rate of oxidation

The rate constant of a reaction is dependent upon its specific conditions. For example, varying only the temperature of the reaction will likely change the rate constant. Calculating the rate constant of a reaction can be done experimentally by using the integrated rate law. The integrated rate law was used to determine the rates of oxidation of the boronic esters. In a reaction where the reactants are A and B and form products, then the rate law is:

$$\text{Rate} = k[A]^x[B]^y \qquad 3.1$$

Where k is the rate constant, [A] and [B] are the concentrations of the reactants and x and y are the rate orders with respect to [A] and [B] respectively. For the boronic ester oxidation with hydrogen peroxide, the rate law can be written as per equation 3.2.

$$\text{Rate} = k[\text{boron}]^x[H_2O_2]^y \qquad 3.2$$

The rate constant is related to the rate at which the concentration of a reactant decreases. However, when there are two reactants, both reactants decrease in concentration and therefore there is more than one variable involved. Thus it would be impossible to tell the rate of the reaction with respect to just one of the reactants. Measuring the pseudo-first order rate constant can solve this issue. By having one reactant in a two-reactant reaction in a large excess, it can be assumed that its concentration does not change significantly, and therefore does not affect the rate of reaction. Therefore, the rate of the reaction can be calculated with respect to the reactant that is in limiting concentration.

To calculate the pseudo-first order rate constant, it has to be assumed that the reaction is first order with respect to the limiting reagent. The rate law for a first order reaction is given by equation 3.3:

$$\frac{d[A]}{dt} = -k[A][B] \qquad 3.3$$

Where [A] is the concentration of the limiting reagent, [B] is the concentration of the other reagent and k is the rate constant. When the concentration of B is in excess, the pseudo-first order rate equation can be used:

$$\frac{d[A]}{dt} = -k_{obs}[A] \qquad 3.4$$

The term k has now changed to k_{obs}, indicating that the rate constant obtained from these calculations are not the true rate of the reaction, but an observed rate based on the experimental data. Rearranging equation 3.4 gives equation 3.5.

$$\frac{d[A]}{[A]} = -k_{obs}dt \qquad 3.5$$

The integrated rate law can be used to find the concentration of a reactant at a certain time point, as well as the rate at that instant. Deriving the pseudo-first order integrated rate law begins by integrating equation 3.5 and rearranging to equation 3.9.

$$\int_{[A]_0}^{[A]_t} \frac{d[A]}{[A]} = \int_{0}^{t} -k_{obs}dt \qquad 3.6$$

$$\ln \frac{[A]_t}{[A]_0} = -k_{obs}t \quad 3.7$$

$$\frac{[A]_t}{[A]_0} = e^{-k_{obs}t} \quad 3.8$$

$$[A]_t = [A]_0 e^{-k_{obs}t} \quad 3.9$$

Equation 3.9 is the integrated rate law for pseudo-first order reactions and is used to calculate the pseudo-first order rate constant for the oxidation of boronic acids.

3.1.4 Aims and objectives

The overall aim of the chapter is to study the rate of oxidation of boronic esters by ROS to develop an understanding of the mechanism of oxidation and the scope for selectively choosing diols to form boronic esters based on their oxidation rates, to influence their pertinence to real-world applications. For example, in anti-cancer prodrugs, a boronic ester that oxidises to an active phenolic drug could be finely tuned so that only certain concentrations of ROS can activate the drug.

A series of boronic esters needed to be synthesised or procured to generate a library of compounds for testing. Some were commercially available, whilst the majority were synthesised from the boronic acid and corresponding diol. Once in hand, the oxidation rates of all the esters had to be measured. There are a range of methods for doing this experimentally; tracking the reaction via UV-Vis was selected as the easiest, both in experimental set-up and as a high throughput of data collection and analysis.

To improve the validity of the results, the equilibrium that a boronic ester is under when in aqueous conditions also had to be investigated.

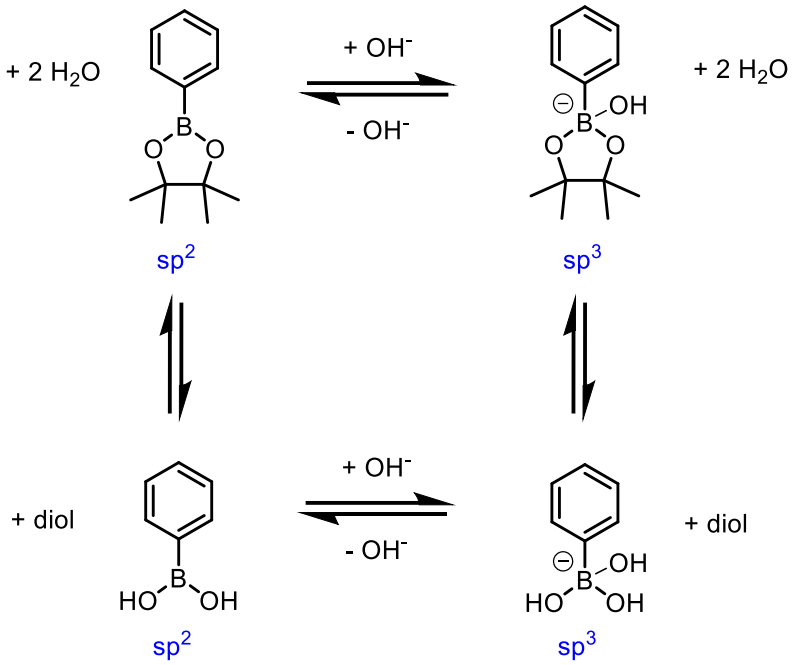

Scheme 3.4 *– Four potential structures of a boronic ester and the equilibrium relationship between them, illustrate here phenylboronic acid and pinacol.*

As seen in **Scheme 3.4**, boronic esters have four potential structures when in aqueous conditions, and the positions of the equilibria are dependent on factors such as pH. In the horizontal equilibria, i.e. left to right, the boron centre is either sp^2 or sp^3 hybridised and is partially depending on the pH of the solution. In the vertical equilibria, i.e. top to bottom, the boronic ester is in equilibrium with the boronic acid and diol and is partially dependent on the binding affinity of the diol to the boronic acid. The positions of the equilibria had to be determined for the conditions in the oxidation experiments so that it was known which species was primarily oxidising. It would be sensible to assume that each of the four structures in **Scheme 3.4** would oxidise at different rates. Therefore, a major aim for the chapter is to develop experimental protocols to assess the equilibria shown.

3.2 Synthesis of boronic esters

Boronic acids and esters are generally commercially available with Sigma Aldrich selling 637 different products.[213] The most common boronic ester commercially available is the pinacol ester.[214] The synthesis of cyclic boronic esters can be achieved via a condensation reaction between the corresponding boronic acid and a 1,2- or 1,3-diol.[215] The continual removal of water with a drying agent such as anhydrous magnesium sulfate or using the Dean-Stark apparatus set up is generally used. This drives the equilibrium towards the boronic ester (**Scheme 3.5**).[216]

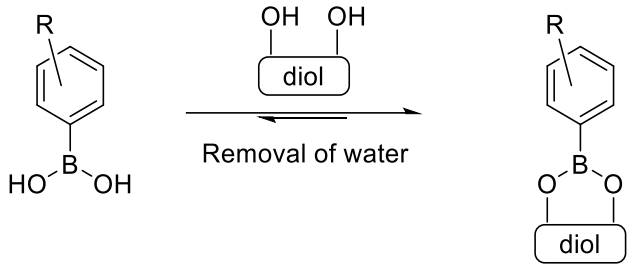

Scheme 3.5 *– Equilibrium between boronic acid and boronic ester being driven to the right through the removal of water.*

A series of boronic esters were synthesised so their relative rates of oxidation could be investigated. The initial step in the library synthesis was the identification of target compounds. Firstly, it was decided to focus on one boronic acid rather than varying the substituent around the ring. Altering the substituent on the aromatic ring changes the electronics and therefore the rate of reaction, with a correlation to its Hammett parameter. Secondly, a range of diols were required to alter properties such as solubility, pK_a, flexibility, and propensity for hydrolysis.

3.2.1 Selection of para*-nitrophenylboronic acid*

The rate experiments were undertaken with *para*-nitrophenylboronic acid and its boronic esters. Focusing on one boronic acid meant there was one fewer variable in

the experiments and a full data set could be collected. The oxidation of *para*-nitrophenylboronic acid produces *para*-nitrophenol. The colorimetric change of this reaction from colourless to yellow was easily quantified via UV-Vis spectrometry, therefore the progression of the reaction could be monitored.

3.2.2 Diol properties

A list of available diols **59a** to **59l** that were used in the oxidation study is shown in **Figure 3.1**.

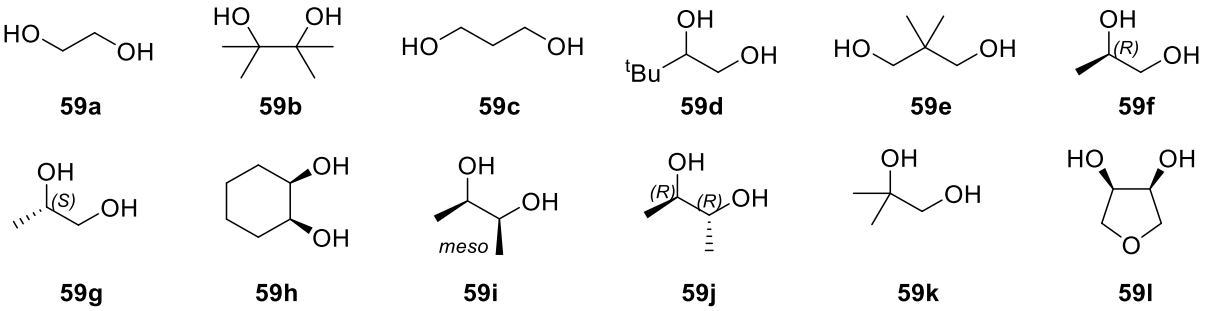

***Figure 3.1** – Structures of the twelve selected diols, compounds **59a** to **59l**.*

A few of the medicinal chemical properties of each ester was taken into consideration when the selection of diols was made. cLogP is the calculated measure of the lipophilicity of a compound, i.e. an indicator of how permeable the compound is across cell membranes. LogS is a measure of the aqueous solubility of a compound. Compounds with low solubility tend to have lower absorption into the body and lower stability, causing them to fail as drug candidates.[217] It is clear that the values outlined in **Table 3.1** are for reference and comparison only, but could be used to further determine the right ester recommendation for each use.

***Table 3.1** – Molecular weight, cLogP and logS as calculated by ChemDraw for the ester of para-nitrophenyl boronic acid and the following diols.*

Property of ester / *Diol*	MW, g mol^{-1}	*cLogP*	*LogS*
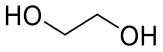	192.97	1.337	-2.554
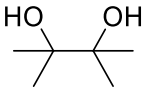	249.07	3.413	-3.973
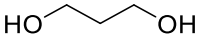	206.99	1.896	-2.902
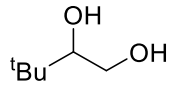	249.07	3.183	-3.768
	235.05	2.934	-3.465
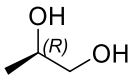	206.99	1.856	-2.927
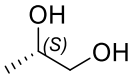	206.99	1.856	-2.927
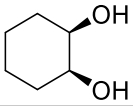	247.06	2.769	-3.788
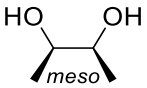	221.02	2.375	-3.300
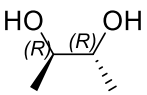	221.02	2.375	-3.300
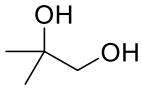	221.02	2.375	-3.265
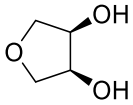	235.00	0.871	-2.546

3.2.3 Synthesis of boronic esters

Para-nitrophenylboronic acid (**60**) was reacted with each of the diols (**59a-l**) in **Figure 3.1** under the conditions outlined in **Scheme 3.6**. The initial reaction was carried out

using 1.0 mmol of boronic acid, 1.2 mmol of diol and 3.0 mmol of anhydrous magnesium chloride. Dichloromethane was used as the solvent (5 mL), to give each reaction a concentration of 200 mM.

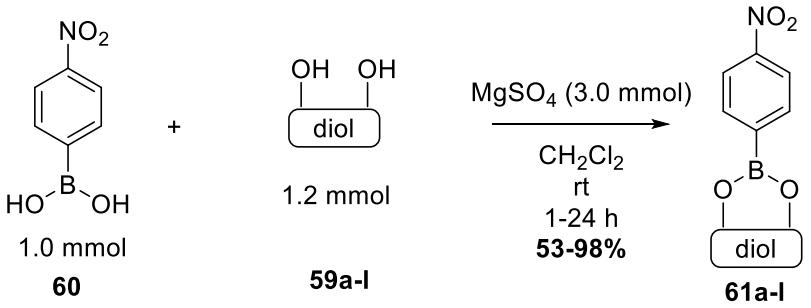

Scheme 3.6 *– General scheme for the synthesis of the para-nitrophenylboronic esters.*

In the case of ethylene glycol and 1,4-anhydroerythritol, the reaction vessel was first flushed with argon and sealed during the reaction to maintain a dry atmosphere. Once the diol was in the reaction mixture, inert gas flow was halted and magnesium sulfate was used to remove water from the reaction. Each reaction was allowed to continue until no boronic acid was visible by TLC, with the curcumin TLC dip being used to test for the boron containing compounds.

Purification of boronic esters is notoriously difficult via standard purification methods such as chromatography, due in part to the Lewis acidity of the boron centre increasing the adsorption onto silica.[218] Recrystallisation is a more facile method of purification of boronate esters.[219] The condensation reactions to form the boronic esters proceeded with few by-products, and thus minimal purification was required. On completion of the reactions as judged by TLC, the reaction mixture was filtered to remove magnesium sulfate and then transferred to a separating funnel. A 0.1 M aqueous solution of

fructose was added (1 mL) to wash the organic fraction which was then dried over anhydrous magnesium sulfate and concentrated *in vacuo*. Fructose binds readily to any unreacted boronic acid, removing it from the organic fraction. A downside to the fructose wash is the equilibrium boronic esters are in with their corresponding boronic acid, reducing the yield of the reactions. However, given the accurate physical organic experiments being undertaken with these compounds, the purity of the compounds was paramount with yields being inconsequential.

The yields for the formation of boronic esters are given in **Table 3.2**. Compound **61b** was available commercially and was already available in-house, therefore was not synthesised and thus diol **59b** is omitted from **Table 3.2**.

Table 3.2 *– Isolated yields for the synthesis of boronic esters for each diol. Reaction set up shown in* ***Scheme 3.6****.*

Diol		Yield, %
59a	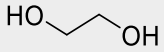	82
59c	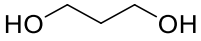	79
59d	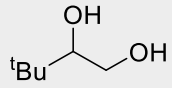	71
59e		80
59f	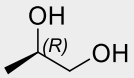	68
59g	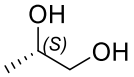	78
59h	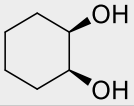	86
59i	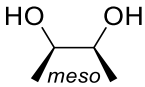	94
59j	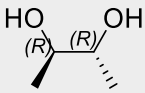	97
59k	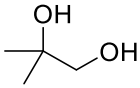	53
59l	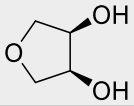	98
Condensation reactions with para*-nitrophenylboronic acid* ***60*** *(1.0 mmol), diol* ***59a*** *to* ***59l*** *(1.2 mmol), and magnesium sulfate (3.0 mmol) to give boronic esters* ***61a*** *to* ***61l****. See* ***Scheme 3.6****.*		

3.3 pK_a measurements of *para*-nitrophenylboronic esters‡

3.3.1 pK_a of boronic acids

The pK_a of a boronic acid is defined as the pH at which there exists equal quantities of neutral boronic acid and negatively charged boronate (**Scheme 3.7**).[220] This is also true for boronic esters, and the pK_a of each is dependent on conditions such as solvent and temperature, therefore it is difficult to compare between values of pK_a calculated using different conditions.

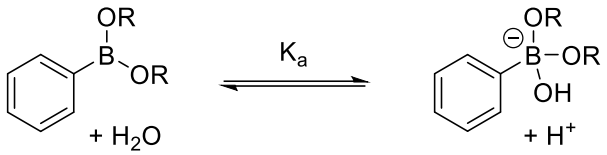

***Scheme 3.7** – Equilibrium between neutral, trigonal planar boron species and anionic, tetrahedral boronate species.*

3.3.2 Experimental pK_a of boronic esters

Obtaining an accurate value for the boronic acid pK_a of a boronic ester requires the two species, neutral boronic ester and anionic boronate, to have different absorbance maxima (λ_{max}). This is the case with *para*-nitrophenylboronic acid and its esters. The first task to carry out with this experiment was making a series of solutions at different pH values. Firstly, a solution of 0.1 molar aqueous sodium phosphate buffer was made and acidified to pH 4. An aliquot (97.5 µL) was removed and 2.5 µL DMSO was added to obtain the pH when in a 97.5:2.5 mixture, as would be the case in this experiment. A larger aliquot of 10 mL was set aside as the first solution. The main solution of aqueous phosphate buffer was basified to the next required pH and the above procedure was repeated until 24 solutions had been made at regular pH intervals

‡ For the remainder of chapter 3, pK_a refers to the boronic acid pK_a.

between pH 4 and pH 10.5. The experiments were set up on 96-well plates using 2.5 µL of boronic ester in DMSO (5 mM) in 24 wells followed by 97.5 µL of the different pH solutions in each well. A UV-Vis spectrum between 220 nm and 800 nm was then obtained.

The output from the experiments gives an absorption data point for each pH of solution being measured. When plotted, a representative graph (**Figure 3.2**) gives a curve with the mid-point of the downward slope giving the pH at which there is a 1:1 ratio between sp^2 and sp^3 boron centres, therefore the boronic acid pK_a of *para*-nitrophenylboronic acid, which is 6.9 under these conditions. This process was repeated with all the boronic ester derivatives of *para*-nitrophenylboronic acid and the results are shown in **Table 3.3**.

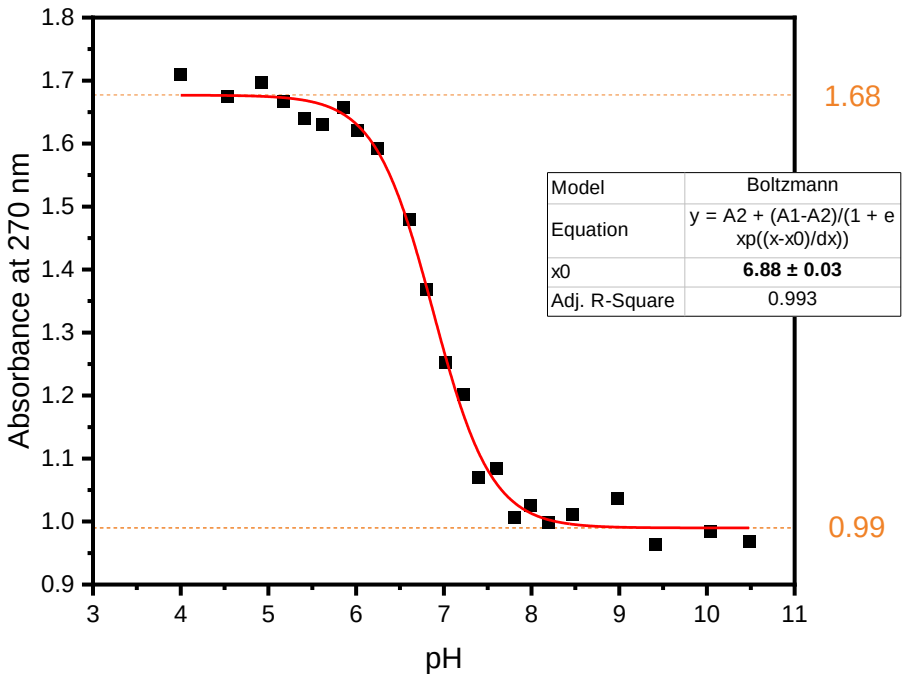

Figure 3.2 *– Graph to show absorbance of compound* ***60*** *at 270 nm as a function of pH. The midpoint of absorbance gives the pH at the point of sp^2:sp^3 ratio is 1:1, i.e. the pK_a of the compound.*

Table 3.3 *– pK_as of the boronic esters of* para*-nitrophenylboronic acid.*

Compound	pK_a ± error
60	6.88 ± 0.03
61a	6.94 ± 0.09
61b	6.87 ± 0.06
61c	6.75 ± 0.10
61d	6.94 ± 0.04
61e	6.96 ± 0.09
61f	7.04 ± 0.12
61g	7.06 ± 0.06
61h	7.04 ± 0.07
61i	7.07 ± 0.08
61j	6.84 ± 0.04
61k	6.81 ± 0.06
61l	6.85 ± 0.06

3.4 Boronic acid-diol affinity measurements

When rates of oxidation were being measured, a fundamental question to ask is whether the rates being measured are the rates of ester oxidation, or of ester hydrolysis followed by oxidation of the boronic acid. By measuring the propensity for hydrolysis, which is related to the binding strength of the diol to the boronic acid, a ranking order could be developed comparing diol binding strength to a particular boronic acid. If this is the not the same ranking order as the rate of oxidation, then it can be assumed that the rate measurements are indeed, at least in part, independent of the equilibrium position of the ester hydrolysis.

3.4.1 Measurement of diol binding strength

Qualitative measurements, i.e. not absolute values, of diol binding strength were adequate to develop a ranking order of relative strengths to compare against the ranking order of rates of oxidation. Alizarin Red S (ARS) is a catechol that binds

strongly to boronic acids and has been used in displacement assays to work out diol binding strength (see chapter 4). Unbound, ARS has low fluorescence emission between 500 nm and 700 nm when excited at 468 nm. When bound to a boronic acid, the fluorescence increases as illustrated in **Figure 3.3**, and quantification of the increase when a competitive binder such as another diol is introduced allows a binding strength to be ascertained. Additionally, unbound ARS at pH 7.4 is red in colour, and when bound to a boronic acid changes colour to orange. Therefore, UV-Vis measurements could also be used to quantify binding, however background absorption is more of an issue with this given that some boronic acids also absorb in the same wavelength region.[221, 222]

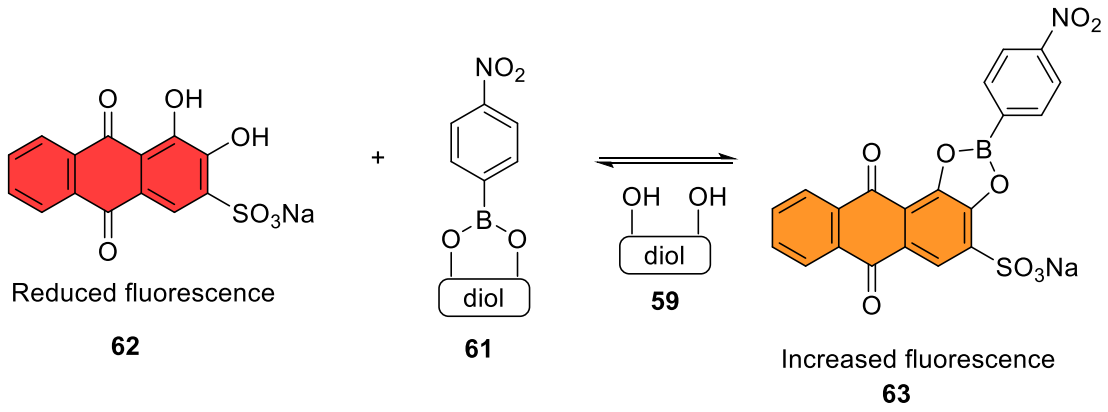

Figure 3.3 *– Unbound ARS (**62**) has reduced fluorescence, bound ARS (**63**) has increased fluorescence. By introducing a competitive binder, such as another diol, the resulting equilibrium gives an indication of diol binding strength.*

To measure the diol binding strength, three stock solutions were made:

A. ARS (**62**) in aqueous sodium phosphate buffer (0.1 M, pH 7.4) to a final concentration of 1.25 x 10^{-4} M.

B. *Para*-nitrophenylboronic acid (**60**) in 5% DMSO and 95% aqueous sodium phosphate buffer (0.1 M, pH 7.4) to a final concentration of 6.3 x 10^{-3} M.

C. Each diol (**59**) in aqueous sodium phosphate buffer (0.1 M, pH 7.4) to a final concentration of 1.5 M.

The experiment was set up in black 96-well plates with each well containing 50 µL of each of the solutions **A**, **B** and **C**. An excitation wavelength of 468 nm was used and fluorescence spectra between 500 nm and 740 nm were taken.

3.4.2 Results of diol binding strength experiment

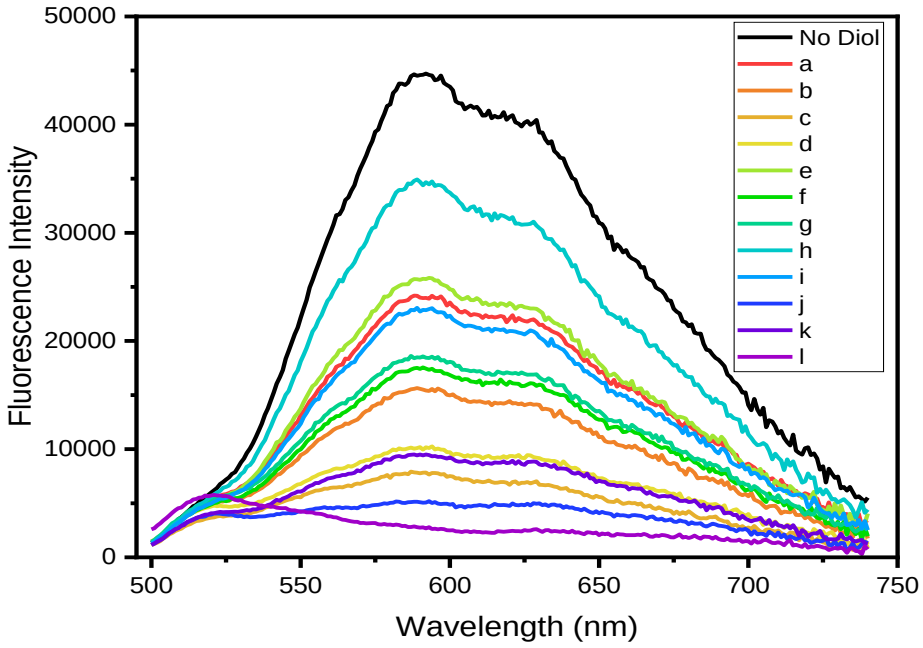

Figure 3.4 *- Emission fluorescence spectra between 500 nm and 740 nm for ARS binding study of all the diols with an excitation wavelength of 468 nm with a slit width of 10 nm.*

Figure 3.4 shows the fluorescence emission spectra between 500 nm and 740 nm after an excitation wavelength of 468 nm of the ARS, *para*-nitrophenylboronic acid and the list of diols. The line in black is where no diol is present, therefore the maximum

fluorescence should be seen with the maximum of ARS bound to *para*-nitrophenylboronic acid. Subsequent coloured lines on the graph have the diol competitively binding to the boronic acid as well as the ARS, with only bound ARS being fluorescent. The level of fluorescence gives an indication of the strength of the binding between *para*-nitrophenylboronic acid and each diol. The fluorescence maximum for bound ARS is 591 nm, and the value for the fluorescence intensity at this wavelength was used to predict the diol binding strength and an outline of these values is shown in **Figure 3.5**. A curious result was the difference in binding strength between diol i and j, where they are diastereoisomers. This could be attributed to a steric clash between the dimethyl groups on the same side and the *p*-orbital of the boron centre, blocking one side and thus causing the boron centre to favour sp^2. However, for the boron to preferentially hybridise to sp^3, the bond angles around the boron need to be as close to 109.5° as possible. The different diastereoisomers may cause different ring strains on the five membered ring, causing the bond angle around the boron to change.

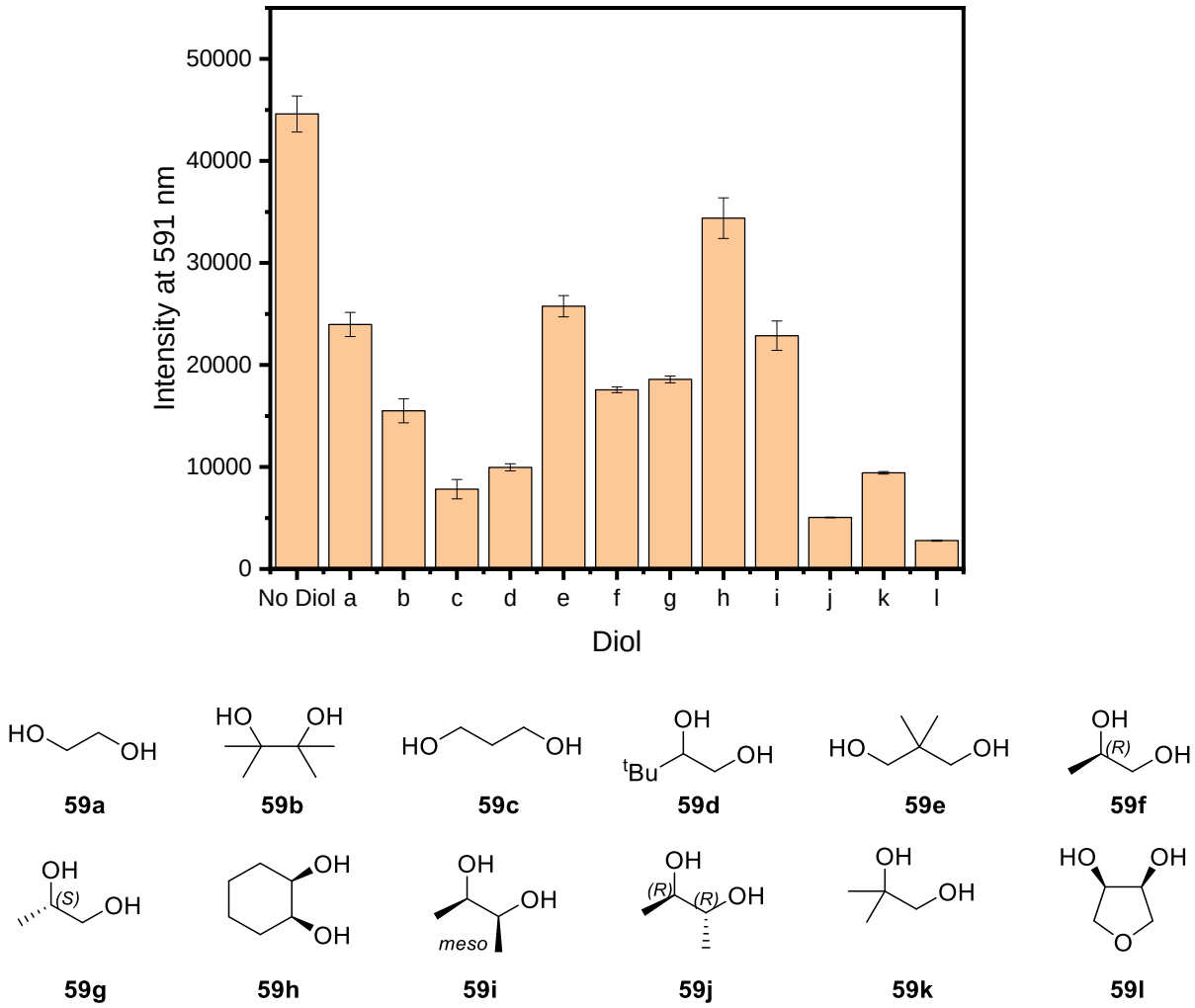

Figure 3.5 *– Bar chart to show the fluorescence intensity at 591 nm (fluorescence maximum) for ARS bound to all the diols giving a relative binding affinity.*

The experiment was carried out in triplicate and the error bars in **Figure 3.5** reflect the standard deviation within the data. The strongest binding diol to boronic acid is diol **l**, the tetrahydrofuran ring derivative. The weakest binding diol is diol **h**, the cyclohexyl derivative. None of the error bars overlap with the control of no diol, indicating that the competitive assay experiment is measuring a binding event between the boronic acid and the diol in each case. Tabulated results in **Table 3.4** outline the value for the fluorescence intensity at 591 nm, the value used to measure the diol binding strength, and the percentage of binding compared with the control, with a higher percentage

indicating more binding to ARS, and therefore weaker binding between the diol and the boronic acid.

Table 3.4 *– Overall results for the fluorescence intensities at 591 nm showing the relative binding affinities of diol to boron.*

Compound	Intensity at 591 nm (RFU)	% of X
60	44606	100
61a	23968	54
61b	15503	35
61c	7826	18
61d	9958	22
61e	25756	58
61f	17558	39
61g	18582	42
61h	34388	77
61i	22871	51
61j	5053	11
61k	9429	21
61l	2778	6

3.5 Rates of oxidation at pH 7.4

The rate of a reaction is dependent on the conditions of the reaction, for example the temperature and the pH. The temperature of all the oxidation experiments was kept at 30 °C. This is slightly warmer than normal room temperature but was selected due to the variable laboratory temperature and the lack of cooling of the microplate reader. When the laboratory temperature was above a certain value, the microplate reader was above normal room temperature, so 30 °C was selected to keep this parameter equal across all experiments. A change in the pH of the solution changes the species present in the system. At high pH, boronic acids are predominantly tetrahedral negatively charged boronates. At low pH, they are predominantly in the trigonal planar neutral form. These are fundamentally different structures with different reactivities. Uncharged boron centres have an empty *p*-orbital for nucleophilic attack, anionic boron centres do not.

3.5.1 sp^2:sp^3 ratio

From the pK_a studies of the boronic esters in section 3.3, all of the *para*-nitrophenylboronic esters are mostly sp^3 hybridised at pH 10, i.e. the equilibrium between the neutral and anionic form of the ester sits towards the anionic boronate. The fraction of sp^2 compared to sp^3 can be measured using the pK_a graphs from section 3.3 by extrapolating the plateau at the maximum and minimum absorbance and finding the absorbance when the pH is 7.4. **Figure 3.6** gives an example of how this is carried out with *para*-nitrophenylboronic acid.

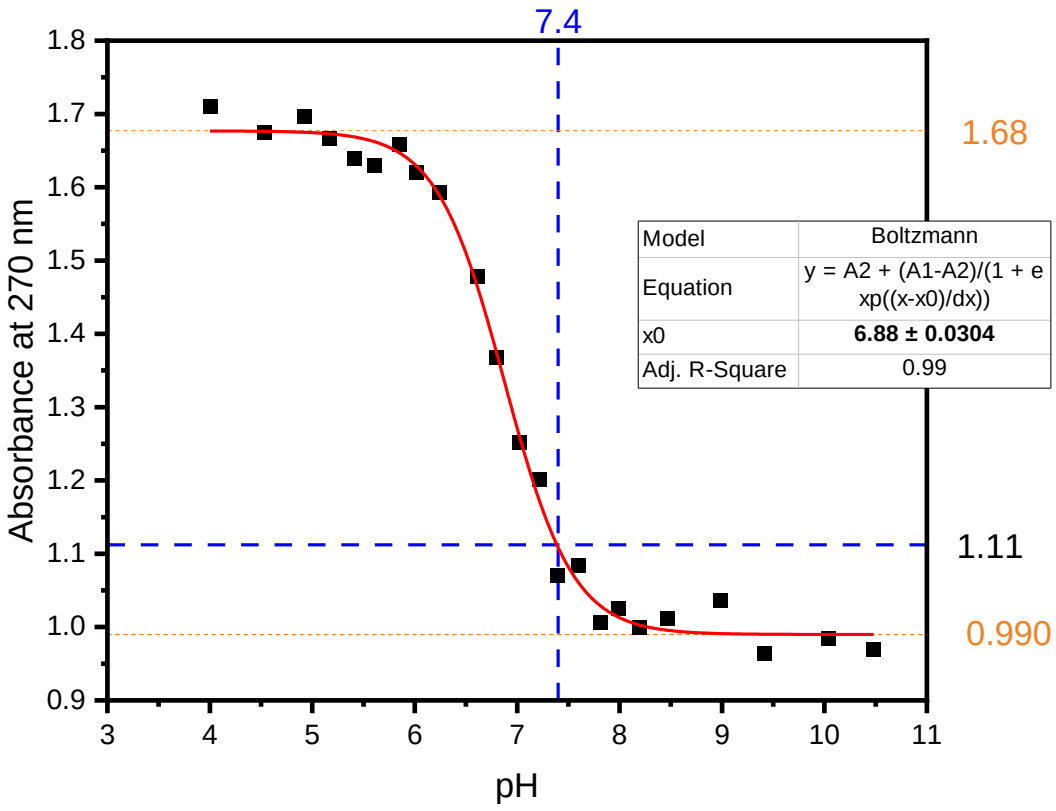

Figure 3.6 *– Graph to show the absorbance at 270 nm of* para*-nitrophenylboronic acid at varying pH values. Orange bisecting lines give a value for the absorbance at the maximum, i.e. all sp^2, and minimum, i.e. all sp^3. Blue bisecting lines give the absorbance value when the pH is 7.4. These three values are used to get the ratio of sp^2 and sp^3 at pH 7.4.*

The sp^2:sp^3 ratio was calculated as a percentage of sp^3 character using equation 3.10, where “abs” is the absorption value. The values are tabulated in **Table 3.5**, and show a variation between the esters of 17%, with the highest values of 82% sp^3 and the lowest value of 65% sp^3.

$$\%sp^3 = \frac{\text{Abs } sp^2 - \text{Abs } sp^3}{\text{Abs } sp^2 - \text{Abs pH 7.4}} \times 100 \qquad 3.10$$

Equation 3.10 shows the method in which the fraction of sp^3 boron was calculated. By extrapolating the highest and lowest plateaus of the graph, the absorption of the fully sp^2 and sp^3 species can be found (Abs sp^2 and Abs sp^3 respectively). The absorption at pH 7.4 is found using the previously described method as shown in **Figure 3.6**.

***Table 3.5** – sp²:sp³ ratio and the %sp³ for the series of* para*-nitrophenylboronic esters at pH 7.4.*

Compound	Ratio sp^2:sp^3	% sp^3
60	18:82	82
61a	28:72	72
61b	27:73	73
61c	22:78	78
61d	26:74	74
61e	29:71	71
61f	35:65	65
61g	33:67	67
61h	34:66	66
61i	30:70	70
61j	18:82	82
61k	19:81	81
61l	18:82	82

3.5.2 Measuring rates

The conditions used for measuring the rate of oxidation of the boronic esters were kept the same as the previous experiments to gather data on hydrolysis rate and pK_a. Temperature was kept at 30 °C, and the same buffer and DMSO ratio was used. 96-

well half-area UV-clear plates were used in all experiments and all measurements were carried out in triplicate. To measure the pseudo-first order rate constant with respect to boronic ester, the concentration of boronic ester must be limiting compared with the concentrations of peroxide, which should be in excess. The concentration of boronic ester used in these instances was 0.1 mM, with peroxide concentrations at 1 mM, 2 mM, 4 mM, 6 mM and 8 mM, i.e. in 10 to 80 equivalents.

The boronic ester was dissolved in 5% DMSO 95% aqueous phosphate buffer solution to a concentration of 0.1 mM, henceforth referred to as solution A. Hydrogen peroxide was diluted from 30% w/w stock to the five concentrations described above, henceforth referred to as solutions B. 50 µL of solution A was added to each well and just before the measurements began, an equal volume of each of solution B were added. Every minute for 60 time points, the absorbance at 405 nm (λ_{max} of *para*-nitrophenolate) was recorded.

To measure the pseudo first order rate constant with respect to peroxide, the limiting reagent in the experiment is peroxide at 0.1 mM and the varied reagents are the boronic esters at the same excesses as previously described. All the experiments were carried out in the same way and the data processing was identical.

The raw data from these experiments are first averaged from the triplicate measurements and zeroed using the background absorbance of the solvent. The resulting graphs show a sharp increase at the start of the reaction followed by a plateau. The initial straight line is related to the initial rate of reaction, and this provides the pseudo-first order rate constant. As the concentration of the variable reagent increases, the initial rate of reaction increases. Once the data has been processed

through baseline corrections, a series of five curves are generated, one for each concentration of the variable species. The example given in **Figure 3.7** is for *para*-nitrophenylboronic acid.

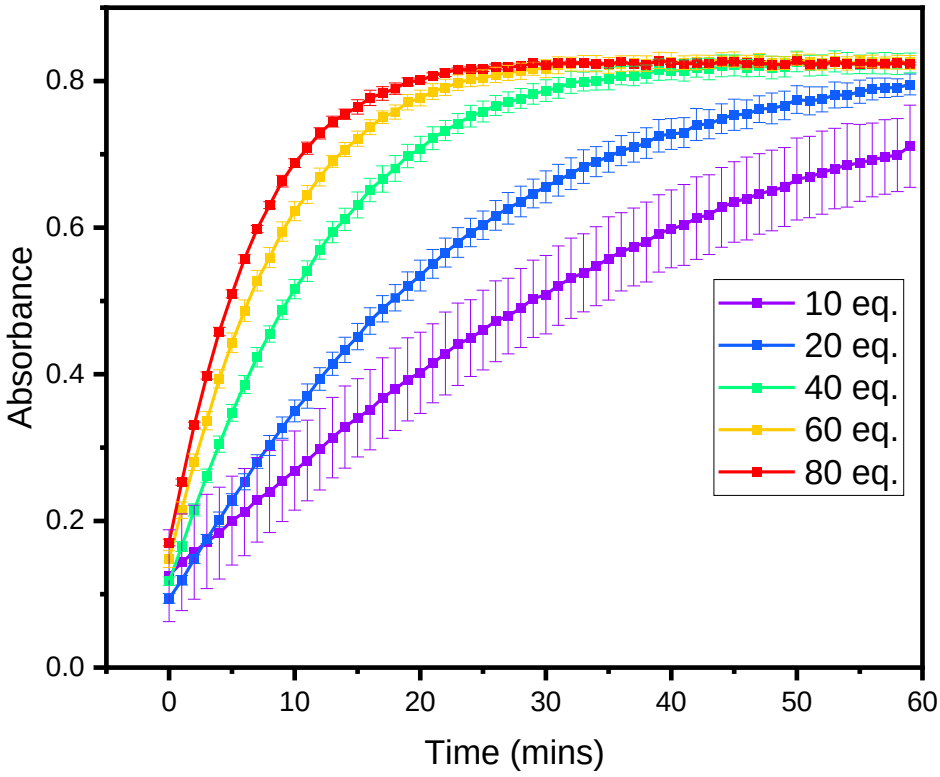

Figure 3.7 *– Graph to show the formation of* para*-nitrophenolate through the oxidation of* para*-nitrophenylboronic acid at five different concentrations of hydrogen peroxide at 10, 20, 40, 60 and 80 equivalents to the boronic acid. X-axis shows time in minutes and the y-axis shows the corrected absorbance at 405 nm.*

The integrated rate law is given by equation 3.11:

$$[\mathrm{A}]_t = [\mathrm{A}]_0 e^{-k_{obs}t} \qquad 3.11$$

The concentration of A can be given by the absorbance, and to calculate the pseudo-first order rate constant, a graph must be drawn of concentration as a function of time.

Taking the natural logarithm of both sides of the integrated rate law (equation 3.11) gives equation 3.12.

$$\ln[\mathrm{A}]_t = \ln[\mathrm{A}]_0 - k_{obs}t \qquad 3.12$$

This equation works when the concentration of the reactant is being measured, however in this case, the concentration of the product, *para*-nitrophenolate is being measured. Therefore, the terms involving the concentration of reactant need to be redefined.

$$[\mathrm{A}]_t = [\mathrm{C}]_f - [\mathrm{C}]_t \qquad 3.13$$

Where $[A]_t$ is the concentration of A at time point t, C is the term for *para*-nitrophenolate, $[C]_f$ is the final concentration of C, and $[C]_t$ is the concentration of C at time point t.

$$[\mathrm{A}]_o = [\mathrm{C}]_f - [\mathrm{C}]_0 \qquad 3.14$$

Where $[A]_0$ is the concentration of A at the start of the reaction, C is the term for *para*-nitrophenolate, $[C]_f$ is the final concentration of C, and $[C]_0$ is the concentration of C at the start of the reaction. A straight line can then be plotted of equation 3.15:

$$\ln[\mathrm{C}]_f - [\mathrm{C}]_t = \ln[\mathrm{C}]_f - [\mathrm{C}]_0 - k_{obs}t \qquad 3.15$$

The graph derived from equation 3.15 should be a straight line with a negative gradient. The absolute value of the gradient gives the observed rate constant k_{obs}. For

the example of *para*-nitrophenylboronic acid, the graph in **Figure 3.8** can be plotted with the five concentrations of hydrogen peroxide in the same five colours as the lines in **Figure 3.7**.

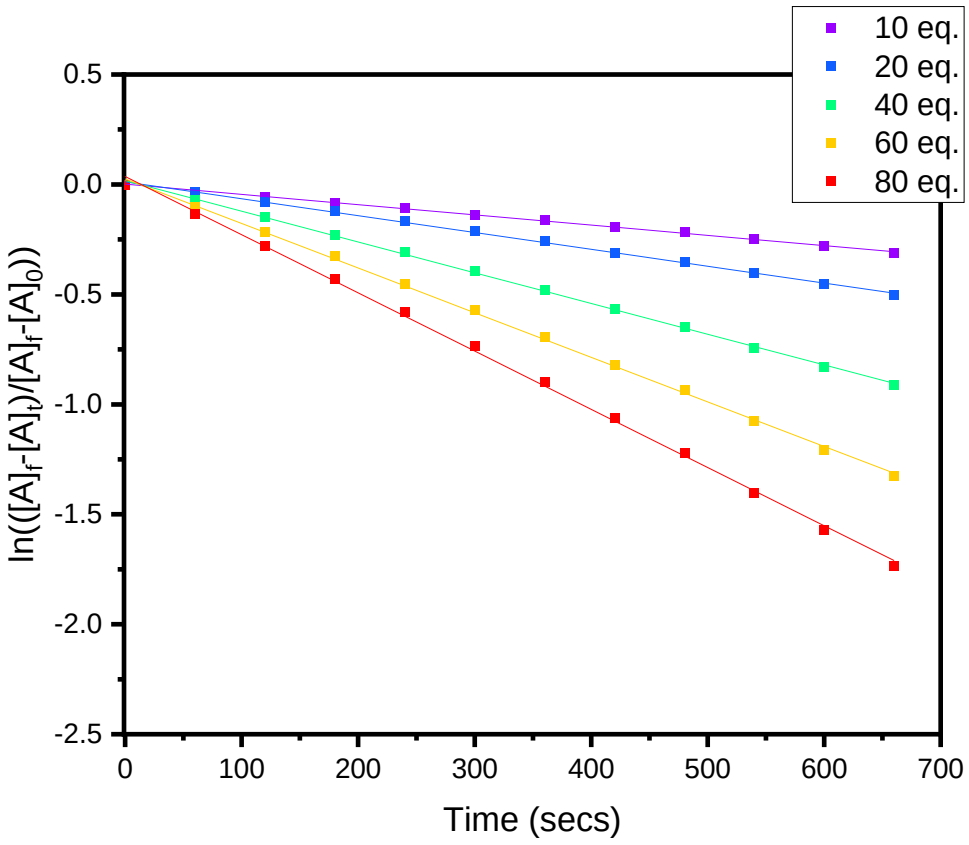

Figure 3.8 *- Graph to show the integrated rate law for the oxidation of* para-*nitrophenylboronic acid. Y-axis is determined by equation 3.15 using the absorbance at 405 nm. X-axis is time in seconds.*

The higher the equivalents of hydrogen peroxide, the steeper the gradient of the line, and therefore the higher the observed rate of reaction, k_{obs}. The final transformation for these data is to combine the five concentrations of hydrogen peroxide in the five experiments to determine the absolute second order rate constant. The gradients of the graph in **Figure 3.8** are first multiplied by -1, then plotted against the concentration of peroxide. This gives a straight line with the gradient equal to the second order rate

constant, k, with units of $M^{-1}s^{-1}$. In the case of the oxidation of *para*-nitrophenylboronic acid, the second order rate constant can be found from the graph in **Figure 3.9**.

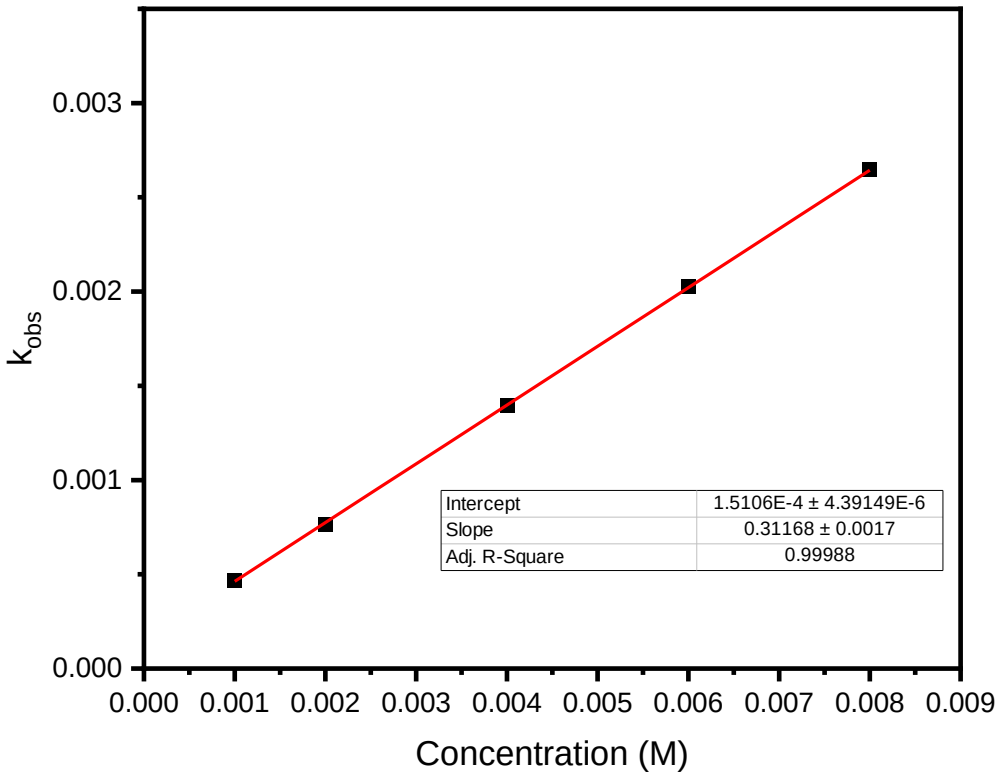

***Figure 3.9** – Graph to show the second order rate constant for the oxidation of* para*-nitrophenylboronic acid. The y-axis is k_{obs} and the x-axis is the concentration of hydrogen peroxide with the slope giving the second order rate constant with units of $M^{-1}s^{-1}$.*

The slope from this graph has a value of 0.311, and so the second order rate constant for the oxidation of *para*-nitrophenylboronic acid at the conditions described above is 0.311 ± 0.002 $M^{-1}s^{-1}$.

3.5.3 Oxidation rates at pH 7.4

The measurements of the second order rate constant for the oxidation of *para*-nitrophenylboronic esters with respect to hydrogen peroxide and with respect to boronic ester at pH 7.4 are outlined in **Table 3.6**, with their averages also calculated,

all with units s^{-1}. The values should be the same if the reaction is first order with respect to both boronic ester and hydrogen peroxide.

Table 3.6 *– Overall results for the second order rate constants of the oxidation of* para*-nitrophenylboronic esters at pH 7.4.*

Compound	k, wrt ester	k, wrt H_2O_2	Average k
60	0.312 ± 0.002	0.384 ± 0.007	0.348 ± 0.036
61a	0.322 ± 0.013	0.192 ± 0.007	0.257 ± 0.065
61b	0.324 ± 0.005	0.381 ± 0.008	0.353 ± 0.029
61c	0.343 ± 0.009	0.398 ± 0.009	0.371 ± 0.028
61d	0.331 ± 0.007	0.364 ± 0.017	0.348 ± 0.0165
61e	0.337 ± 0.006	0.330 ± 0.019	0.334 ± 0.004
61f	0.310 ± 0.004	0.245 ± 0.007	0.278 ± 0.033
61g	0.298 ± 0.005	0.246 ± 0.009	0.272 ± 0.026
61h	0.291 ± 0.003	0.344 ± 0.004	0.318 ± 0.0265
61i	0.333 ± 0.007	0.329 ± 0.010	0.331 ± 0.002
61j	0.284 ± 0.012	0.296 ± 0.004	0.290 ± 0.006
61k	0.286 ± 0.005	0.242 ± 0.010	0.264 ± 0.022
61l	0.277 ± 0.011	0.141 ± 0.010	0.209 ± 0.068

3.5.4 Conclusion

The data in **Table 3.6** show a consistency between values of k when hydrogen peroxide was in excess and when ester was in excess. This indicated that the oxidation of *para*-nitrophenylboronic esters under these conditions process first order with respect to peroxide and first order with respect to the ester, thus indicating that the reaction is second order overall. This is consistent with the mechanism involving both species in the rate-determining step.

3.6 Rates of oxidation measurements at pH 10

3.6.1 Difference to pH 7.4

The rate of many reactions is dependent on the pH.[223] From the pK_a graphs in section **3.3**, all the boronic esters are majority anionic boronate form at pH 10.This is contrary to pH 7.4 where the position of the equilibrium between boronate and neutral gave a mix of the two species. Therefore, when the boronic esters are oxidised at pH 10, they are almost entirely the negatively charged boronate species meaning a difference in the rate of reaction. This reduces the number of variables when probing the reaction as the boronic ester was a single species rather than a dynamic equilibrium between the charged species and neutral species. The experimental set-up for this set of results was carried out in the same way as the methods for pH 7.4, aside from using a N-cyclohexyl-3-aminopropanesulfonic acid (CAPS) buffer at pH 10.

3.6.2 Oxidation rates at pH 10

The overall results for the second order rate constants at pH 10 are outlined in **Table 3.7**

Table 3.7 *- Overall results for the second order rate constants of the oxidation of* para*-nitrophenylboronic esters at pH 10.*

Compound	k, wrt ester	k, wrt H_2O_2	Average k
60	0.578 ± 0.006	0.594 ± 0.041	0.568 ± 0.008
61a	0.583 ± 0.005	0.586 ± 0.005	0.585 ± 0.002
61b	0.625 ± 0.006	0.535 ± 0.038	0.580 ± 0.045
61c	0.619 ± 0.013	0.577 ± 0.023	0.598 ± 0.021
61d	0.582 ± 0.028	0.575 ± 0.013	0.579 ± 0.004
61e	0.605 ± 0.007	0.660 ± 0.026	0.633 ± 0.028
61f	0.572 ± 0.023	0.692 ± 0.024	0.632 ± 0.060
61g	0.598 ± 0.008	0.602 ± 0.034	0.600 ± 0.002
61h	0.567 ± 0.031	0.506 ± 0.013	0.537 ± 0.031

61i	0.617 ± 0.014	0.640 ± 0.023	0.629 ± 0.012
61j	0.661 ± 0.018	0.599 ± 0.023	0.630 ± 0.031
61k	0.635 ± 0.012	0.538 ± 0.027	0.587 ± 0.049
61l	0.532 ± 0.010	0.129 ± 0.004	0.331 ± 0.2015

3.6.3 Conclusion

Similar to the results at pH 7.4, there is little variation in the rate data when changing esters, however the rates with respect to peroxide and with respect to ester are consistent, indicating an overall second order rate constant for this reaction under these conditions. The rates are all higher than the rates at pH 7.4, indicating a pH dependency on the reaction.

Both sets of data for each pH have a different measurement for the final diol, compound **61l**. In both cases, the second order rate constant with respect to the boronic ester is not significantly different to the other diols. However, the rate constant with respect to peroxide is significantly lower than that of the other diols, and the rate constant for the same diol with respect to the ester. This unusual result could indicate that another mechanism is occurring where the rate is not the same order with respect to both peroxide and ester. However, the graph giving the second order rate constant with respect to both constituents gives a straight line, indicating first order. One possible reason for the change in rate could be down to an equilibrium taking place when compound **61l** is in aqueous solution. Tetrahydrofuran can be made through the dehydration of 1,4-butanediol.[224] It is therefore plausible that the equilibrium shown in **Scheme 3.8** is occurring in the oxidation experiments, followed by the condensation reaction with hydrolysed boronic acid. If there is a mixture of these species (compounds **61l**, **64** and **65**) when the oxidation measurements are taking place, then

the value for the second order rate constant is not reliable as any of the species (compounds **61l**, **64** and **65**) could be oxidising.

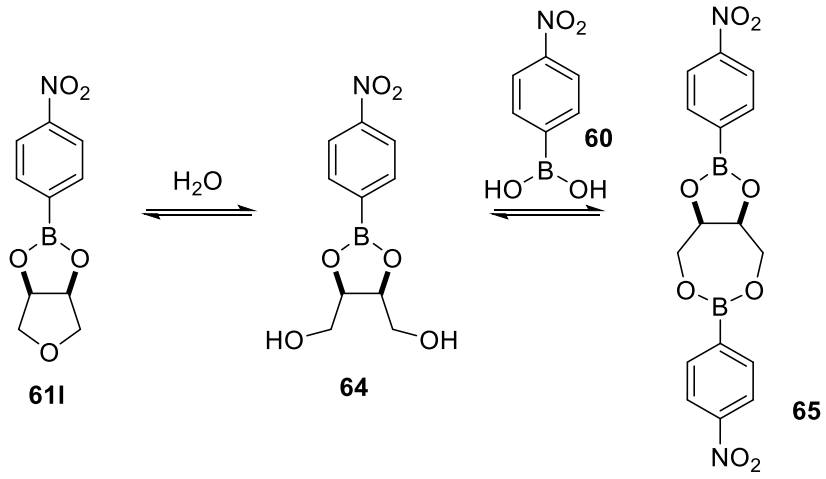

Scheme 3.8 *– Potential equilibrium of compound* ***61l*** *in aqueous conditions to form compound* ***64*** *and subsequent condensation with* para*-nitrophenylboronic acid* ***60*** *to compound* ***65****.*

3.7 Extending the scope in future work

Whilst the study into the oxidation of the twelve *para*-nitrophenylboronic esters gives a preliminary overview of results, the research output is limited to the specific set of conditions. Ideally, the study would be extended to measure a range of pHs, temperatures, substituents on the ring and a wider range of esters, however this was impossible with the current set up due to time constraints. In the future, to increase output, an automated system to set-up experiments, collect and analyse data to increase our understanding of the chemistry is required. However, given the cost implications and complexity, all the experiments were set-up manually. Efforts were made to extend the scope of the research, however certain issues were raised that were unable to be solved in the timeframe, although were paramount in informing

decisions to gather the previously reported data. An overview of the issues found are outlined in this section and how they can be overcome in future work.

3.7.1 Issues with oxidation studies at pH 4

Oxidation rate measurements were carried out for pH 10, where over 95% of the boron species present was sp^3 hybridised, and at pH 7.4, where there was a mix of sp^2 and sp^3. At pH 4, the equilibrium of sp^2 to sp^3 lies almost entirely at sp^2. However, there were a number of issues encountered with the measurements at this pH.

The pH range where sodium phosphate buffer is within buffer range is 5.8 – 8. As with the pH 10 measurements that were carried out in CAPS buffer, a new buffer was required for pH 4. Sigma-Aldrich's list of biological buffers does not feature a buffer with a pH range lower than pH 5.5.[225] Citrate buffer has been used previously to achieve pHs in the range of 4 to 7.[226] However, the chemistry of citric acid with three carboxylic acid groups and an alcohol make it an excellent binder to boron, as exemplified in its use in the formulation of the anti-cancer drug ixazomib.[227] A buffer that binds to boronic acids is not suitable for precise rate measurements as additional binding events would skew the results. There were limited buffer systems to achieve low pH where the buffer would not interfere with boron and the results of the experiment, with an acetate buffer being used for some preliminary experiments.

All the oxidation measurements discussed in this thesis were possible due to the absorption characteristics of *para*-nitrophenol. The pK_a of *para*-nitrophenol is 7.15 at 25 °C.[228] This means that at pHs above 7.15, *para*-nitrophenol is deprotonated and in its *para*-nitrophenolate form, which is yellow in colour and an absorption maximum at

405 nm. At pHs below 7.15, it is in its neutral form and is colourless, meaning its chromophore changed, and it has a λ_{max} of 318 nm. For the phenolate, its λ_{max} is at 405 nm, which is in the visible range and is not near the absorptions of the other components of the reaction such as buffer or peroxide. The absorption measurements taken at this wavelength are therefore not necessarily all due to an increase in the concentration of phenol, and therefore the oxidation data could be skewed.

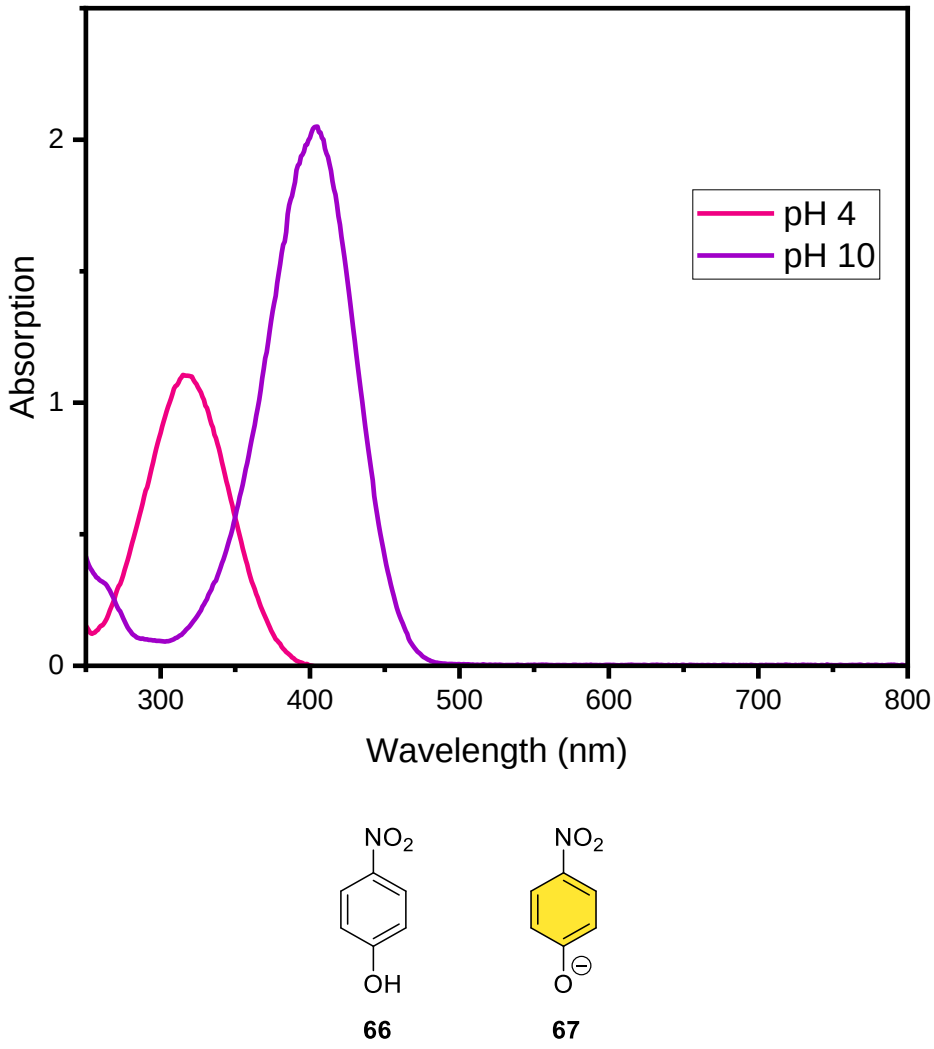

Figure 3.10 *– UV-Vis spectra of* para*-nitrophenol (at pH 4, red line, compound* ***66****) and* para*-nitrophenolate (at pH 10, purple line, compound* ***67****), with both compounds in a 0.1 mM concentration in PBS.*

3.7.2 Catechol as a diol

2-Hydroxyphenol (**Figure 3.11**, compound **68**), commonly known as catechol, was a diol of interest for this study as only alkyl diols had been studied to date. The aromaticity provided a point of difference that could have allowed the reaction to act differently under the experimental conditions of this study.

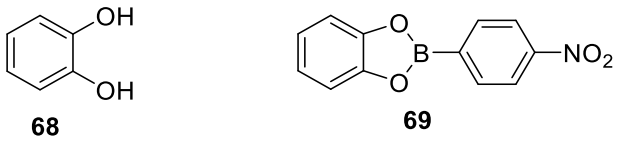

68 **69**

Figure 3.11 *– Structures of catechol (left, compound **68**) and* para-*nitrophenylboronic acid catechol ester (right, compound **69**).*

The first challenge with using catechol was the synthesis of *para*-nitrophenylboronic acid catechol ester (**Figure 3.11**, compound **69**), as the reaction failed when using the condensation conditions used for the rest of the boronic ester syntheses. Increasing the equivalence of magnesium sulfate in the reaction to remove water and drive the equilibrium towards the ester did not give any better results.

The presence of catechol disrupts the UV-Vis absorption measurements as it has a strong UV absorption itself. Therefore, if the compounds were to be synthesised, an alternative method of measuring the oxidation rate would be required. This is a major limitation of this method, given any diol with a chromophore that overlaps the wavelengths of interest would interrupt the results.

3.7.3 Substituent change

Changing the substituent on the aromatic ring changes the electronics of the ring, and therefore changes the electronics of the boron centre. The electron withdrawing nature of the *para*-nitro group draws electron density away from the boron centre into the ring, increasing its Lewis acidity and propensity to accept a Lewis base. Altering the electronics of the ring by changing the substituent and subsequently changing the electron density about the boron centre could alter its propensity for oxidation, change the rate of oxidation, or change the mechanism. Therefore, gathering oxidation rate data for a range of substituents about the ring could help to better understand the global mechanism.

3.7.4 Future work

The work outlined in chapter 3 only scratches the surface of the data that could be gathered on the kinetics of the oxidation of boronic acids and esters. As evidenced, boron species adopt different configurations and reactivities depending on the pH of the solution. Expanding the scope of the experiments to include a wider pH range would give insight into how reactive each configuration of boron is, and whether the reaction mechanism changes depending on pH. Initial work would have to be carried out to find a suitable buffer system for low pH experiments, and a method for tracking the progression of the reaction.

A wider range of diols would hopefully give a larger change in the oxidation rates, as the rates obtained in these experiments are very close together. It can be seen that by using the tetrahydrofuran derived diol that changing the nature of the diol can change the chemistry drastically. Increasing the number of diols to include not only

alkyl, but also aromatic and heteroatoms could give a broader use for this study with more real-world applications.

4 Alizarin Red S

Alizarin Red S was used in the oxidation studies to produce a ranking order of binding strengths of the diols to the boronic acid. This was a method where comparisons could be made between the diols, but no definitive binding constants could be calculated. Chapter 4 outlines the preliminary experiments undertaken to develop a method for calculating absolute binding constants between boronic acids and diols.

4.1 Background

4.1.1 Structure

Alizarin Red S (ARS) is an anthraquinone derivative featuring a catechol on one of the aromatic rings with an adjacent sulfonic acid sodium salt (**Figure 4.1**, compound **62**). The sodium sulfonate salt increases its solubility in water and the 1,2-diol facilitates binding to boronic acids and to calcium, leading to its incorporation in imaging and sensing applications.

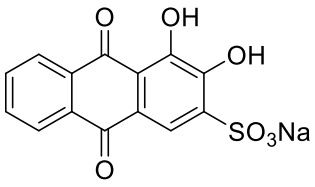

62

***Figure 4.1** – Chemical structure of Alizarin Red S (ARS, **62**).*

Dependent on the pH of the solution, ARS exists as several deprotonated forms. At pHs below 2.7, ARS in its quadruple protonated form can be detected. At pH 12 and above, ARS is fully deprotonated.

4.1.2 Sensing

4.1.2.1 Calcium sensing

Previously, ARS has been used as a sensor for calcium ions in histopathology and to measure bone density. Calcium ions can bind or chelate to ARS molecules and alter the colour, allowing quantitative analysis of calcium ions in tissues.[229, 230] This is useful for tracking changes caused by diseases such as calcium pyrophosphate dihydrate crystal deposition disease, a form of arthritis, and for quantifying calcium deposits in zebrafish skeletons.[231] Upon binding of calcium, ARS visually changes colour from pink to orange-red.[232-234]

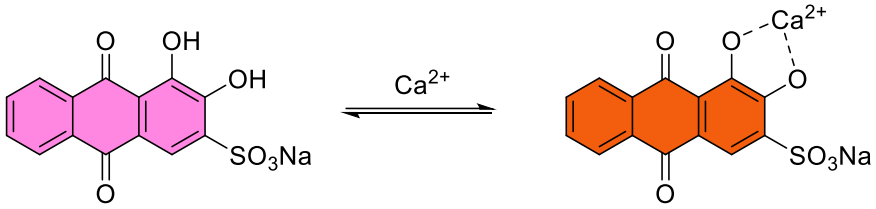

62 **70**

***Figure 4.2** – Complexation of ARS with a calcium ion causes a colour change from pink to orange-red and is used as a stain.*

4.1.2.2 Copper sensing

ARS can be used to detect other species by utilising a competitive binding assay. For example, it has been used to measure the amount of Cu^{2+} ions by measuring the reduction of binding between ARS and boric acid.[235] Copper forms a fluorescent complex with ARS (**Figure 4.3**, compound **71**). Copper ions also form a complex with boric acid. By increasing the copper-boric acid complex concentration, the copper-ARS complex concentration decreases, reducing fluorescence.

A copper-ARS complex has a higher fluorescence intensity than non-complexed ARS (**Figure 4.3**). This has been used as an indicator to detect the amino acid cysteine which undergoes a redox reaction with copper, where copper ions are reduced and thiol on the cysteine is oxidised.[236] As a competitive binding assay, the introduction of cysteine causes the copper to unbind from ARS, reducing the fluorescence. This reduction of fluorescence can be measured to quantify the amount of cysteine present in the sample.[237]

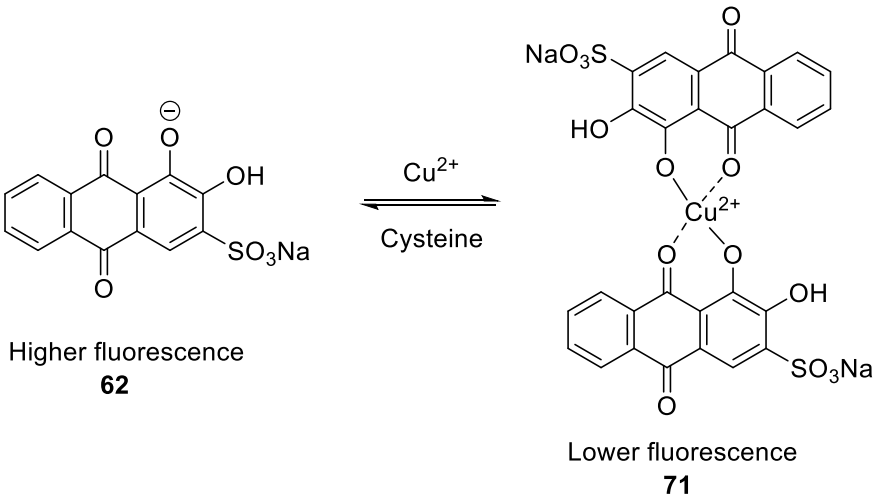

Higher fluorescence
62

Lower fluorescence
71

Figure 4.3 *– Reversible complexation of ARS with a copper ion, reversed by cysteine. Introduction of copper ion decreases the fluorescence of ARS, and cysteine reverses this to increase the fluorescence.*

4.1.2.3 Dopamine sensing

Dopamine is a catecholamine that acts as a neurotransmitter. Detection of dopamine can be performed using the same method outlined for the sensing of copper ions. Through knowing the association constant between boronic acid and ARS, the change in fluorescence intensity can be used to measure the amount of dopamine through a competitive binding assay.[238, 239]

4.2 pH dependency

4.2.1 Setting up samples

The resonance forms of ARS depend upon the pH of the solution. The first pK_a of ARS is between 4 and 6 and the second is between 10 and 12. There is a significant colour difference when ARS is dissolved in different pH buffers as seen in **Figure 4.4**. Three sodium phosphate buffer solutions were made using hydrochloric acid or sodium hydroxide to alter the pH to 4 or pH 12, which are outside of the buffer range of sodium phosphate buffer (pH 5.8 to 8.0). A 0.25 mM solution of ARS was then made using these solutions.

***Figure 4.4** – Alizarin Red S (2.5 x 10^{-4} mol dm^{-3}) in sodium phosphate buffer at pH 4.0, 7.4 and 12.0 (left to right).*

The solution is yellow at pH 4, red at pH 7.4 and purple at pH 12, following the different protonation states of the compound. At pH 4, ARS is likely to be in its fully protonated form, with a single deprotonation at pH 7.4 and double deprotonation at pH 12. The UV-Vis spectra for these in PBS are shown in **Figure 4.5**.

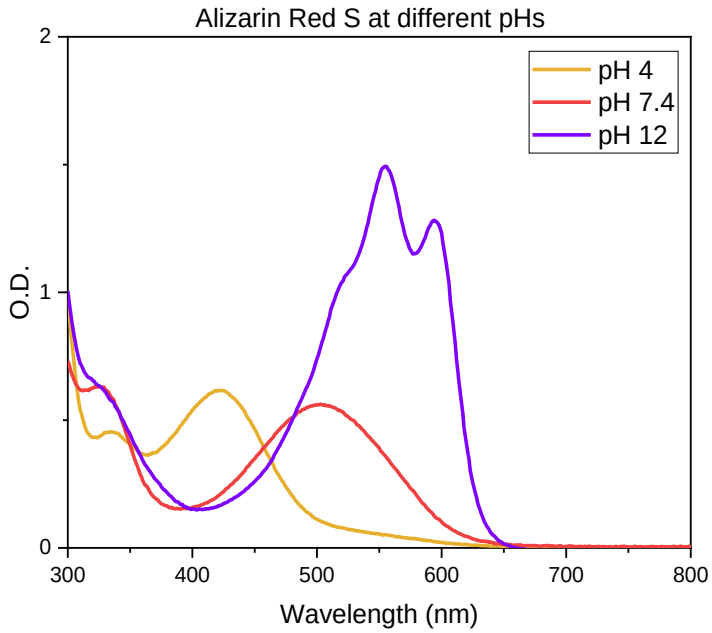

Figure 4.5 *– UV-Vis spectra of Alizarin Red S (0.1 mM) at 3 different pHs in 97.5% PBS and 2.5% DMSO at 30 °C.*

4.2.2 pH 12 change

Once the ARS solution had been transferred to a microplate for analysis, it was left for 24 hours to observe any changes that may occur. The solutions at pH 4 and pH 7.4 did not change (measured by UV-Vis and fluorescence), however there was a large change in the solution at pH 12. To see how long was needed for this change to take place, a UV-Vis spectrum of the solution was taken every 20 minutes over a 12-hour period.

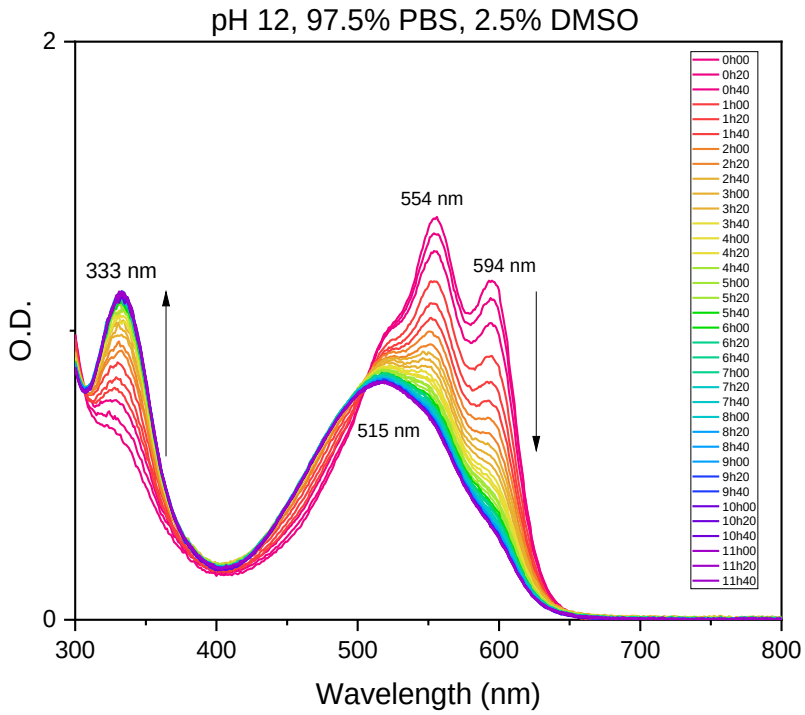

Figure 4.6 *– UV-Vis spectra of ARS (0.1 mM, pH 12) in PBS and DMSO (2.5%) taken every 20 minutes for a 12 hour period.*

When the solution is first pipetted into the plate there are two maxima, one at 554 nm and another at 594 nm. Over time, these decrease in intensity and a new maximum at 333 nm increases in intensity. The spectrum at the end of the 12 hours resembles the spectrum taken at pH 7.4, indicating that the double deprotonated ARS is singly protonating over time. This was unexpected, as the stock solution was stored in a glass volumetric flask, not under inert atmosphere and the only manipulation this solution has had is being transferred to a microplate and diluted with 2.5% DMSO and PBS. To investigate the phenomenon, the same experiment was carried out but without diluting with DMSO and PBS as shown in **Figure 4.7**.

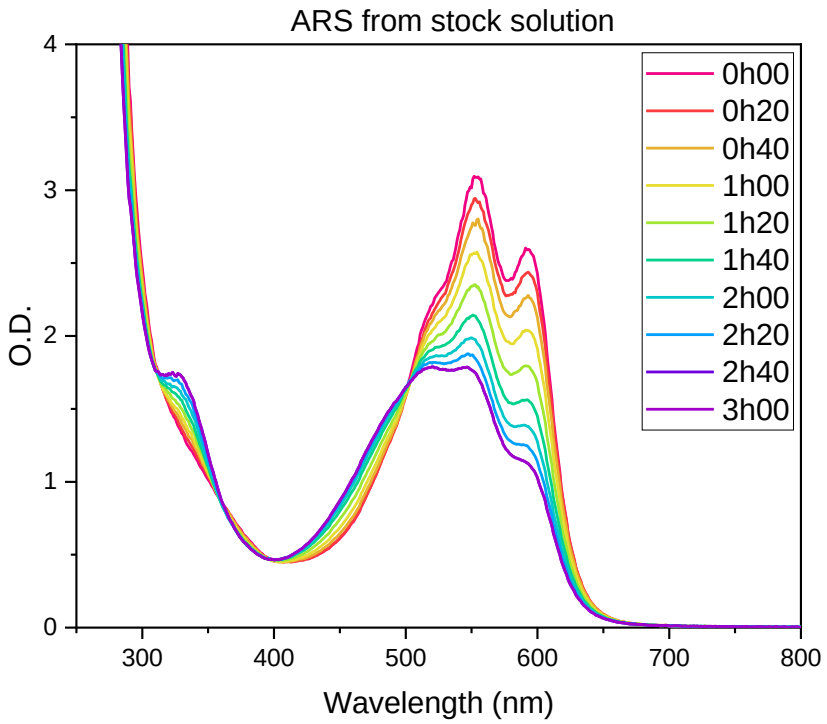

Figure 4.7 *– UV-Vis spectra of ARS (0.25 mM, pH 12) in PBS (100%) taken every 20 minutes for a 3 hour period.*

ARS stock solution was transferred to the microplate by pipette and a UV-Vis spectrum was taken every 20 minutes. The same change whereby the absorption at 554 nm and 592 nm is reducing occurs even when not diluted with additional PBS and DMSO (**Figure 4.7**).

UV-Vis spectroscopy measures the transition of electrons to the excited state from the ground state through the absorption of light radiation. It was theorised that the act of irradiating the sample every time a spectrum was recorded could be having an effect on the ARS molecules, causing a potential change in species. To test this hypothesis, a parallel set of experiments was carried out with a spectrum taken every five minutes on one sample and every 30 minutes on another for a total of one hour (**Figure 4.8**).

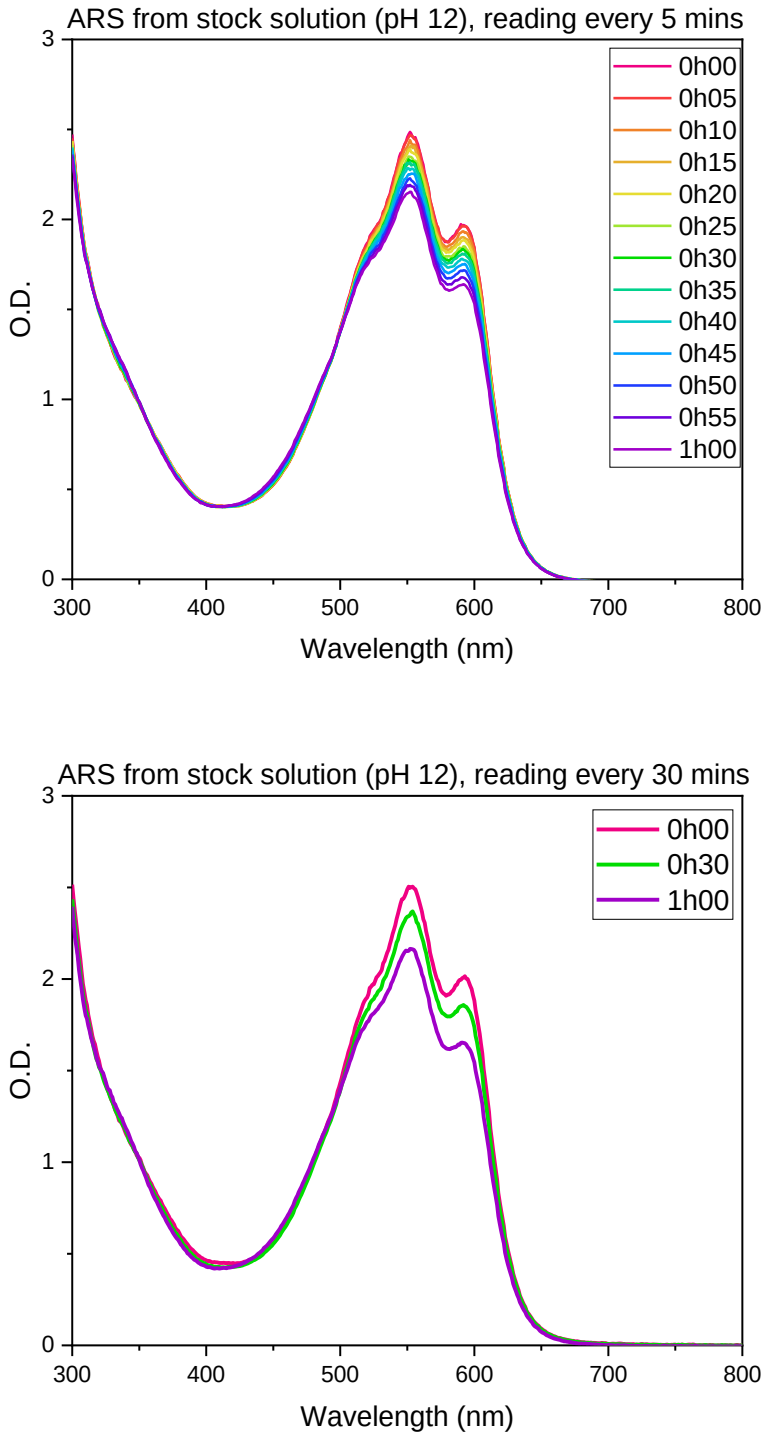

Figure 4.8 *– UV-Vis spectra between 300 and 800 nm of ARS solution at pH 12 with measurements taken every 5 minutes (above) and every 30 minutes (below).*

Optical density at λ_{max} changes at the same rate regardless of how many times a spectrum is recorded, indicating that the act of irradiating the sample with light does not cause the change in species.

4.2.2.1 Plastic vs. quartz

The microplates used are plastic and the volumetric flask that the stock solution was stored in is glass. To see if this has any effect on the change of species, a UV-Vis spectrum was taken of the stock solution in a quartz cuvette with a PTFE cap.

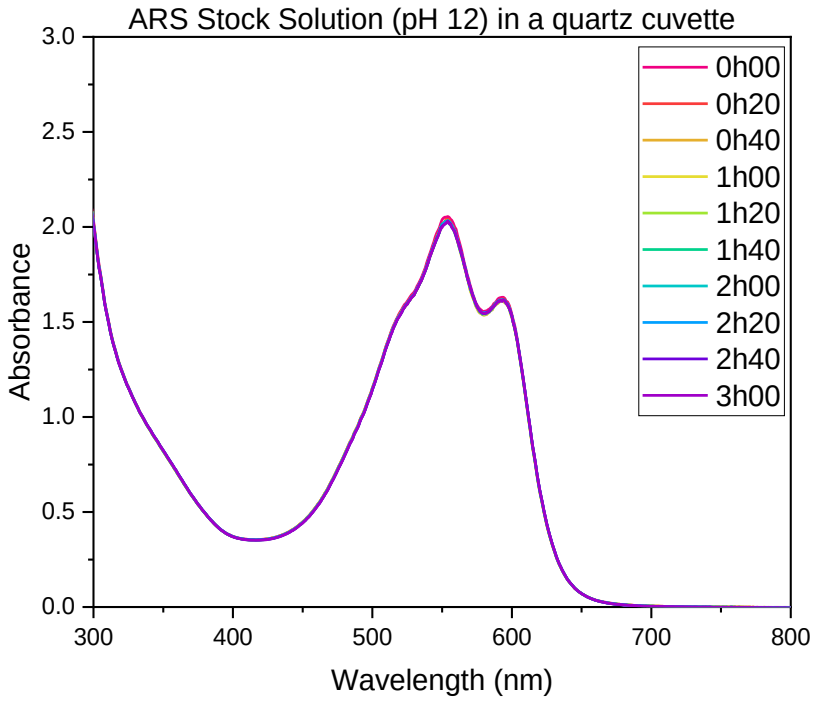

***Figure 4.9** – UV-Vis spectra between 300 and 800 nm of ARS solution at pH 12 with measurements taken every 20 minutes recorded in a quartz cuvette.*

There was no change in the spectra over time as seen when recorded on the microplate reader. This is either due to the quartz cuvette or because the cuvette was sealed from the air. The cuvette was left with the cap off overnight and there was a significant colour change from purple to red, as evidence by the UV-Vis spectrum recorded in the morning (**Figure 4.10**). The pH of the solution was measured when red to be 9.62, a significant decrease from the original stock solution of 12, supporting the hypothesis that the double deprotonated ARS becomes singly protonated. This follows allowing air to change the system. We theorise that carbon dioxide from the

atmosphere dissolves in the solution forming carbonic acid, reducing the pH in the well that is outside of buffer range.[240]

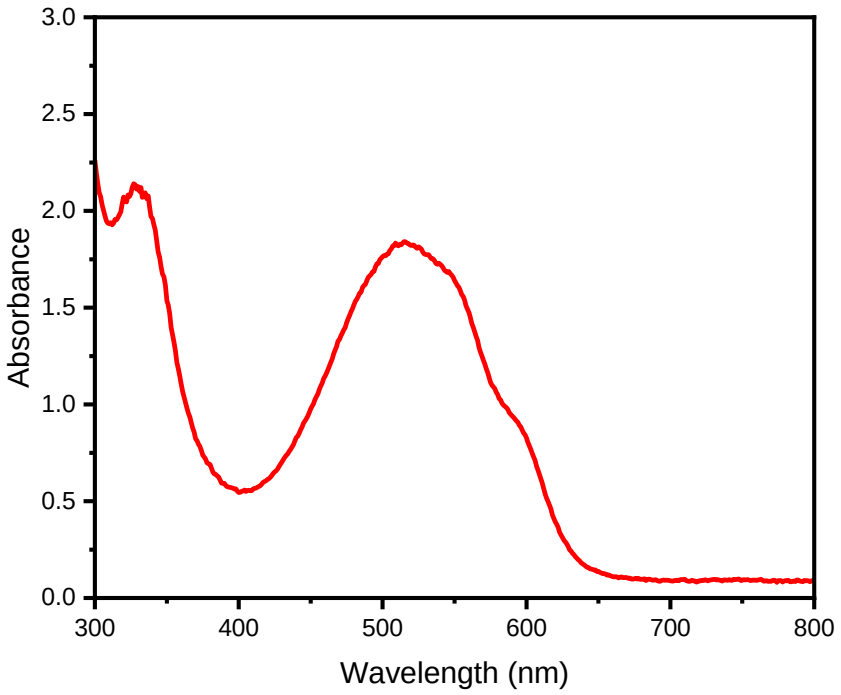

Figure 4.10 *– UV-Vis spectrum between 300 and 800 nm of ARS solution at pH 12 recorded in the quartz cuvette after being exposed to air overnight.*

4.2.2.2 Alternative buffers

To overcome the issue with the changing pH when PBS was outside the buffer range, a series of solutions of ARS were made with different buffers. Three buffers at pH 10 were selected to be investigated: carbonate buffer, glycine buffer and CAPS buffer. For reference, PBS adjusted to pH 10 and an aqueous sodium hydroxide solution were also prepared. ARS solutions of 2.5 x 10^{-4} M were made up in the different buffers and non-buffers and their pHs were retested following dissolution of ARS. The pH was rechecked 24 hours later to confirm whether it had changed over time after being stored in polypropylene centrifuge tubes without the caps.

***Table 4.1** – ARS dissolved in five buffer solutions to a concentration of 2.5 x 10^{-4} M and the pH measured immediately after making the solution and after 24 hours.*

Buffer	*pH straight after dissolution of ARS*	*pH after 24 hours*
NaOH (aq)	9.99	9.63
PBS	9.90	8.58
Carbonate	10.07	10.04
Glycine	10.02	10.00
CAPS	10.02	10.01

A UV-Vis spectrum for each buffer was recorded immediately after making the solutions between 250 and 800 nm (**Figure 4.11**). The results showed very similar spectra for CAPS and carbonate buffer, and similar spectra for PBS and glycine. The unbuffered showed a very different spectrum and was therefore disregarded as a potential system. PBS was also removed as a potential based on the change in pH it experiences over time.

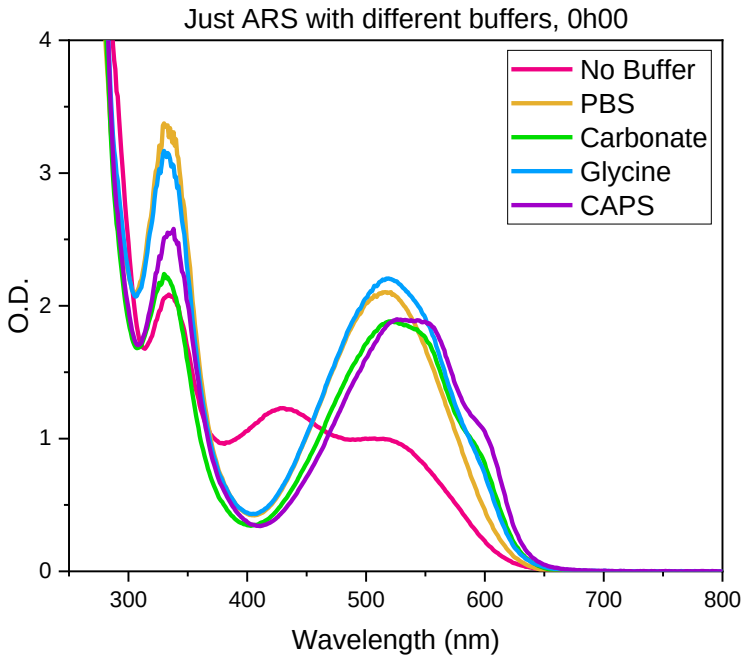

***Figure 4.11** – UV-Vis spectra between 250 nm and 800 nm of ARS (2.5 x 10^{-4} M) in five different solvent systems.*

Fluorescence emission spectra were also recorded immediately after making the solutions along with 10 equivalents of phenylboronic acid (**Figure 4.12**). The excitation wavelength was 468 nm and the emission spectra were recorded between 500 nm and 740 nm. Unbuffered aqueous sodium hydroxide and PBS showed the highest fluorescence intensity at the λ_{max} of 592 nm, however these two buffer systems had been disregarded from previous experiments. Among the other three buffers, CAPS showed the highest fluorescence intensity. This was considered optimal, as the maximum change of fluorescence intensity between bound and unbound ARS would allow for more reliable measurements to be taken with respect to measuring binding constants.

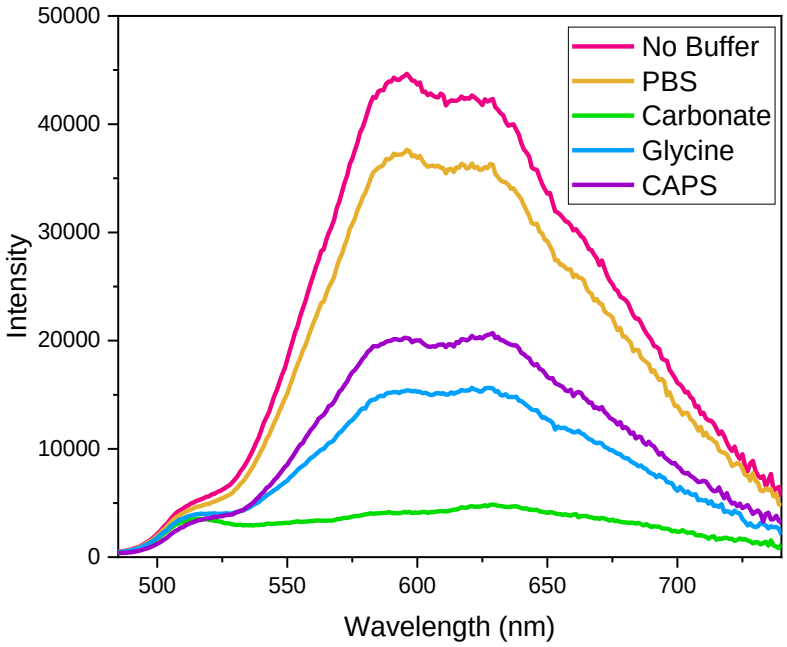

***Figure 4.12** – Fluorescence emission spectra between 500 nm and 740 nm with an excitation wavelength of 468 nm of ARS (2.5 x 10^{-4} M) and phenylboronic acid (2.5 x 10^{-3} M) in five different solvent systems.*

ARS stock solution in PBS at pH 12 was kept in a glass volumetric flask with the lid on and therefore no circulating air. When needed, the flask was unstoppered briefly, and

the necessary quantity was taken. PBS at pH 12 is no longer within the buffer range and so any small change in acidity can affect the pH greatly. Therefore, if experiments require ARS solution at high pH, and PBS is being used as the solvent, then the reading needs to be taken immediately or under an inert atmosphere. This is difficult to achieve using a microplate reader, and so an alternative method for measuring high pH ARS is to use CAPS buffer. Given the different fluorescence and UV-Vis spectra obtained using different buffers, it is clear that readings between different buffers cannot be compared.

4.3 Binding constant determination using ARS

4.3.1 Boronic acid binding to alizarin

Arylboronic acids bind to ARS reversibly. The extent to which they bind can be measured as unbound ARS is non-fluorescent and bound is fluorescent. The change in fluorescence can be measured as a function of concentration of boronic acid and the association constant can then be found.

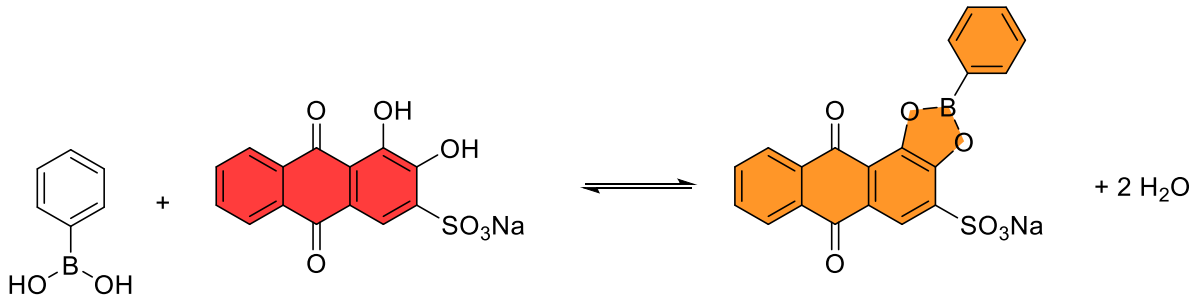

Scheme 4.1 *– General equilibrium between ARS and phenylboronic acid, and the bound form.*

4.3.1.1 Benesi-Hildebrand equation

The Benesi-Hildebrand method can be used to find the association constant between two species in a 1:1 complex.[241] The complexation between boronic acids and ARS is a 1:1 complex and so, using the Benesi-Hildebrand equation (4.1), a graph of $1/[BA]$ (x-axis) *versus* $1[\Delta I]$ (y-axis) can be plotted.

$$\frac{1}{(\mathrm{I}-\mathrm{I}_0)} = \frac{1}{\mathrm{k_{a1}}(\mathrm{I_{max}}-\mathrm{I}_0)}\frac{1}{[\mathrm{BA}]} + \frac{1}{(\mathrm{I_{max}}-\mathrm{I}_0)} \qquad 4.1$$

Where I is the fluorescence intensity of the bound ARS mixture, I_0 is the fluorescence intensity of unbound ARS, I_{max} is the maximum fluorescence intensity, BA is boronic acid and k_{a1} is the association constant. The plot gives a linear fit and the gradient and intercept can be used to find the association constant, k_{a1}. The gradient is given by equation 4.2.

$$\mathrm{gradient} = \frac{1}{\mathrm{k_{a1}}(\mathrm{I_{max}}-\mathrm{I}_0)} \qquad 4.2$$

The intercept is given by equation 4.3.

$$\mathrm{y-intercept} = \frac{1}{(\mathrm{I_{max}}-\mathrm{I}_0)} \qquad 4.3$$

Rearrangement of these equations gives equation 4.4.

$$\mathrm{k_{a1}} = \frac{\mathrm{gradient}}{\mathrm{y-intercept}} \qquad 4.4$$

4.3.1.2 K_a between ARS and phenylboronic acid at pH 7.4

The binding constant of phenylboronic acid to ARS has been previously calculated by Spingsteen and Wang in PBS, without DMSO. They calculated the value to be 1300 M^{-1} under these conditions.[222] Fluorescence emission spectra were recorded (excitation 468 nm) between 500 nm and 740 nm (**Figure 4.13**). The difference in fluorescence between unbound ARS (absence of boronic acid) and bound ARS (presence of boronic acid) was used to obtain the absolute binding constants.

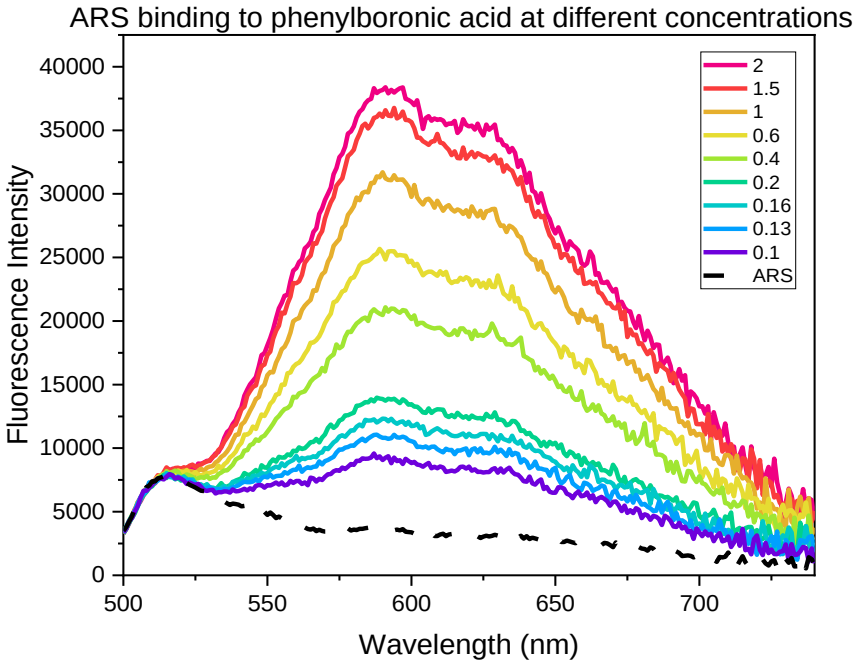

***Figure 4.13** – Fluorescence emission spectrum of phenyboronic acid at different concentrations (0.1 to 2 mM) and ARS (1 x 10^{-2} mM). Spectra were taken between 500 nm and 740 nm with an excitation wavelength of 468 nm. All solutions were made using 5% DMSO in PBS.*

The area under each curve was calculated and $I - I_0$ was determined, with I being the area under the curve of each concentration of boronic acid and I_0 being the area under the curve for just ARS. The reciprocal of $I - I_0$ was plotted against the reciprocal of the concentration of phenylboronic acid and k_{a1} was calculated using equation 4.4

to be 1170 M^{-1} ± 146. This is in line with the literature value obtained by Springsteen and Wang for a similar system.

4.3.1.3 Ka between ARS and further boronic acids

The substituents of an aromatic ring change its electron density. In turn, this alters the reactivity of other groups around the aromatic ring, i.e., the lower the electron density of an aromatic ring, the faster the rate of nucleophilic aromatic substitution. For example, the presence of an *ortho*- or *para*-nitro group drastically increases the rate of the reaction.[242, 243] Following the protocol outlined in 4.3.1.1 and 4.3.1.2, the association constants between ARS and a series of boronic acids were determined and tabulated compared to their Hammett parameter in **Table 4.2**. The conditions used were the same used for phenylboronic acid, at pH 7.4, in PBS (95%) and DMSO (5%).

***Table 4.2** – Different substituent phenylboronic acids and their association constants given to three significant figures with errors.*

Boronic acid 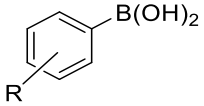	*Association constant k_a, M^{-1}*	*Hammett parameter, σ*
4-OH	131 ± 83	-0.37
4-OMe	341 ± 144	-0.27
4-^{t}Bu	883 ± 57	-0.20
3-NMe_2	1340 ± 89	-0.15
H	1170 ± 146	0.00
4-F	1260 ± 155	0.06
3-OMe	1960 ± 24	0.12
3-OH	1650 ± 80	0.12
4-Br	3123 ± 35	0.23
3-Br	4640 ± 135	0.39
4-CO_2H	1920 ± 74	0.45
4-NO_2	7490 ± 189	0.78

Boronic acids in **Table 4.2** are in order according to their Hammett parameter, σ, with the most electron donating at the top (4-OH) and most electron-withdrawing at the bottom (4-NO_2).[244] When Hammett parameter is plotted against the association constant, they form a general trend, with the carboxylic acid as an outlier. This is likely due to the carboxylic acid being anionic at pH 7.4, and therefore having a more electron donating nature than in its neutral form. The σ value for the carboxylate anion at the *para*- position is 0.00, the same as no substituent. The σ value for *para*-carboxylic acid is 0.45, and both are shown in the graph in **Figure 4.14**.[244]

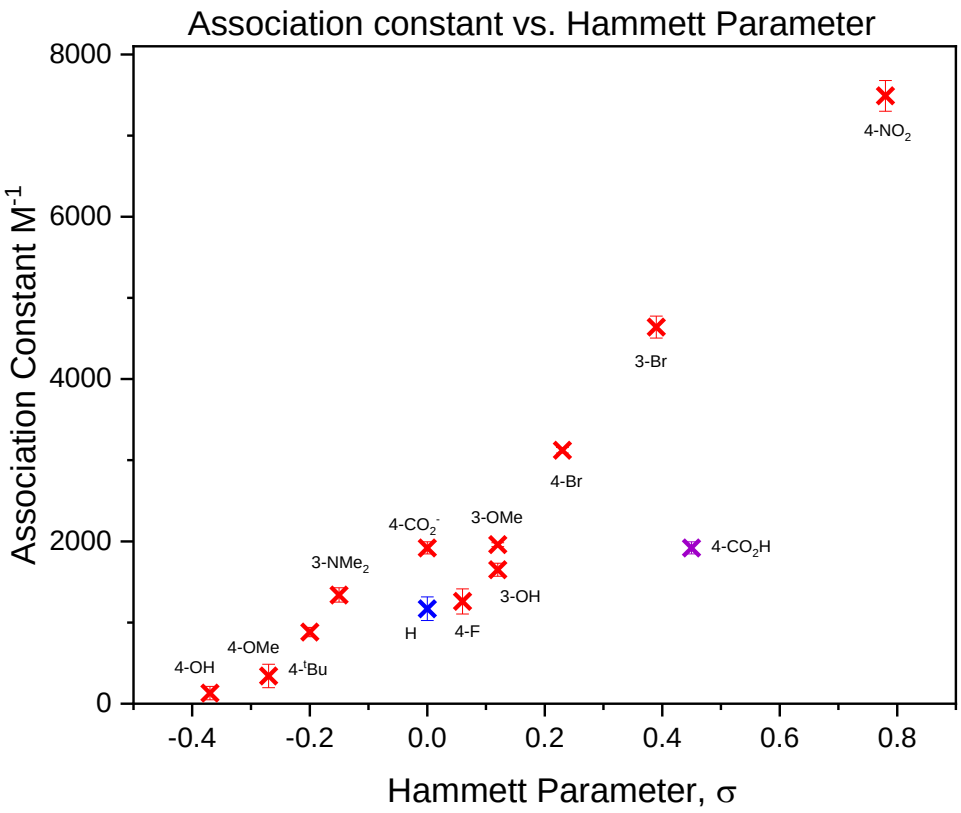

Figure 4.14 *– Graph showing the association constant in M^{-1} of different phenyl boronic acids as a function of their Hammett parameter at pH 7.4, calculated from an ARS binding study. Shown in purple is the* para*-carboxylic acid boronic acid that will likely be the anion at pH 7.4. Shown in blue is a proton, set as the '0' reference value.*

4.3.2 Binding constant of boronic acids to diols

It is possible to use the relative binding affinity of boronic acids to ARS to measure the association constant between boronic acids and other diols. As ARS-boronic acid complex is fluorescent, it can be used as a marker to measure the binding of the boronic acids to other diols in a three-component system (**Scheme 4.2**).

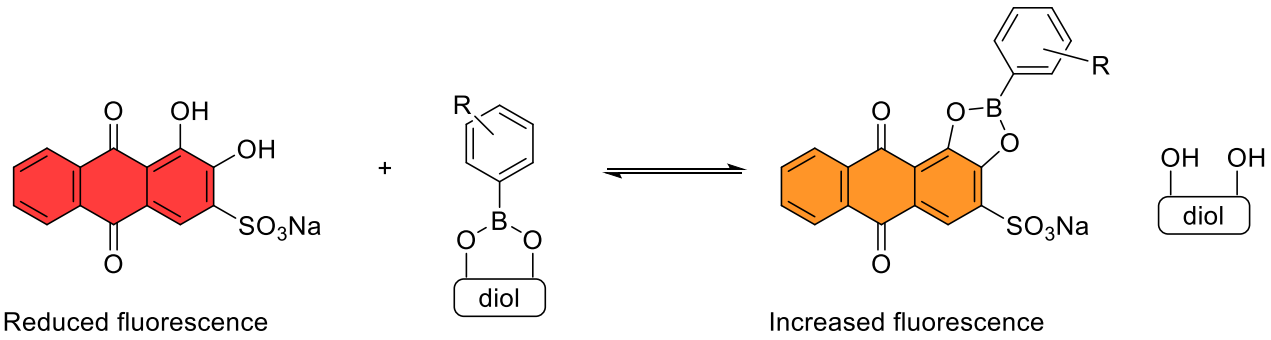

***Scheme 4.2** – Lower fluorescence when ARS is unbound than when bound to a boronic acid. The greater the binding of boronic acid to diol, the lower the binding to ARS and therefore the lower the fluorescence.*

If all the boronic acid is bound to ARS, then the system will be at maximum fluorescence. When a different diol is added, it competitively binds to the boronic acid, reducing the amount of ARS-boronic acid bound complex and thus reducing the fluorescence. Measuring this reduction of fluorescence as a function of concentration of diol and using the association constant between the boronic acid and ARS can give an absolute value for the association constant between boronic acid and diol. This is using an extension of the Benesi-Hildebrand equation with new terms defined. Calculated values Q and [S]/P are then plotted, where Q and P are defined in equations 4.5 and 4.6 respectively, and [S] is the concentration of the diol.

$$\mathrm{Q} = \frac{\mathrm{I_{max}} - \mathrm{I_x}}{\mathrm{I_x}} \qquad 4.5$$

Where I_{max} is the maximum fluorescence which is achieved when there is no diol present, and all the ARS is bound to boronic acid. I_x is the fluorescence intensity at each concentration of diol.

$$\mathrm{P} = [\mathrm{BA}] - \frac{1}{\mathrm{Q}k_a} - \frac{[\mathrm{ARS}]}{\mathrm{Q}+1} \qquad 4.6$$

Where $[BA]$ is the concentration of boronic acid, Q is defined by equation 4.5, k_a is the association constant between the boronic acid and ARS calculated from the experiments outline in section 4.3.1, and $[ARS]$ is the concentration of ARS. The gradient of the plot of Q vs. [S]/P gives the binding constant between the diol and the boronic acid.

4.3.3 Dopamine and phenylboronic acid

Springsteen and Wang outlined the methods to obtain the association constants between phenylboronic acid and a range of diols.[222] Dopamine was selected as the diol as it had a high binding affinity to phenylboronic acid as shown by Ali *et al*.[239] Several iterations of different concentrations of the three components were tried before the following concentrations were decided upon.

Table 4.3 *– Final well concentrations of ARS, phenylboronic acid and dopamine to determine the binding constant between dopamine and phenylboronic acid.*

Component	*Concentration, mM*
ARS	0.01
Phenylboronic acid	2
Dopamine	50 to 0.15

The experiment was carried out by first making three stock solutions:

A. ARS in aqueous sodium phosphate buffer (0.1 M, pH 7.4) to a final concentration of 3×10^{-5} M.

B. Phenylboronic acid in 5% DMSO and 95% aqueous sodium phosphate buffer (0.1 M, pH 7.4) to a final concentration of 6×10^{-3} M.

C. Dopamine hydrochloride in aqueous sodium phosphate buffer (0.1 M, pH 7.4) to a final concentration of 0.15 M.

50 µL stock solution C was transferred to the top well of a black 96-well plate. Serial dilution across the subsequent 11 wells to gave 12 different concentrations of dopamine, each with a volume of 50 µL. 50 µL of stock solutions A and B were then added to each well. An excitation wavelength of 468 nm was used with a slit width of 10 nm. Fluorescence intensity spectra were taken between 500 and 740 nm. A representative graph of this is shown in **Figure 4.15**. The red line indicates the highest concentration of dopamine at 50 mM. The purple line indicates the lowest concentration of dopamine at 0.15 mM. The black line shows the fluorescence intensity without dopamine.

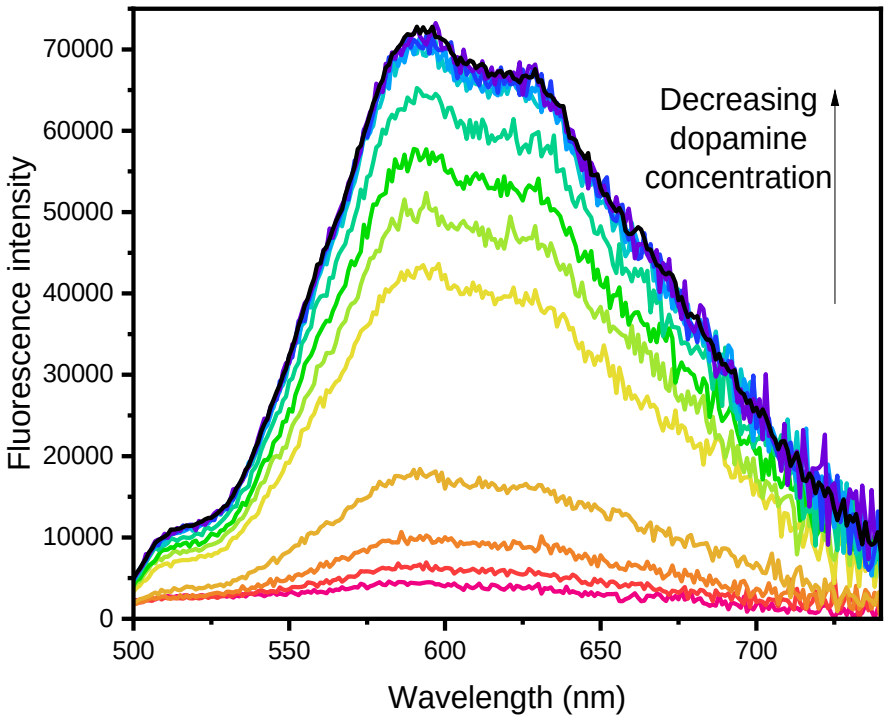

Figure 4.15 *– Representative graph showing how the fluorescence intensity changes based on the concentration of dopamine in the sample, with the highest concentration in red (50 mM) and lowest concentration in purple (0.15 mM).*

Using the equation outlined in section 4.3.2, and the value for the binding constant between phenylboronic acid and ARS of 1170 M^{-1}, the calculated binding constant of dopamine to phenylboronic acid at pH 7.4 is 617.0 ± 21.5 M^{-1}. A previous study determined the binding constant between dopamine and phenylboronic acid in PBS at pH 7.4 to be around 820 M^{-1}.[239] An issue that arose was the lack of difference between the fluorescence intensities when no dopamine was present and when very low concentrations were present. To obtain the data above, the lowest four concentrations of dopamine were omitted from the data set.

4.4 Conclusion and future work

Alizarin Red S is a useful fluorescent sensor for detecting and quantifying boronic acids and can be used effectively to calculate binding constants of boronic acids to

diols when the binding affinity is strong. It has been used to measure the binding constant between dopamine and phenylboronic acid, which was possible as they bind strongly. When the same method was applied to the diols investigated in chapter 3, the far weaker binding strength could not be measured as the difference in the fluorescence intensities were not great enough.

In future, the concentrations of the reagents should be looked at to be able to obtain the binding constants for boronic acids and diols. This could then be compared with other methods of obtaining the binding strength, such as isothermal titration calorimetry (ITC).

5 Final remarks and future work

The synthesis of aniline-containing derivatives of PTL was carried out using an alternative synthetic route to previous work in the group and other literature. Although the final compounds did not show potency against CLL, the barriers to their synthesis that have been overcome adds to the organic synthetic toolbox for use with other similar substrates. Studies within the research group by project students supervised by the author of this thesis revealed activity against CLL for phenol-containing derivatives of PTL. Future work on this project could investigate the structure-activity relationship (SAR) of phenol derivatives in the pursuit of more potent drugs against CLL.

Building up the picture of how boronic acids and esters undergo oxidation would involve an extension of the study outlined in this thesis through changing individual parameters and carrying out the same experimental methods to measure the oxidation rates. Given the ease of measuring the formation of *para*-nitrophenolate, extending the study to use a wide range of pHs would help to feed experimental data into the computational calculations. This could be carried out far more easily with liquid handlers and robotics to automate the gathering of data instead of running the experiments by hand. This would eliminate human error in the experiments and increase volume and quality of data through the use of a high throughput system. Further studies on the ARS competitive binding assay would feed into this work and if the method was validated against isothermal titration calorimetry, then it paves the way for a rapid screening of binding characteristics of boronic acids and diols.

6 Experimental

All commercially available solvents, catalysts and reagents were purchased from suppliers and used without further purification. Proton NMR spectra were recorded at 300 MHz on a Bruker AVIII300 NMR spectrometer or at 400 MHz on a Bruker AVIII400 NMR spectrometer. Carbon NMR spectra are proton decoupled and were recorded at 101 MHz on a Bruker AVIII400 NMR spectrometer. Fluorine NMR spectra were recorded at 377 MHz on a Bruker AVIII400 NMR spectrometer. Boron NMR spectra were recorded at 128 MHz on a Bruker AVIII400 NMR spectrometer. Chemical shifts (δ) were reported in ppm relative to TMS (δ 0.00) for 1H NMR and to chloroform (δ 77.16) for 13C NMR spectroscopy; coupling constants (J) are expressed in Hertz (Hz). The following abbreviations are used for multiplicities: s = singlet, d = doublet, t = triplet, q = quartet, quint = quintet, m = multiplet, pent = pentet, hex = hextet, and br = broad. Mass spectra were recorded on an electrospray MS Waters LCT Time of Flight Mass Spectrometer. Infrared Spectra Varian 660-IR FT-IR spectrometer at room temperature using an ATR attachment. Melting points were measured using a StuartTM digital melting point apparatus (SMP10) and reported as a range. Specific optical rotations were recorded on an Optical PolAAr 2001 automatic polarimeter at room temperature. The X-ray crystal structures were determined using an Agilent SuperNova X-ray diffractometer with an Atlas detector (wavelength 1.5418 Å).

6.1 Chapter 2 – PTL derivatives synthesis

6.1.1 Extraction of PTL

Feverfew was grown at Winterbourne gardens on the University of Birmingham campus. The flowers and stalks were harvested and allowed to dry for a week in a

greenhouse. The dried plant matter was cut into ~1 cm long pieces and simmer in water (100 g plant material to 1 L of water) for 10 minutes at 80 °C. The water was collected, and the same plant material was simmered twice more in water for 10 minutes at 80 °C. The collected water was allowed to cool and partitioned with chloroform. The organic fraction was collected, and the aqueous layer extracted twice more with chloroform. The combined organic fractions were concentrated *in vacuo*, and the crude material was subjected to column chromatography (silica gel, 0-30% hexane/ethyl acetate). The appropriate fractions were collected and concentrated *in vacuo*, and the resulting white solid was recrystallised in ice-cold diethyl ether to afford parthenolide as a white crystalline solid.

6.1.2 Biological data

Biological data was obtained at the Institute of Cancer Research at the University of Birmingham. MEC1 cells were obtained from the American Type Culture Collection and were cultures in RPMI 1640 medium with 10% fetal bovine serum (Sigma-Aldrich). MEC1 cells were seeded at a density of 25000 cells per well in a 96 well plate to a volume of 200 µL. The cells were treated with the compound at varying concentrations, and cell viability was determined through the reduction of resazurin. A final well concentration of resazurin of 50 µg/mL was added to each well and they were incubated at 37 °C for 3 hours. Reduction of resazurin was measured on a PheraSTAR FS plate reader. Cell viability was calculated by finding the difference of cells alive between the control and the treated.

6.1.3 Aniline derivatives

All NMR spectra are published in Tetrahedron (2020).[193] NMR resonances for compound **41a** are fully assigned. NMR resonances for subsequent compounds have new resonances assigned.

*6.1.3.1 General procedure **A***

To a 1:1 water-methanol (0.2 mmol) solution of parthenolide (1 equiv.), the corresponding aniline (1.2 equiv.) and squaric acid (10 mol%) were added. The resulting solution was stirred at 50 °C for 48 hours. The solution was allowed to cool to room temperature and the solvent was removed *in vacuo*. The residual was extracted with dichloromethane, the combined organic layers were washed with brine and then dried over anhydrous magnesium sulfate, filtered, and solvent removed *in vacuo*. The product was isolated by flash chromatography over silica gel.

*6.1.3.2 Synthesis of compound **41a***

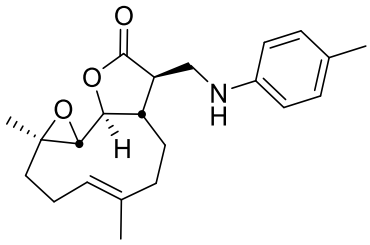

(3*R*,3a*S*,9a*R*,10a*R*,10b*S*,*E*)-6,9a-Dimethyl-3-((p-tolylamino)methyl)-3a,4,5,8,9,9a,10a,10b-octahydrooxireno[2',3':9,10]cyclodeca[1,2-b]furan-2(3H)-one (41a). Following the general procedure **A**, a mixture of parthenolide (100 mg, 0.403 mmol), *p*-toluidine (52 mg, 0.483 mmol) and squaric acid (5 mg, 0.040 mmol) was stirred at 50 °C in 1:1 water:methanol (2 mL total) for 48 hours. The title compound

was obtained as a white solid in 51% yield (73 mg). **Rf** = 0.65 (hexane:ethyl acetate, 1:1); **^{1}H NMR** (400 MHz, $CDCl_3$) δ 7.01 (2H, d, Ar*H*), 6.58 (2H, d, Ar*H*), 5.13 (1H, d, *H*C-C=O), 4.28 (1H, s, N*H*), 3.84 (1H, t, C=C*H*), 3.56 (1H, d, N-C*H*H), 3.36 (1H, d, N-CH*H*), 2.69 (1H, d, epoxide-C*H*), 2.60 to 2.51 (1H, m, O=C-O-C*H*), 2.43 to 2.27 (2H, m, CH_2), 2.24 (3H, s, Me), 2.20 to 1.93 (5H, m, CH_2 (multiple)), 1.76 to 1.60 (1H, m, C*H*H), 1.69 (3H, s, Me), 1.28 (3H, s, Me), 1.19 (1H, td, C*H*); **^{13}C NMR** (101 MHz, $CDCl_3$) δ 176.5 (C=O), 145.4 (NArCq), 134.3 (ArCq), 129.9 (ArCH), 127.6 (C=C), 125.3 (C=C), 113.6 (ArCH), 82.5 (CO), 66.3 (CO), 61.6 (CO), 47.4 (CH), 46.8 (CH), 42.5 (CH_2), 41.1 (CH_2), 36.6 (CH_2), 30.1 (CH_2), 24.1 (CH_2), 20.4 (CH_3), 17.2 (CH_3), 16.9 (CH_3); **IR** (neat, cm-1) 3363 (NH), 1747 (C=O); **HRMS** (TOF MS ES+) m/z: [M+H]+ calc. for $C_{22}H_{30}NO_3^+$ 356.2224, found 356.2226; **mp** 200-203 °C; **$[\alpha]_D^{22}$** = -12.81° (c 2.0, CH_2Cl_2).

*6.1.3.3 Synthesis of compound **41b***

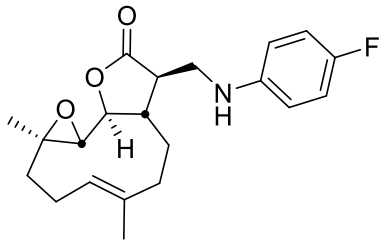

(3*R*,3a*S*,9a*R*,10a*R*,10b*S*,*E*)-3-(((4-Fluorophenyl)amino)methyl)-6,9a-dimethyl-3a,4,5,8,9,9a,10a,10b-octahydrooxireno[2',3':9,10]cyclodeca[1,2-b]furan-2(3H)-one (41b). Following the general procedure **A**, a mixture of parthenolide (100 mg, 0.403 mmol), 4-fluoroaniline (54 mg, 0.483 mmol) and squaric acid (5 mg, 0.040 mmol) was stirred at 50 °C in 1:1 water:methanol (2 mL total) for 48 hours. The title compound was obtained as a white solid in 35% yield (51 mg). **Rf** = 0.57 (hexane:ethyl acetate,

1:1); **^{1}H-NMR** (400 MHz, $CDCl_3$) δ 6.97 to 6.86 (2H, m), 6.66 to 6.56 (2H, m), 5.15 (1H, d, *J* 12.3), 4.37 (1H, s), 3.87 (1H, t, *J* 9.0), 3.54 (1H, dd, *J* 13.5, 3.8), 3.34 (1H, dd, *J* 13.5, 7.1), 2.70 (1H, d, *J* 8.9), 2.56 (1H, ddd, *J* 12.4, 7.1, 3.8), 2.47 to 2.28 (2H, m), 2.22 to 1.91 (5H, m), 1.81 to 1.67 (1H, m), 1.70 (3H, s), 1.29 (3H, s), 1.27 to 1.14 (1H, m); **^{13}C-NMR** (101 MHz, $CDCl_3$) δ 176.4, 157.5, 144.0, 134.2, 125.4, 116.0, 115.8, 114.5 (d, $J_{C\text{-}F}$ 10 Hz), 82.6, 66.2, 61.6, 47.3, 46.9, 43.0, 41.1, 36.5, 30.1, 24.1, 17.2, 16.9; **^{19}F-NMR** (377 MHz, $CDCl_3$) δ -126.8; **IR** (neat, cm^{-1}) 3371 (NH), 1748 (C=O); **HRMS** (TOF MS ES+) *m/z*: $[M+H]^+$ calc. for $C_{21}H_{27}NO_3^+$ 360.1974, found 360.1975; **mp** 121-124 °C; **$[\alpha]_D^{22}$ = -**19.39° (c 0.5, CH_2Cl_2).

*6.1.3.4 Synthesis of compound **41c***

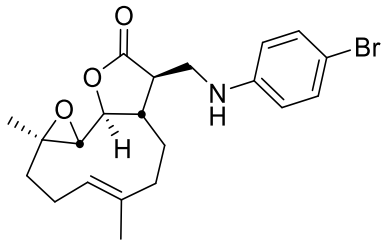

(3*R*,3a*S*,9a*R*,10a*R*,10b*S*,*E*)-3-(((4-Bromophenyl)amino)methyl)-6,9a-dimethyl-3a,4,5,8,9,9a,10a,10b-octahydrooxireno[2',3':9,10]cyclodeca[1,2-b]furan-2(3H)-one (41c). Following the general procedure **A**, a mixture of parthenolide (100 mg, 0.403 mmol), 4-bromoaniline (83 mg, 0.483 mmol) and squaric acid (5 mg, 0.040 mmol) was stirred at 50 °C in 1:1 water:methanol (2 mL total) for 48 hours. The title compound was obtained as a white solid in 9% yield (15 mg). **Rf** = 0.57 (hexane:ethyl acetate, 1:1); **^{1}H-NMR** (400 MHz, $CDCl_3$) δ 7.31 to 7.23 (2H, m), 6.58 to 6.49 (2H, m), 5.14 (1H, d, *J* 12.1), 4.48 (1H, t, *J* 6.8), 3.91 to 3.82 (1H, m), 3.59 to 3.52 (1H, m) 3.39 to 3.31 (1H, m), 2.69 (1H, d, *J* 8.9), 2.59 to 2.52 (1H, m), 2.45 to 2.28 (2H, m), 2.21 to

1.93 (5H, m), 1.79 to 1.70 (1H, m), 1.70 (3H, s), 1.29 (3H, s), 1.30 to 1.16 (1H, m); **^{13}C-NMR** (101 MHz, $CDCl_3$) δ 176.3, 146.7, 134.2, 132.2, 125.5, 114.9, 109.9, 82.6, 66.2, 61.6, 60.4, 47.4, 46.9, 42.1, 41.1, 36.5, 30.1, 24.1, 17.2, 16.9, 14.2; **IR** (neat, cm^{-1}) 3380 (NH), 1760 (C=O); **HRMS** (TOF MS ASAP+) *m/z*: $[M+H]^+$ calcd. for $C_{21}H_{27}BrNO_3^+$ 420.1174 found 420.1179; **mp** 182-184 °C; **$[\alpha]_D^{22}$** = 9.70° (c 0.5, CH_2Cl_2).

*6.1.3.5 Synthesis of compound **41d***

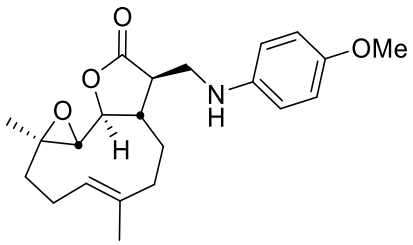

(3*R*,3a*S*,9a*R*,10a*R*,10b*S*,*E*)-3-(((4-Methoxyphenyl)amino)methyl)-6,9a-dimethyl-3a,4,5,8,9,9a,10a,10b-octahydrooxireno[2',3':9,10]cyclodeca[1,2-b]furan-2(3H)-one (41d). Following the general procedure **A**, a mixture of parthenolide (100 mg, 0.403 mmol), 4-methoxyaniline (60 mg, 0.483 mmol) and squaric acid (5 mg, 0.040 mmol) was stirred at 50 °C in 1:1 water:methanol (2 mL total) for 48 hours. The title compound was obtained as a white solid in 54% yield (81 mg). **Rf** = 0.50 (hexane:ethyl acetate, 1:1); **^{1}H-NMR** (400 MHz, $CDCl_3$) δ 6.84 to 6.75 (2H, m), 6.68 to 6.60 (2H, m), 5.13 (1H, d, *J* 12.2), 4.21 (1H, s), 3.85 (1H, t, *J* 9.0), 3.75 (3H, s), 3.53 (1H, dd, *J* 13.5 & 3.8), 3.33 (1H, dd, *J* 13.5 & 7.0), 2.70 (1H, d, *J* 8.9), 2.56 (1H, ddd, *J* 12.3, 6.9 & 3.8), 2.45 to 2.26 (2H, m), 2.21 to 1.91 (6H, m), 1.78 to 1.65 (1H, m), 1.69 (3H, s), 1.28 (3H, s), 1.20 (1H, td, *J* 13.0 & 5.9); **^{13}C-NMR** (101 MHz, $CDCl_3$) δ 176.6, 152.7, 141.8, 134.3, 125.3, 115.0, 82.6, 66.2, 61.6, 55.8, 47.2, 46.9, 43.4, 41.1, 36.6, 30.0, 24.1,

17.2, 16.9; **IR** (neat, cm^{-1}) 3365 (NH), 1747 (C=O); **HRMS** (TOF MS ES+) *m/z*: $[M+H]^+$ calcd. for $C_{22}H_{30}NO_4^+$ 372.2175, found 372.2174; **mp** 145-147 °C; **$[\alpha]_D^{22}$** = -16.62° (c 1.0, CH_2Cl_2).

*6.1.3.6 Synthesis of compound **41e***

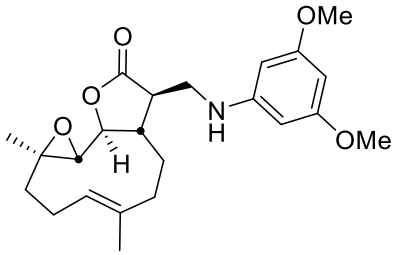

(3*R*,3a*S*,9a*R*,10a*R*,10b*S*,*E*)-3-(((3,5-Dimethoxyphenyl)amino)methyl)-6,9a-dimethyl-3a,4,5,8,9,9a,10a,10b-octahydrooxireno[2',3':9,10]cyclodeca[1,2-b]furan-2(3H)-one (41e). Following the general procedure **A**, a mixture of parthenolide (100 mg, 0.403 mmol), 3,5-dimethoxyaniline (74 mg, 0.483 mmol) and squaric acid (5 mg, 0.040 mmol) was stirred at 50 °C in 1:1 water:methanol (2 mL total) for 48 hours. The title compound was obtained as a white solid in 26% yield (42 mg). **Rf** = 0.50 (hexane:ethyl acetate, 1:1); **^{1}H-NMR** (400 MHz, $CDCl_3$) δ 5.91 (1H, t, *J* 2.1), 5.83 (2H, d, *J* 2.1), 5.13 (1H, dd, *J* 11.9 & 2.3), 4.47 (1H, s), 3.86 (1H, t, *J* 9.0), 3.75 (6H, s), 3.56 (1H, dd, *J* 14.5 & 3.3), 3.36 (1H, dd, *J* 13.8 & 6.8), 2.69 (1H, d, *J* 8.9), 2.57 (1H, ddd, *J* 12.3, 6.8 & 3.7), 2.46 to 2.27 (2H, m), 2.21 to 1.94 (4H, m), 1.80 to 1.70 (1H, m), 1.69 (3H, s), 1.29 (3H, s), 1.20 (1H, td, *J* 13.4 & 6.3); **^{13}C-NMR** (101 MHz, $CDCl_3$) δ 176.4, 161.9, 149.7, 134.3, 125.4, 92.1, 90.4, 82.6, 66.2, 61.6, 55.2, 47.5, 46.8, 41.8, 41.0, 36.6, 30.1, 24.1, 17.2, 16.9; **IR** (neat, cm^{-1}) 3389 (NH), 1761 (C=O); **HRMS** (TOF MS ES+) *m/z*: $[M+H]^+$ calcd. for $C_{23}H_{32}NO_5^+$ 402.2280, found 402.2285; **mp** 110-112 °C; **$[\alpha]_D^{22}$** = -5.02° (c 2.0, CH_2Cl_2).

*6.1.3.7 Synthesis of compound **41f***

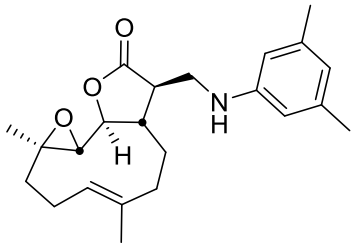

(3*R*,3a*S*,9a*R*,10a*R*,10b*S*,*E*)-3-(((3,5-Dimethylphenyl)amino)methyl)-6,9a-dimethyl-3a,4,5,8,9,9a,10a,10b-octahydrooxireno[2',3':9,10]cyclodeca[1,2-b]furan-2(3H)-one (41f). Following the general procedure **A**, a mixture of parthenolide (100 mg, 0.403 mmol), 3,5-dimethylaniline (54 mg, 0.483 mmol) and squaric acid (5 mg, 0.040 mmol) was stirred at 50 °C in 1:1 water:methanol (2 mL total) for 48 hours. The title compound was obtained as a white solid in 28% yield (42 mg). **Rf** = 0.62 (hexane:ethyl acetate, 1:1); **^{1}H-NMR** (400 MHz, $CDCl_3$) δ 6.41 (1H, s), 6.28 (2H, s), 5.12 (1H, dd, *J* 12.1 & 2.3), 4.27 (1H, s), 3.84 (1H, t, *J* 9.0), 3.58 (1H, dd, *J* 13.8 & 3.8), 3.39 (1H, dd, *J* 13.8 & 6.3), 2.68 (1H, d, *J* 8.9), 2.55 (1H, ddd, *J* 12.3, 6.3 & 3.8), 2.45 to 2.27 (2H, m), 2.24 (6H, s), 2.20 to 1.95 (5H, m), 1.79 to 1.66 (1H, m), 1.70 (3H, s), 1.29 (3H, s), 1.19 (1H, td, *J* 13.0 & 6.0); **^{13}C-NMR** (101 MHz, $CDCl_3$) δ 176.4, 147.9, 139.1, 134.3, 125.4, 120.2, 111.3, 82.5, 66.2, 61.6, 47.8, 46.7, 42.0, 41.0, 36.6, 30.1, 24.1, 21.5, 17.2, 16.9; **IR** (neat, cm^{-1}) 3382 (NH), 1755 (C=O); **HRMS** (TOF MS ES+) *m/z*: $[M+H]^+$ calcd. for $C_{23}H_{32}NO_3^+$ 370.2383, found 370.2382; **mp** 196-197 °C; **$[\alpha]_D^{22}$** = 11.08° (c 0.5, CH_2Cl_2).

*6.1.3.8 Synthesis of compound **41g***

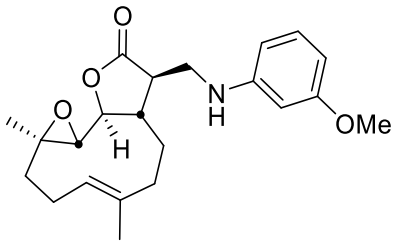

(3*R*,3a*S*,9a*R*,10a*R*,10b*S*,*E*)-3-(((3-Methoxyphenyl)amino)methyl)-6,9a-dimethyl-3a,4,5,8,9,9a,10a,10b-octahydrooxireno[2',3':9,10]cyclodeca[1,2-b]furan-2(3H)-one (41g). Following the general procedure **A**, a mixture of parthenolide (80 mg, 0.32 mmol), 3-methoxyaniline (48 mg, 0.384 mmol) and squaric acid (4 mg, 0.030 mmol) was stirred at 50 °C in 1:1 water:methanol (2 mL total) for 48 hours. The title compound was obtained as a white solid in 24% yield (28 mg). **Rf** = 0.52 (hexane:ethyl acetate, 1:1); **^{1}H-NMR** (400 MHz, $CDCl_3$) δ 7.10 (1H, t, *J* 8.1), 6.31 (1H, dd, *J* 8.2 & 2.4), 6.26 (1H, dd, *J* 8.0 & 2.2), 6.20 (1H, t, *J* 2.3), 5.13 (1H, d, *J* 12.2 & 2.4), 4.43 (1H, s), 3.85 (1H, t, *J* 9.0), 3.77 (3H, s), 3.58 (1H, dd, *J* 14.1 & 3.6), 3.39 (1H, dd, *J* 13.8 & 6.7), 2.69 (1H, d, *J* 8.9), 2.56 (1H, ddd, *J* 12.3, 6.7 & 3.8), 2.46 to 2.25 (2H, m), 2.20 to 1.94 (5H, m), 1.79 to 1.66 (1H, m), 1.69 (3H, s), 1.29 (3H, s), 1.27 to 1.14 (1H, m); **^{13}C NMR** (101 MHz, $CDCl_3$) δ 176.4, 161.0, 149.2, 134.3, 130.2, 125.4, 106.3, 103.4, 99.4, 82.6, 66.2, 61.6, 55.2, 47.6, 46.8, 41.9, 41.0, 36.6, 30.1, 24.1, 17.2, 16.9; **IR** (neat, cm^{-1}) 2930 (NH), 1762 (C=O); **HRMS** (TOF MS ES+) *m/z*: $[M+H]^+$ calcd. for $C_{22}H_{30}NO_4^+$ 372.2175, found 372.2177; **mp** 154-156 °C; **$[\alpha]_D^{22}$** = -17.31° (c 1.0, CH_2Cl_2).

*6.1.3.9 Synthesis of compound **41h***

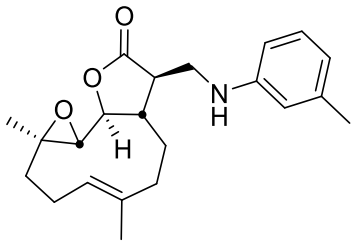

(3*R*,3a*S*,9a*R*,10a*R*,10b*S*,*E*)-6,9a-Dimethyl-3-((m-tolylamino)methyl)-3a,4,5,8,9,9a,10a,10b-octahydrooxireno[2',3':9,10]cyclodeca[1,2-b]furan-2(3H)-one (41h). Following the general procedure **A**, a mixture of parthenolide (80 mg, 0.32 mmol), m-toluidine (42 mg, 0.384 mmol) and squaric acid (4 mg, 0.030 mmol) was stirred at 50 °C in 1:1 water:methanol (2 mL total) for 48 hours. The title compound was obtained as a white solid in 18% yield (20 mg). **Rf** = 0.64 (hexane:ethyl acetate, 1:1); **^{1}H-NMR** (400 MHz, $CDCl_3$) δ 7.08 (1H, t, *J* 7.5), 6.57 (1H, d, *J* 7.2), 6.50 to 6.43 (2H, m), 5.12 (1H, dd, *J* 12.2 & 3.8), 4.35 (1H, s), 3.85 (1H, t, *J* 9.0), 3.58 (1H, dd, *J* 13.8 & 3.9), 3.40 (1H, dd, *J* 13.8 & 6.6), 2.68 (1H, d, *J* 8.9), 2.56 (1H, ddd, *J* 12.2, 6.5 & 3.8), 2.45 to 2.30 (2H, m), 2.28 (3H, s), 2.20 to 1.95 (5H, m), 1.79 to 1.66 (1H, m), 1.69 (3H, s), 1.29 (3H, s), 1.19 (1H, td, *J* 13.0 & 5.9); **^{13}C NMR** (101 MHz, $CDCl_3$) δ 176.4, 147.8, 139.3, 134.3, 129.3, 125.4, 119.2, 114.2, 110.4, 82.6, 66.2, 61.6, 47.6, 46.8, 42.0, 41.0, 36.6, 30.1, 24.1, 21.6, 17.2, 16.9; **IR** (neat, cm^{-1}) 3385 (NH), 1761 (C=O); **HRMS** (TOF MS ES+) *m/z*: $[M+H]^+$ calc. for $C_{22}H_{30}NO_3^+$ 356.2224, found 356.2230; **mp** 154-156 °C; **$[\alpha]_D^{22}$** = -7.62° (c 0.5, CH_2Cl_2).

*6.1.3.10 Synthesis of compound **41i***

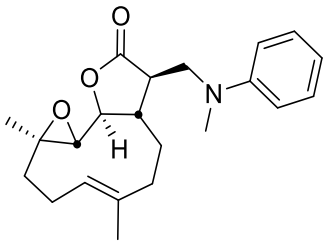

(3*R*,3a*S*,9a*R*,10a*R*,10b*S*,*E*)-6,9a-Dimethyl-3-((methyl(phenyl)amino)methyl)-3a,4,5,8,9,9a,10a,10b-octahydrooxireno[2',3':9,10]cyclodeca[1,2-b]furan-2(3H)-one (41i). Following the general procedure **A**, a mixture of parthenolide (100 mg, 0.403 mmol), *N*-methylaniline (52 mg, 0.483 mmol) and squaric acid (5 mg, 0.040 mmol) was stirred at 50 °C in 1:1 water:methanol (2 mL total) for 48 hours. The title compound was obtained as a white solid in 8% yield (9 mg). **Rf** = 0.67 (hexane:ethyl acetate, 1:1); **^{1}H-NMR** (400 MHz, $CDCl_3$) δ 7.29 to 7.22 (2H, m), 6.79 to 6.70 (3H, m), 5.05 (1H, dd, *J* 11.8 & 2.3), 4.01 (1H, dd, *J* 15.4 & 4.9), 3.79 (1H, t, *J* 9.0), 3.65 (1H, dd, *J* 15.5 & 6.1), 3.01 (3H, s), 2.74 to 2.62 (2H, m), 2.41 to 2.28 (1H, m), 2.19 to 2.03 (4H, m), 1.96 to 1.86 (1H, m), 1.79 to 1.68 (1H, m), 1.64 (3H, s), 1.65 to 1.53 (1H, m), 1.26 (3H, s), 1.19 (1H, td, *J* 13.0 & 5.9); **^{13}C NMR** (101 MHz, $CDCl_3$) δ 176.0, 149.0, 134.4, 129.5, 125.0, 117.2, 112.5, 82.3, 66.5, 61.6, 52.1, 48.1, 46.4, 40.9, 39.6, 36.6, 30.4, 24.1, 17.2, 16.9; **IR** (neat, cm^{-1}) 1760 (C=O); **HRMS** (TOF MS ES+) *m/z*: $[M+H]^+$ calc. for $C_{22}H_{30}NO_3^+$ 356.2224, found 356.2232; **mp** 153-156 °C; **$[\alpha]_D^{22}$** = -124.65° (c 1.0, CH_2Cl_2).

*6.1.3.11 Synthesis of compound **41j***

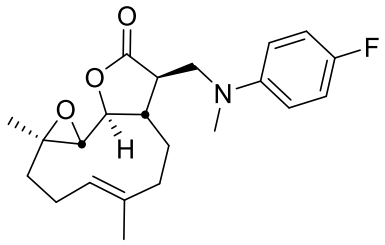

(3*R*,3a*S*,9a*R*,10a*R*,10b*S*,*E*)-3-(((4-Fluorophenyl)(methyl)amino)methyl)-6,9a-dimethyl-3a,4,5,8,9,9a,10a,10b-octahydrooxireno[2',3':9,10]cyclodeca[1,2-b]furan-2(3H)-one (41j). Following the general procedure **A**, a mixture of parthenolide (80 mg, 0.32 mmol), 4-fluoro-N-methylaniline (48 mg, 0.384 mmol) and squaric acid (4 mg, 0.030 mmol) was stirred at 50 °C in 1:1 water:methanol (2 mL total) for 48 hours. The title compound was obtained as a white solid in 8% yield (9 mg). **Rf** = 0.64 (hexane:ethyl acetate, 1:1); **^{1}H-NMR** (400 MHz, $CDCl_3$) δ 7.02 to 6.91 (2H, m), 6.75 to 6.65 (2H, m), 5.07 (1H, dd, *J* 12.2 and 2.0), 3.92 (1H, dd, *J* 15.4 and 4.9), 3.80 (1H, t, *J* 9.0), 3.60 (1H, dd, *J* 15.4 and 6.0), 2.97 (3H, s), 2.67 (1H, d, *J* 8.9), 2.63 (1H, ddd, *J* 11.9, 6.0 and 4.9), 2.44 to 2.28 (1H, m), 2.19 to 2.06 (4H, m), 1.89 (1H, dd, *J* 15.2 and 6.6), 1.76 (1H, t, *J* 13.0), 1.65 (3H, s), 1.66 to 1.54 (1H, m), 1.27 to 1.13 (4H, m); **^{13}C-NMR** (101 MHz, $CDCl_3$) δ 176.0, 145.8, 134.3, 125.1, 115.9, 115.7, 113.9, 113.9, 82.3, 66.5, 61.6, 52.8, 48.1, 46.4, 41.0, 40.1, 36.6, 30.3, 24.1, 17.2, 16.9; **^{19}F-NMR** (377 MHz, $CDCl_3$) δ -128.0; **IR** (neat, cm^{-1}) 1761 (C=O); **HRMS** (TOF MS ASAP+) *m/z*: $[M+H]^+$ calc. for $C_{22}H_{29}FNO_3^+$ 374.2131, found 374.2141; **mp** 131-134 °C; **$[\alpha]_D^{22}$** = 34.97° (c 1.0, CH_2Cl_2).

*6.1.3.12 Synthesis of compound **41k***

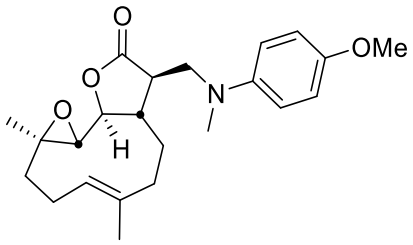

(3*R*,3a*S*,9a*R*,10a*R*,10b*S*,*E*)-3-(((4-Methoxyphenyl)(methyl)amino)methyl)-6,9a-dimethyl-3a,4,5,8,9,9a,10a,10b-octahydrooxireno[2',3':9,10]cyclodeca[1,2-b]furan-2(3H)-one (41k). Following the general procedure **A**, a mixture of parthenolide (80 mg, 0.32 mmol), 4-methoxy-N-methylaniline (53 mg, 0.384 mmol) and squaric acid (4 mg, 0.030 mmol) was stirred at 50 °C in 1:1 water:methanol (2 mL total) for 48 hours. The title compound was obtained as a white solid in 36% yield (45 mg). **Rf** = 0.64 (hexane:ethyl acetate, 1:1); **^{1}H-NMR** (400 MHz, $CDCl_3$) δ 6.90 to 6.81 (2H, m), 6.79 to 6.71 (2H, m), 5.08 (1H, dd, *J* 9.8 and 2.1), 3.89 (1H, dd, *J* 15.2 and 4.8), 3.80 (1H, t, *J* 9.2), 3.76 (3H, s), 3.52 (1H, dd, *J* 15.3 and 6.2), 2.93 (3H, s), 2.68 (1H, d, *J* 8.9), 2.62 (1H, ddd, *J* 11.9, 6.0 and 4.8), 2.44 to 2.28 (1H, m), 2.21 to 2.07 (4H, m), 1.93 (1H, dd, *J* 14.8 and 6.6), 1.78 (1H, t, *J* 12.7), 1.64 (3H, s), 1.63 to 1.51 (1H, m), 1.27 (3H, s), 1.25 to 1.15 (1H, m); **^{13}C-NMR** (101 MHz, $CDCl_3$) δ 176.2, 152.2, 144.0, 134.5, 125.0, 115.0, 114.9, 82.3, 66.5, 61.6, 55.8, 53.2, 48.1, 46.5, 41.0, 40.4, 36.6, 30.3, 24.1, 17.2, 16.9; **IR** (neat, cm^{-1}) 1766 (C=O); **HRMS** (TOF MS ASAP+) *m/z*: $[M+H]^+$ calc. for $C_{23}H_{32}NO_4^+$ 386.2331, found 386.2330; **mp** 146-148 °C; **$[\alpha]_D^{22}$** = 81.72° (c 2.0, CH_2Cl_2).

6.1.4 XRD of compound 41a

XRD data published in Tetrahedron (2020).[193]

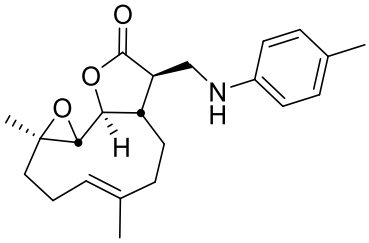

Single crystals of compound **41a** were prepared through vapour diffusion of hexane into dichloromethane. A suitable crystal was selected and submitted for single crystal XRD. Crystal Data for $C_{22}H_{29}NO_3$ (*M* =355.46 g/mol): monoclinic, space group $P2_1$ (no. 4), *a* = 11.1281(3) Å, *b* = 7.1835(2) Å, *c* = 11.8050(3) Å, *β* = 93.143(2)°, *V* = 942.26(4) Å^3, *Z* = 2, *T* = 100.00(10) K, μ(CuKα) = 0.654 mm^{-1}, *Dcalc* = 1.253 g/cm^3, 33890 reflections measured (7.5° ≤ 2Θ ≤ 148.854°), 3695 unique (R_{int} = 0.0431, R_{sigma} = 0.0198) which were used in all calculations. The final R_1 was 0.0287 (I > 2σ(I)) and wR_2 was 0.0719 (all data).

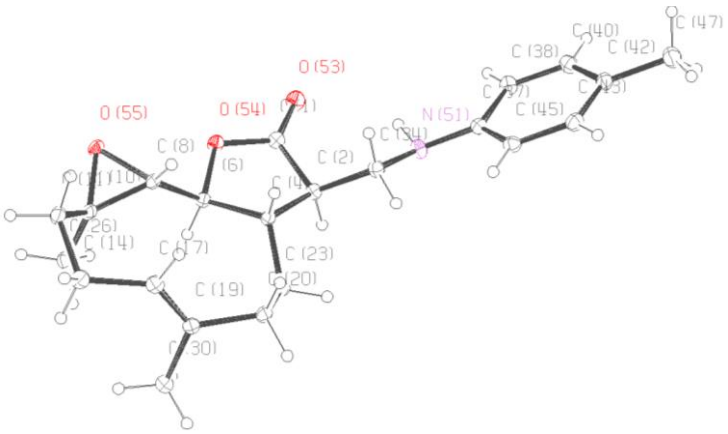

6.1.5 Molecular docking

Chimera, a free-to-use software made by UCSF, was downloaded alongside the Autodock Vina add-on. The structure of NF-κB was obtained from the Protein Data Bank (PDB) using the PDB ID 2RAM.[245] This PDB ID presents NF-κB with two protein

chains and DNA, and so the DNA was removed and only protein chain A was selected. The standard dock prep program in Chimera was used to prepare the protein using the default settings with additional solvent molecules removed. The substrate file was prepared by first drawing the compound in ChemDraw with all stereochemistry, then copy and pasting it into Chem3D and subjecting it to an MM2 minimisation. This file was then saved as a .mol file to be transferred into Chimera. Standard Autodock Vina code was used with the default settings to obtain the docking score and lowest energy poses.

6.1.6 ALF01 amine synthesis

*6.1.6.1 Synthesis of compound **47***

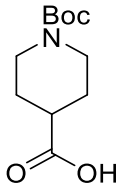

***N*-Boc-Piperidine-4-carboxylic acid (47).** To a solution of piperidine-4-carboxylic acid (6.46 g, 50 mmol) in THF (50 mL) cooled to 0 °C was added dropwise a solution of di-*tert*-butyl carbamate (19.10 g, 87.5 mmol, 1.75 eq.) dissolved in aqueous sodium hydroxide (50 mL, 1 M). After stirring for 30 minutes, the solution as allowed to warm to room temperature and was stirred for 18 hours. The resulting mixture was concentrated *in vacuo* to half its original volume and then adjusted to pH 5-6 by addition of aqueous HCl (1 M). The white precipitate formed was collected by suction filtration and then taken up in chloroform (~100 mL) and this organic solution was dried over anhydrous magnesium sulfate. The solvent was removed *in vacuo* to give compound **47** as a white powder (10.56 g, 92%). **^{1}H NMR** (400 MHz, CDCl3) δ 4.03

(s, 2H), 2.86 (t, *J* = 12.6 Hz, 2H), 2.51 (tt, *J* = 11.0, 3.9 Hz, 1H), 1.92 (d, *J* = 13.1 Hz, 2H), 1.62 (dd, *J* = 10.9, 4.4 Hz, 1H), 1.46 (s, 9H); **^{13}C NMR** (101 MHz, $CDCl_3$) δ 195.3, 42.1, 31.2, 28.4, 27.4; **IR** ν (cm^{-1}) 3187 (O-H) 2975 (C-H) 1801 (C=O) 1679 (C=O); **MS** *m/z* 229 (M^+, 100%), 170 (M – ^{t}Bu, 64).

*6.1.6.2 Synthesis of compound **49***

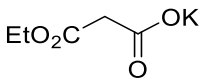

Ethyl potassium malonate (49). Potassium hydroxide (5.61 g, 0.1 mol) dissolved in ethanol (100 mL) was added dropwise over 30 minutes to a stirring solution of diethyl malonate (15 mL, 0.1 mol) dissolved in ethanol (100 mL). Upon addition of the potassium hydroxide, a significant amount of white precipitate formed. The mixture was left stirring vigorously for 18 hours. The mixture was concentrated *in vacuo* and white crystals formed which were filtered and washed with diethyl ether. The crystals were air dried to give compound **49** as a white crystalline solid (14.28 g, 84%). **^{1}H NMR** (400 MHz, D_2O) δ 4.08 (q, *J* = 7.2 Hz, 2H), 3.19 (s, 2H), 1.16 (t, *J* = 7.2 Hz, 3H); **^{13}C NMR** (101 MHz, D_2O) δ 174.25, 171.54, 62.09, 44.72, 13.25; **MS** *m/z* 131 (M^+ - K^+) IR ν (cm^{-1}) 2984 (C-H) 1726 (C=O) 1595 (C=O); **mp** 195 °C – 196 °C.

*6.1.6.3 Synthesis of compound **50** (1st route)*

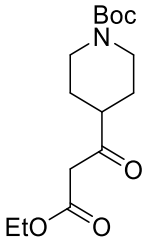

***tert*-Butyl 4-(3-ethoxy-3-oxopropanoyl)piperidine-1-carboxylate (50)**. Ethyl potassium malonate **49** (3.71 g, 21.8 mmol, 2.5 eq.), magnesium chloride (2.49 g, 26.2 mmol, 3.0 eq.) and DMAP (106 mg, 0.9 mmol, 0.1 eq.) were added at 0 °C to a 1:2 solution of acetonitrile (9 mL) and tetrahydrofuran (18 mL). The mixture was allowed to warm to room temperature and was stirred for 5 h. In a separate flask, *N*-Boc-piperidine-4-carboxylic acid **47** (2.00 g, 8.7 mmol, 1.0 eq.) and carbonyl diimidazole (1.84 g, 11.3 mmol, 1.3 eq.) were added at 0 °C to tetrahydrofuran (20 mL). The mixture was allowed to warm to room temperature and was stirred for 4 h. The latter mixture was added to the former at 0 °C. Triethylamine (3.6 mL, 26.2 mmol, 3.0 eq.) was added to the reaction and this was allowed to stir for 18 h at room temperature. The solvent was evaporated *in vacuo* and the resultant mixture was adjusted to pH 4 with aqueous HCl (1 M). This was extracted in ethyl acetate (3 x 50 mL) and the combined organic fractions were washed with aqueous HCl (1 M, 50 mL), then aqueous NaOH (1 M, 50 mL), then brine (50 mL). This was dried over anhydrous magnesium sulfate, filtered and concentrated *in vacuo* to form the crude product as a yellow oil. This was subjected to flash column chromatography (silica, hexane / ethyl acetate gradient elution) to give the pure product **50** as a colourless oil (1.76 g, 67%). **^{1}H NMR** (300 MHz, $CDCl_3$) δ 4.37 – 4.05 (m, 2H), 3.50 (s, 1H), 2.62 (tt, *J* = 11.3, 3.7 Hz, 1H), 2.05 (s, 1H), 1.85 (d, *J* = 12.9 Hz, 1H), 1.78 – 1.48 (m, 3H), 1.46 (d, *J* = 2.0 Hz, 12H), 1.43 – 1.23 (m, 3H), 1.25 (d, *J* = 6.1 Hz, 1H); **^{13}C NMR** (101 MHz, $CDCl_3$) 204.13, 167.27, 154.62, 79.54, 61.16, 48.65, 47.26, 43.14, 28.41, 27.23, 14.22; **IR** ν (cm^{-1}) 2975 (C-H) 1747, 1684 (C=O); **MS** *m/z* 322 (M^+ + Na^+)

*6.1.6.4 Synthesis of compound **51** (for 2nd route to compound **50**)*

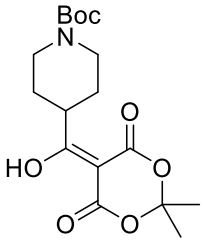

***tert*-Butyl 4-((2,2-dimethyl-4,6-dioxo-1,3-dioxan-5-ylidene)(hydroxy)methyl)piperidine-1-carboxylate (51).** Compound **47** (2.50 g, 10.92 mmol, 1.0 eq.), Meldrum's acid (1.73 g, 12.01 mmol, 1.1 eq.) and DMAP (2.13 g, 17.47 mmol, 1.6 eq.) were dissolved in dichloromethane (50 mL) at room temperature. Once all the reagents were in solution, a solution of DCC (2.70 g, 13.10 mmol, 1.2 eq.) in dichloromethane (50 mL) was added dropwise and the resulting mixture was stirred at room temperature for 24 h. The mixture was filtered through cotton wool and the residue washed with dichloromethane (20 mL). The combined organic filtrate was washed with aqueous HCl (1 M, 10 mL) and the organic layer was dried over anhydrous sodium sulfate, filtered and concentrated *in vacuo*. The crude material was used directly in the next step without purification. **^{1}H NMR** (400 MHz, $CDCl_3$) δ 4.22 (2H, br s), 3.95 (1H, tt, *J* 11.5 & 3.6 Hz), 2.82 (2H, t, *J* 11.8 Hz), 1.91 to 1.56 (11H, m), 1.46 (9H, s).

*6.1.6.5 Synthesis of compound **50** (2nd route)*

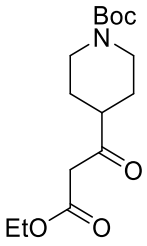

***tert*-Butyl 4-(3-ethoxy-3-oxopropanoyl)piperidine-1-carboxylate (50)**. The crude material **51** was dissolved in ethanol (50 mL) and heated to reflux. After 18 h, the reaction was allowed to cool to reflux and the solvent removed *in vacuo* to give the crude product as a pale yellow oil. This was subjected to flash column chromatography (silica, hexane / ethyl acetate gradient elution) to give compound **50** as a colourless oil (2.60 g, 82% over 2 steps). Data is consistent with other compound **50** from section 6.1.6.3.

*6.1.6.6 Synthesis of compound **53***

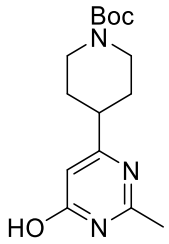

***tert*-Butyl-4-(6-hydroxy-2-methylpyrimidin-4-yl)piperidine-1-carboxylate (53).** Acetamidine hydrochloride (611 mg, 6.46 mmol, 1.1 eq.) and potassium carbonate (1.62 g, 11.74 mmol, 2.0 eq.) was dissolved in water (7 mL). A solution of compound **50** (1.76 g, 5.87 mmol, 1.0 eq.) dissolved in methanol (7 mL) was added to the aqueous mixture and this was stirred at reflux for 12 h. The reaction was cooled to room temperature and quenched with a solution of saturated aqueous ammonium chloride (7 mL). This was extracted in dichloromethane (3 x 10 mL) and washed with water. The combined organic layers were dried over anhydrous sodium sulfate, filtered and concentrated *in vacuo*. The resulting white material was subjected to flash column chromatography (silica, dichloromethane / methanol gradient elution) to give **53** as a white solid (1.33 g, 77%). **^{1}H NMR** (400 MHz, $CDCl_3$) δ 13.29 (s, 1H), 4.23 (s, 1H), 4.14 – 4.07 (m, 2H), 2.79 (t, *J* = 12.6 Hz, 3H), 2.61 – 2.41 (m, 3H), 2.17 (d, *J* = 1.1 Hz, 3H), 1.94 – 1.80 (m, 3H), 1.65 – 1.44 (m, 3H), 1.47 (s, 9H); **^{13}C NMR** (101 MHz, $CDCl_3$)

δ 172.27, 165.81, 158.43, 154.57, 107.56, 79.45, 77.43, 77.11, 76.80, 43.65, 43.24, 28.36, 28.15, 27.36, 21.54; **IR** ν (cm^{-1}) 3250 (br), 2931, 1685, 1658; **MS** *m/z* 316 (M^+ + Na^+).

*6.1.6.7 Synthesis of ALF amine, compound **44***

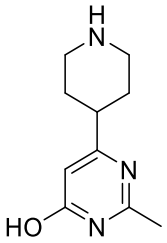

2-methyl-6-(piperidin-4-yl)pyrimidin-4-ol (44). Compound **53** (180 mg, 0.61 mmol) was dissolved in dichloromethane (3 mL) and cooled to 0 °C. Trifluoroacetic acid (3 mL, 4.47 mmol) was added dropwise to the mixture which was allowed to stir for 6 h at room temperature. The solvent was removed *in vacuo* to give the crude product as a yellow oil. Ethyl acetate (5 mL) was added and a white solid was formed which was then filtered and washed with chloroform. This was concentrated *in vacuo* giving the pure product **44** as a white solid (96 mg, 83%). **^{1}H NMR** (400 MHz, Methanol-d_4) δ 6.19 (1H, s), 3.51 (2H, dt, *J* 11.9, 3.0), 3.12 (2H, td, *J* 13.0, 3.1), 2.80 (1H, tt, *J* 11.7, 3.6), 2.43 to 2.35 (2H, m), 2.13 (1H, s), 2.10 (1H, s), 2.00 to 1.87 (2H, m); **^{13}C NMR** (101 MHz, Methanol-d_4) δ 169.21, 164.39, 161.33, 159.71, 107.90, 43.50, 40.17, 26.79, 19.88, 19.65; **HRMS** (ES+) m/z: $[M + H]^+$ calc. for $C_{10}H_{16}N_3O^+$: 194.1293, found: 194.1292.

6.2 Chapter 3 – Boronic ester oxidation

Oxidation rates were determined by measuring the UV-Vis spectra of the solutions on a BMG Clariostar Microplate Reader.

6.2.1 Curcumin dip

The curcumin dip can be used to visualise boron containing compounds, where curcumin is dissolved in methanol and acidified to ensure protonation of the curcumin.[246] Boron containing compounds make a complex with curcumin that stains the TLC plate orange, indicating a positive presence of boron in the TLC spot (**Figure 6.1**).

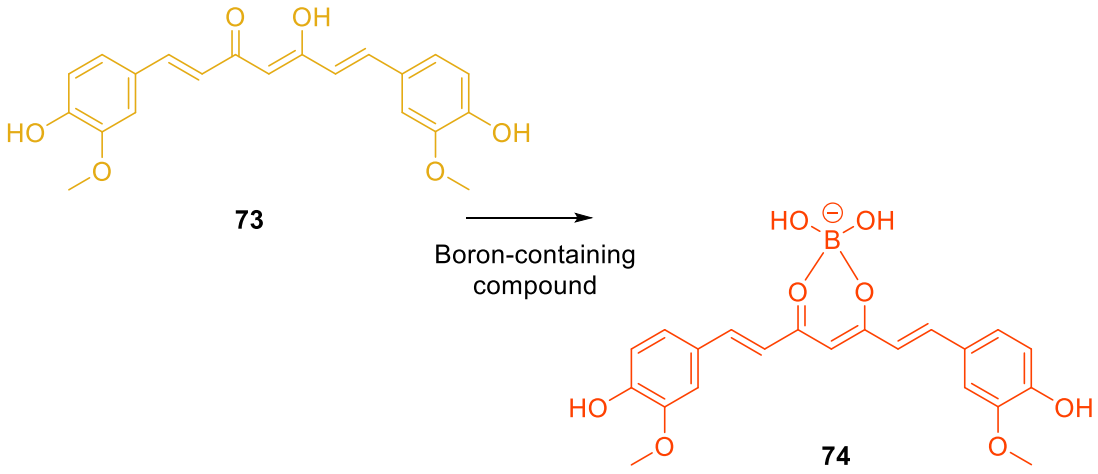

Figure 6.1 *– Colour change of curcumin when in the presence of a boron-containing compound.*

6.2.2 Synthesis

*6.2.2.1 General procedure **B***

Boronic acid (1 mmol), diol (1.1 mmol, 1.1 equiv.) and anhydrous magnesium sulfate (3 mmol, 3 equiv.) was added to the reaction vessel with dichloromethane (5 mL). The reaction was stirred at room temperature until deemed finished by TLC. The reaction mixture was filtered through cotton wool, added to a separating funnel and washed with water (5 mL). The organic fraction was then washed with a fructose solution (0.1 M in water) and dried over anhydrous magnesium sulfate. The solvent was removed

in vacuo and any further purification was carried out via flash column chromatography to form the product.

*6.2.2.2 Synthesis of compound **61a***

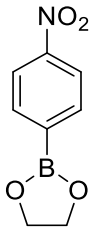

2-(4-nitrophenyl)-1,3,2-Dioxaborolane (61a). Following general procedure **B**, a mixture of 4-nitrophenylboronic acid (84 mg, 0.50 mmol), ethylene glycol (31 µL, 0.55 mmol, 1.1 equiv.) and $MgSO_4$ (180 mg, 1.50 mmol, 3.0 equiv.) was stirred at room temperature in dichloromethane (5 mL) for 5 hours. The title compound was obtained as a yellow solid in 82% yield (79 mg, 0.41 mmol). **mp** 161-163 °C; **^{1}H NMR** (400 MHz, $CDCl_3$) δ 8.25 to 8.17 (2H, m, Ar*H*-C-N), 8.02 to 7.94 (2H, m, Ar*H*-C-B), 4.44 (4H, s, C*H*$_2$); **^{11}B NMR** (128 MHz, $CDCl_3$) δ 31.2; **^{13}C NMR** (101 MHz, $CDCl_3$) δ 150.0 (*Ar*-N), 135.8 (*Ar*-C-N), 122.6 (*Ar*-C-B), 66.4 (*C*H_2-O); **IR** ν (cm^{-1}) 1598w; **HRMS** (ASAP+) m/z: $[M+H]^+$ calc. for $C_8H_8{}^{10}BNO_4^+$: 193.0661, found: 193.0668.

*6.2.2.3 Synthesis of compound **61c***

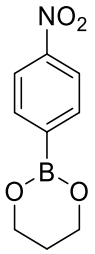

2-(4-nitrophenyl)-1,3,2-Dioxaborinane (61c). Following general procedure **B**, a mixture of 4-nitrophenylboronic acid (167 mg, 1.0 mmol), 1,3-propanediol (80 µL, 1.1 mmol, 1.1 equiv.) and $MgSO_4$ (360 mg, 3.0 mmol, 3.0 equiv.) was stirred at room temperature in dichloromethane (5 mL) for 5 hours. The title compound was obtained as a yellow solid in 79% yield (164 mg, 0.79 mmol). **mp** 122-124 °C; **^{1}H NMR** (400 MHz, $CDCl_3$) δ 8.20-8.12 (2H, m, Ar*H*-C-N), 7.95 to 7.86 (2H, m, Ar*H*-C-B), 4.19 (4H, t, *J* 5.5, C*H*$_2$O), 2.09 (2H, p, *J* 5.5, C*H*$_2$(CH$_2$)$_2$); **^{11}B NMR** (128 MHz, $CDCl_3$) δ 26.6; **^{13}C NMR** (101 MHz, $CDCl_3$) δ 149.5 (*Ar*-N), 134.6 (*Ar*-C-N), 122.3 (*Ar*-C-B), 62.2 (*C*H$_2$-O), 27.3 (*C*H$_2$(CH$_2$)$_2$); **IR** ν (cm^{-1}) 2964w, 1518s; **HRMS** (ASAP+) m/z: $[M+H]^+$ calc. for $C_9H_{11}{}^{11}BNO_4^+$: 208.0781, found: 208.0793.

*6.2.2.4 Synthesis of compound **61d***

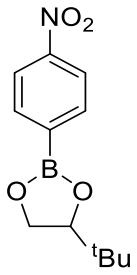

4-(*tert*-butyl)-2-(4-nitrophenyl)-1,3,2-Dioxaborolane (61d). Following general procedure **B**, a mixture of 4-nitrophenylboronic acid (167 mg, 1.0 mmol), 3,3-dimethyl-1,2-butanediol (130 mg, 1.1 mmol, 1.1 equiv.) and $MgSO_4$ (360 mg, 3.0 mmol, 3.0 equiv.) was stirred at room temperature in dichloromethane (5 mL) for 5 hours. The title compound was obtained as a yellow solid in 71% yield (177 mg, 0.71 mmol). **mp** 83-84 °C; **^{1}H NMR** (400 MHz, $CDCl_3$) δ 8.25 to 8.16 (2H, m, Ar*H*-C-N), 8.02 to 7.92 (2H, m, Ar*H*-C-B), 4.38 to 4.27 (2H, m, C*H*$_2$O), 4.24 to 4.14 (1H, m, C*H*), 0.96 (9H, s, (C*H*$_3$)$_3$); **^{11}B NMR** (128 MHz, $CDCl_3$) δ 30.8; **^{13}C NMR** (101 MHz, $CDCl_3$) δ 150.0 (*Ar*-

N), 135.8 (*Ar*-C-N), 122.5 (*Ar*-C-B), 85.5 (*C*HO^{t}Bu), 67.5 (*C*H_2O), 33.9 (*C*(CH_3)$_3$), 24.6 (*C*H_3); **IR** ν (cm^{-1}) 2963w, 1522s; **HRMS** (ASAP+) m/z: $[M+H]^+$ calc. for $C_{12}H_{17}{}^{11}BNO_4^+$: 250.1251, found: 250.1264.

*6.2.2.5 Synthesis of compound **61e***

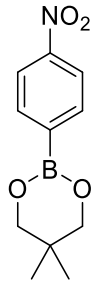

5,5-Dimethyl-2-(4-nitrophenyl)-1,3,2-dioxaborinane (61e). Following general procedure **B**, a mixture of 4-nitrophenylboronic acid (167 mg, 1.0 mmol), neopentyl glycol (114 mg, 1.1 mmol, 1.1 equiv.) and $MgSO_4$ (360 mg, 3.0 mmol, 3.0 equiv.) was stirred at room temperature in dichloromethane (5 mL) for 5 hours. The title compound was obtained as a yellow solid in 80% yield (189 mg, 0.80 mmol). **R_f** 0.32 (hexane/ethyl acetate 8:2); **mp** 110-111 °C; **^{1}H NMR** (400 MHz, $CDCl_3$) δ 8.21 to 8.13 (2H, m, Ar*H*-C-N), 7.99 to 7.91 (2H, m, Ar*H*-C-B), 3.80 (4H, s, CH_2O) 1.04 (6H, s, (CH_3)$_2$); **^{11}B NMR** (128 MHz, $CDCl_3$) δ 26.2; **^{13}C NMR** (101 MHz, $CDCl_3$) δ 149.6 (*Ar*-N), 134.8 (*Ar*-C-N), 122.3 (*Ar*-C-B), 72.5 (*C*H_2O), 31.9 (*C*(CH_3)$_3$), 21.9 (*C*H_3); **IR** ν (cm^{-1}) 2966w, 2938w, 1596m; **HRMS** (ASAP+) m/z: $[M]^+$ calc. for $C_{11}H_{15}{}^{11}BNO_4^+$: 236.1094, found: 236.1105.

*6.2.2.6 Synthesis of compound **61f***

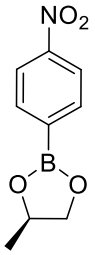

(*R*)-4-Methyl-2-(4-nitrophenyl)-1,3,2-dioxaborolane (61f). Following general procedure **B**, a mixture of 4-nitrophenylboronic acid (167 mg, 1.0 mmol), (*R*)-1,2-propanediol (81 µL, 1.1 mmol, 1.1 equiv.) and $MgSO_4$ (360 mg, 3.0 mmol, 3.0 equiv.) was stirred at room temperature in dichloromethane (5 mL) for 5 hours. The title compound was obtained as a yellow solid in 68% yield (140 mg, 0.68 mmol). **mp** 91-93 °C; **^{1}H NMR** (400 MHz, $CDCl_3$) δ 8.28 to 8.16 (2H, m, Ar*H*-C-N), 8.00 to 7.91 (2H, m, Ar*H*-C-B), 4.78 (1H, tq, *J* 7.5 & 6.3, C*H*OCH_3), 4.50 (1H, dd, *J* 8.9 & 7.8, C*H*HO), 3.94 (1H, dd, *J* 9.0 & 7.3, CH*H*O), 1.44 (3H, d, *J* 6.2, C*H*$_3$); **^{11}B NMR** (128 MHz, $CDCl_3$) δ 30.8; **^{13}C NMR** (101 MHz, $CDCl_3$) δ 150.0 (*Ar*-N), 135.7 (*Ar*-C-N), 122.5 (*Ar*-C-B), 74.4 (*C*HO), 72.9 (*C*H_2O), 21.8 (*C*H_3); **IR** ν (cm^{-1}) 2977w, 2902w, 1515s; **HRMS** (ASAP+) m/z: $[M+H]^+$ calc. for $C_9H_{11}{}^{11}BNO_4^+$: 208.0781, found: 208.0788.

*6.2.2.7 Synthesis of compound **61g***

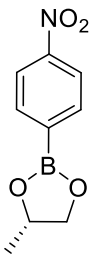

(*S*)-4-Methyl-2-(4-nitrophenyl)-1,3,2-dioxaborolane (61g). Following general procedure **B**, a mixture of 4-nitrophenylboronic acid (167 mg, 1.0 mmol), (*S*)-1,2-propanediol (81 µL, 1.1 mmol, 1.1 equiv.) and $MgSO_4$ (360 mg, 3.0 mmol, 3.0 equiv.) was stirred at room temperature in dichloromethane (5 mL) for 5 hours. The title compound was obtained as a yellow soild in 78% yield (161 mg, 0.78 mmol). **mp** 90-92 °C; **^{1}H NMR** (400 MHz, $CDCl_3$) δ 8.27 to 8.17 (2H, m, Ar*H*-C-N), 8.01 to 7.91 (2H, m, Ar*H*-C-B), 4.78 (1H, tq, *J* 7.6 & 6.2, C*H*OCH_3), 4.51 (1H, dd, *J* 9.0 & 7.8, C*H*HO), 3.95 (1H, dd, *J* 8.9 & 7.3, CH*H*O), 1.45 (3H, d, *J* 6.2, C*H*$_3$); **^{11}B NMR** (128 MHz, $CDCl_3$) δ 31.0; **^{13}C NMR** (101 MHz, $CDCl_3$) δ 150.0 (*Ar*-N), 135.8 (*Ar*-C-N), 122.6 (*Ar*-C-B), 74.4 (*C*HO), 72.9, (*C*H_2O), 21.8 (*C*H_3); **IR** ν (cm^{-1}) 2977w, 2902w, 1515s; **HRMS** (ASAP+) m/z: $[M+H]^+$ calc. for $C_9H_{11}{}^{11}BNO_4^+$: 208.0781, found: 208.0789.

*6.2.2.8 Synthesis of compound **61h***

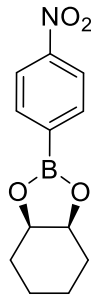

(3a*R*,7a*S*)-2-(4-nitrophenyl)Hexahydrobenzo[*d*][1,3,2]dioxaborole (61h). Following general procedure **B**, a mixture of 4-nitrophenylboronic acid (167 mg, 1.0 mmol), *cis*-1,2-cyclohexanediol (128 mg, 1.1 mmol, 1.1 equiv.) and $MgSO_4$ (360 mg, 3.0 mmol, 3.0 equiv.) was stirred at room temperature in dichloromethane (5 mL) for 5 hours. The title compound was obtained as a yellow solid in 86% yield (213 mg, 0.86 mmol). **mp** 104-107 °C; **^{1}H NMR** (400 MHz, $CDCl_3$) δ 8.23 to 8.19 (2H, m, Ar*H*-C-N), 7.99 (2H, dt, *J* 8.7 & 1.7, Ar*H*-C-B), 4.62 to 4.56 (2H, m, C*H*O), 1.97 to 1.75 (4H, m,

Cy*H*), 1.65 to 1.53 (2H, m, Cy*H*), 1.46 to 1.35 (2H, m, Cy*H*); **^{11}B NMR** (128 MHz, $CDCl_3$) δ 31.5; **^{13}C NMR** (101 MHz, $CDCl_3$) δ 150.0 (*Ar*-N), 135.8 (*Ar*-C-N), 122.5 (*Ar*-C-B), 76.2 (*C*HO), 28.5 (*C*H_2CHO), 19.1 ((*C*H_2)$_2$CH_2); **IR** ν (cm^{-1}) 2943m, 1517s; **HRMS** (ASAP+) m/z: $[M]^+$ calc. for $C_{12}H_{15}{}^{11}BNO_4^+$: 248.1094, found: 248.1098.

*6.2.2.9 Synthesis of compound **61i***

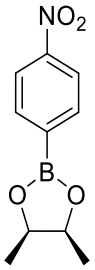

(4*S*,5*R*)-4,5-Dimethyl-2-(4-nitrophenyl)-1,3,2-dioxaborolane (61i). Following general procedure **B**, a mixture of 4-nitrophenylboronic acid (167 mg, 1.0 mmol), *meso*-2,3-butanediol (99 mg, 1.1 mmol, 1.1 equiv.) and $MgSO_4$ (360 mg, 3.0 mmol, 3.0 equiv.) was stirred at room temperature in dichloromethane (5 mL) for 5 hours. The title compound was obtained as a yellow solid in 94% yield (208 mg, 0.94 mmol). **mp** 132-134 °C; **^{1}H NMR** (400 MHz, $CDCl_3$) δ 8.20 (2H, d, *J* 8.7, Ar*H*-C-N), 7.97 (2H, d, *J* 8.7, Ar*H*-C-B), 4.81 to 4.72 (2H, m, C*H*OCH_3), 1.32 (6H, d, *J* 6.2, CH_3); **^{11}B NMR** (128 MHz, $CDCl_3$) δ 30.7; **^{13}C NMR** (101 MHz, $CDCl_3$) δ 149.9 (*Ar*-N), 135.7 (*Ar*-C-N), 122.5 (*Ar*-C-B), 76.5 (*C*HO), 16.6 (*C*H_3); **IR** ν (cm^{-1}) 1600m; **HRMS** (ASAP+) m/z: $[M+H]^+$ calc. for $C_{10}H_{13}{}^{10}BNO_4^+$: 221.0974, found: 221.0975.

*6.2.2.10 Synthesis of compound **61j***

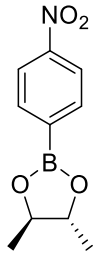

(4*R*,5*R*)-4,5-Dimethyl-2-(4-nitrophenyl)-1,3,2-dioxaborolane (61j). Following general procedure **B**, a mixture of 4-nitrophenylboronic acid (167 mg, 1.0 mmol), *(R, R)*-(-)-2,3-butanediol (100 µL, 99 mg, 1.1 mmol, 1.1 equiv.) and $MgSO_4$ (360 mg, 3.0 mmol, 3.0 equiv.) was stirred at room temperature in dichloromethane (5 mL) for 5 hours. The title compound was obtained as a yellow solid in 97% yield (215 mg, 0.97 mmol). **mp** 111-113 °C; **^{1}H NMR** (400 MHz, $CDCl_3$) δ 8.20 (2H, dt, *J* 8.6 *&* 1.9, Ar*H*-C-N), 7.97 (2H, dt, *J* 8.7 *&* 1.7, Ar*H*-C-B), 4.27 to 4.17 (2H, m, C*H*OCH_3), 1.41 (6H, dd, *J* 6.0 *&* 1.7, C*H*$_3$); **^{11}B NMR** (128 MHz, $CDCl_3$) δ 29.8; **^{13}C NMR** (101 MHz, $CDCl_3$) δ 149.9 (*Ar*-N), 135.7 (*Ar*-C-N), 122.5 (*Ar*-C-B), 81.2 (*C*HO), 20.9 (*C*H$_3$); **IR** ν (cm^{-1}) 1600w, 1517m; **HRMS** (EI+) m/z: $[M]^+$ calc. for $C_{10}H_{12}{}^{10}BNO_4{}^+$: 222.0896, found: 222.0892.

*6.2.2.11 Synthesis of compound **61k***

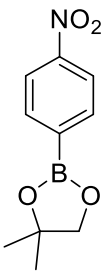

4,4-Dimethyl-2-(4-nitrophenyl)-1,3,2-dioxaborolane (61k). Following general procedure **B**, a mixture of 4-nitrophenylboronic acid (167 mg, 1.0 mmol), 2-methylpropane-1,2-diol (99 µL, 99 mg, 1.1 mmol, 1.1 equiv.) and $MgSO_4$ (360 mg, 3.0 mmol, 3.0 equiv.) was stirred at room temperature in dichloromethane (5 mL) for 5 hours. The title compound was obtained as a yellow solid in 53% yield (118 mg, 0.53 mmol). **mp** 108-110 °C; **^{1}H NMR** (400 MHz, $CDCl_3$) δ 8.20 (2H, d, *J* 8.7, Ar*H*-C-N), 7.96 (2H, d, *J* 8.7, Ar*H*-C-B), 4.11 (2H, s, C*H*$_2$), 1.47 (6H, s, C*H*$_3$); **^{11}B NMR** (128 MHz, $CDCl_3$) δ 30.7; **^{13}C NMR** (101 MHz, $CDCl_3$) δ 149.9 (*Ar*-N), 135.7 (*Ar*-C-N), 122.5 (*Ar*-C-B), 81.2 (*C*$_q$O), 77.9 (*C*H$_2$O), 28.4 (*C*H$_3$); **IR** ν (cm^{-1}) 1600w, 1520s; **HRMS** (ASAP+) m/z: $[M+H]^+$ calc. for $C_{10}H_{13}{}^{10}BNO_4^+$: 221.0974, found: 221.0978.

*6.2.2.12 Synthesis of compound **61l***

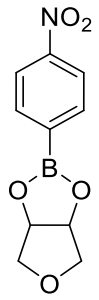

2-(4-Nitrophenyl)tetrahydrofuro[3,4-d][1,3,2]dioxaborole (61l). Following general procedure **B**, a mixture of 4-nitrophenylboronic acid (167 mg, 1.0 mmol), 1,4-anhydroerythritol (90 µL, 114 mg, 1.1 mmol, 1.1 equiv.) and $MgSO_4$ (360 mg, 3.0 mmol, 3.0 equiv.) was stirred at room temperature in dichloromethane (5 mL) for 5 hours. The title compound was obtained as a yellow solid in 98% yield (231 mg, 0.98 mmol). **mp** 181-183 °C; **^{1}H NMR** (400 MHz, $CDCl_3$) δ 8.23 to 8.18 (2H, m, Ar*H*-C-N), 7.98 to 7.92 (2H, m, Ar*H*-C-B), 5.15 (2H, dd, *J* 2.5, 1.3, C*H*HOC*H*H), 4.18 (2H, dd, *J* 10.4, 1.2, C*H*OB), 3.61 to 3.53 (2H, m, CH*H*OCH*H*); **^{11}B NMR** (128 MHz, $CDCl_3$) δ

30.5; **^{13}C NMR** (101 MHz, $CDCl_3$) δ 150.0 (*Ar*-N), 135.9 (*Ar*-C-N), 122.6 (*Ar*-C-B), 82.3 (*C*H_2O), 74.6 (*C*HO); **IR** ν (cm^{-1}) 1600m, 1515s; **HRMS** (ASAP+) m/z: $[M+H]^+$ calc. for $C_{10}H_{11}{}^{10}BNO_5^+$: 235.0767, found: 235.0768.

7 References

1. Globocan, Cancer Today, https://gco.iarc.fr/today/home, (accessed July 2022).
2. C. Baker, *Cancer: Summary of Statistics (England)*, House of Commons Library, 2021.
3. H. K. Matthews, C. Bertoli and R. A. M. de Bruin, *Nat. Rev. Mol. Cell Bio.*, 2022, **23**, 74-88.
4. E. S. Gilbert, *Int. J. Radiat. Biol.*, 2009, **85**, 467-482.
5. J. Orazio, S. Jarrett, A. Amaro-Ortiz and T. Scott, *Int. J. Mol. Sci.*, 2013, **14**.
6. T. J. Key, K. E. Bradbury, A. Perez-Cornago, R. Sinha, K. K. Tsilidis and S. Tsugane, *BMJ*, 2020, **368**, m511.
7. D. S. Chan, R. Lau, D. Aune, R. Vieira, D. C. Greenwood, E. Kampman and T. Norat, *PLoS One*, 2011, **6**, e20456.
8. R. Takachi, M. Inoue, T. Shimazu, S. Sasazuki, J. Ishihara, N. Sawada, T. Yamaji, M. Iwasaki, H. Iso, Y. Tsubono and S. Tsugane, *Am. J. Clin. Nutr.*, 2010, **91**, 456-464.
9. L. Jacob, M. Freyn, M. Kalder, K. Dinas and K. Kostev, *Oncotarget*, 2018, **9**, 17420-17429.
10. H. Rumgay, K. Shield, H. Charvat, P. Ferrari, B. Sornpaisarn, I. Obot, F. Islami, V. E. P. P. Lemmens, J. Rehm and I. Soerjomataram, *Lancet Oncol.*, 2021, **22**, 1071-1080.
11. A. Bansal, M. P. Singh and B. Rai, *Int. J. Appl. Basic Med. Res.*, 2016, **6**, 84-89.
12. S. Klasberg, T. Bitard-Feildel and L. Mallet, *Bioinf. Biol. Insights*, 2016, **10**, 121-131.
13. E. V. Koonin and A. S. Novozhilov, *IUBMB Life*, 2009, **61**, 99-111.
14. P. D. Sun, C. E. Foster and J. C. Boyington, *Curr. Protoc. Protein Sci.*, 2004, **Chapter 17**, 1711-1717.1711.
15. A. J. Bruce Alberts, Juliam Lewis, Martin Raff, Keith Roberts, Peter Walter, Garland Science, 4th edn., 2002, ch. Protein Function.
16. S. Martínez Cuesta, S. A. Rahman, N. Furnham and J. M. Thornton, *Biophys. J.*, 2015, **109**, 1082-1086.
17. D. Grandér, *Med. Oncol.*, 1998, **15**, 20-26.
18. M. A. Feitelson, A. Arzumanyan, R. J. Kulathinal, S. W. Blain, R. F. Holcombe, J. Mahajna, M. Marino, M. L. Martinez-Chantar, R. Nawroth, I. Sanchez-Garcia, D. Sharma, N. K. Saxena, N. Singh, P. J. Vlachostergios, S. Guo, K. Honoki, H. Fujii, A. G. Georgakilas, A. Bilsland, A. Amedei, E. Niccolai, A. Amin, S. S. Ashraf, C. S. Boosani, G. Guha, M. R. Ciriolo, K. Aquilano, S. Chen, S. I. Mohammed, A. S. Azmi, D. Bhakta, D. Halicka, W. N. Keith and S. Nowsheen, *Semin. Cancer Biol.*, 2015, **35**, S25-S54.
19. M. Jagannathan-Bogdan and L. I. Zon, *Development*, 2013, **140**, 2463-2467.
20. W. Zakrzewski, M. Dobrzyński, M. Szymonowicz and Z. Rybak, *Stem Cell. Res. Ther.*, 2019, **10**, 68.
21. A. P. Ng and W. S. Alexander, *Cell Death Discovery*, 2017, **3**, 17002.
22. H. Kawamoto and N. Minato, *Int. J. Biochem. Cell Biol.*, 2004, **36**, 1374-1379.
23. A. Birbrair and P. S. Frenette, *Ann. N. Y. Acad. Sci.*, 2016, **1370**, 82-96.
24. J. Y. Lee and S. H. Hong, *Int. J. Stem Cells*, 2020, **13**, 1-12.

25. L. M. Silla, F. Dulley, R. Saboya, E. Paton, F. Kerbauy, M. Arantes Ade and N. Hamerschlak, *Rev. Bras. Hematol. Hemoter.*, 2013, **35**, 56-61.
26. J. Bolaños-Meade and R. A. Brodsky, *Curr. Opin. Oncol.*, 2009, **21**, 158-161.
27. Y. Dong, O. Shi, Q. Zeng, X. Lu, W. Wang, Y. Li and Q. Wang, *Exp. Hematol. Oncol.*, 2020, **9**, 14.
28. C. R. UK, Leukaemia (all subtypes combined) statistics, https://www.cancerresearchuk.org/health-professional/cancer-statistics/statistics-by-cancer-type/leukaemia, (accessed July, 2022).
29. N. J. Short, M. E. Rytting and J. E. Cortes, *Lancet*, 2018, **392**, 593-606.
30. M. Hallek, T. D. Shanafelt and B. Eichhorst, *Lancet*, 2018, **391**, 1524-1537.
31. J. W. Vardiman, *Chem. Biol. Interact.*, 2010, **184**, 16-20.
32. D. A. Arber, A. Orazi, R. Hasserjian, J. Thiele, M. J. Borowitz, M. M. Le Beau, C. D. Bloomfield, M. Cazzola and J. W. Vardiman, *Blood*, 2016, **127**, 2391-2405.
33. E. A. Shephard, R. D. Neal, P. W. Rose, F. M. Walter and W. Hamilton, *Br. J. Gen. Pract.*, 2016, **66**, e182-188.
34. Y. Kikushige, F. Ishikawa, T. Miyamoto, T. Shima, S. Urata, G. Yoshimoto, Y. Mori, T. Iino, T. Yamauchi, T. Eto, H. Niiro, H. Iwasaki, K. Takenaka and K. Akashi, *Cancer Cell*, 2011, **20**, 246-259.
35. C. R. UK, Chronic lymphocytic leukaemia (CLL) incidence statistics, https://www.cancerresearchuk.org/health-professional/cancer-statistics/statistics-by-cancer-type/leukaemia-cll/incidence#heading-One, (accessed July, 2022).
36. M. Hallek, B. D. Cheson, D. Catovsky, F. Caligaris-Cappio, G. Dighiero, H. Döhner, P. Hillmen, M. Keating, E. Montserrat, N. Chiorazzi, S. Stilgenbauer, K. R. Rai, J. C. Byrd, B. Eichhorst, S. O'Brien, T. Robak, J. F. Seymour and T. J. Kipps, *Blood*, 2018, **131**, 2745-2760.
37. M. Hallek and O. Al-Sawaf, *Am. J. Hematol.*, 2021, **96**, 1679-1705.
38. A. C. Rawstron, K.-A. Kreuzer, A. Soosapilla, M. Spacek, O. Stehlikova, P. Gambell, N. McIver-Brown, N. Villamor, K. Psarra, M. Arroz, R. Milani, J. de la Serna, M. T. Cedena, O. Jaksic, J. Nomdedeu, C. Moreno, G. M. Rigolin, A. Cuneo, P. Johansen, H. E. Johnsen, R. Rosenquist, C. U. Niemann, W. Kern, D. Westerman, M. Trneny, S. Mulligan, M. Doubek, S. Pospisilova, P. Hillmen, D. Oscier, M. Hallek, P. Ghia and E. Montserrat, *Cytometry, Part B*, 2018, **94**, 121-128.
39. B. Jakšić, V. Pejša, S. Ostojić-Kolonić, I. Kardum-Skelin, S. Bašić-Kinda, B. Coha, V. Gverić-Krečak, R. Vrhovac, O. Jakšić, I. Aurer, J. Sinčić-Petričević, A. Načinović-Duletić and D. Nemet, *Acta Clin. Croat.*, 2018, **57**, 190-215.
40. W. G. Wierda, S. O'Brien, X. Wang, S. Faderl, A. Ferrajoli, K.-A. Do, J. Cortes, D. Thomas, G. Garcia-Manero, C. Koller, M. Beran, F. Giles, F. Ravandi, S. Lerner, H. Kantarjian and M. Keating, *Blood*, 2007, **109**, 4679-4685.
41. G. Dighiero, K. Maloum, B. Desablens, B. Cazin, M. Navarro, R. Leblay, M. Leporrier, J. Jaubert, G. Lepeu, B. Dreyfus, J.-L. Binet, P. Travade, F.-L. Turpin, G. Tertian and A. Bichoffe, *N. Engl. J. Med.*, 1998, **338**, 1506-1514.
42. C. Shustik, R. Mick, R. Silver, A. Sawitsky, K. Rai and L. Shapiro, *Hematol. Oncol.*, 1988, **6**, 7-12.
43. X. C. Badoux, M. J. Keating, X. Wang, S. M. O'Brien, A. Ferrajoli, S. Faderl, J. Burger, C. Koller, S. Lerner, H. Kantarjian and W. G. Wierda, *Blood*, 2011, **117**, 3016-3024.
44. R. Szász, B. Telek and Á. Illés, *Pathol. Oncol. Res.*, 2021, **27**, 1609742.

45. C. S. Tam, S. O'Brien, W. Wierda, H. Kantarjian, S. Wen, K. A. Do, D. A. Thomas, J. Cortes, S. Lerner and M. J. Keating, *Blood*, 2008, **112**, 975-980.
46. N. Kutsch, R. Busch, J. Bahlo, J. Mayer, M. Hensel, G. Hopfinger, G. Hess, U. von Grünhagen, C.-M. Wendtner, A. Maria Fink, K. Fischer, M. Hallek and B. Eichhorst, *Leuk. Lymphoma*, 2017, **58**, 399-407.
47. A. P. Skarbnik and S. Faderl, *Ther. Adv. Hematol.*, 2017, **8**, 99-105.
48. J. C. Barrientos, *Cancer Control*, 2015, **22**, 17-23.
49. G. Y. Liou and P. Storz, *Free Radic. Res.*, 2010, **44**, 479-496.
50. J. Fang, T. Seki and H. Maeda, *Adv. Drug Delivery Rev.*, 2009, **61**, 290-302.
51. L. Khandrika, B. Kumar, S. Koul, P. Maroni and H. K. Koul, *Cancer Lett.*, 2009, **282**, 125-136.
52. L. A. Sena and N. S. Chandel, *Mol. Cell*, 2012, **48**, 158-167.
53. J. Zhang, X. Wang, V. Vikash, Q. Ye, D. Wu, Y. Liu and W. Dong, *Oxid. Med. Cell. Longev.*, 2016, **2016**, 4350965.
54. M. P. Murphy, *Biochem. J.*, 2008, **417**, 1-13.
55. P. K. Jensen, *Biochim. Biophys. Acta*, 1966, **122**, 157-166.
56. G. Loschen, A. Azzi, C. Richter and L. Flohé, *FEBS Lett.*, 1974, **42**, 68-72.
57. F. Muller, *J. Am. Aging Assoc.*, 2000, **23**, 227-253.
58. H. Sies and D. P. Jones, *Nat. Rev. Mol. Cell Bio.*, 2020, **21**, 363-383.
59. T. Finkel, *J. Cell Biol.*, 2011, **194**, 7-15.
60. A. B. Al-Mehdi, V. M. Pastukh, B. M. Swiger, D. J. Reed, M. R. Patel, G. C. Bardwell, V. V. Pastukh, M. F. Alexeyev and M. N. Gillespie, *Sci. Signaling*, 2012, **5**, ra47.
61. M. Schieber and Navdeep S. Chandel, *Curr. Biol.*, 2014, **24**, R453-R462.
62. K. Ito, A. Hirao, F. Arai, K. Takubo, S. Matsuoka, K. Miyamoto, M. Ohmura, K. Naka, K. Hosokawa, Y. Ikeda and T. Suda, *Nat. Med.*, 2006, **12**, 446-451.
63. S. Yalcin, X. Zhang, J. P. Luciano, S. K. Mungamuri, D. Marinkovic, C. Vercherat, A. Sarkar, M. Grisotto, R. Taneja and S. Ghaffari, *J. Biol. Chem.*, 2008, **283**, 25692-25705.
64. C. L. Bigarella, R. Liang and S. Ghaffari, *Development*, 2014, **141**, 4206-4218.
65. A. V. Kudryavtseva, G. S. Krasnov, A. A. Dmitriev, B. Y. Alekseev, O. L. Kardymon, A. F. Sadritdinova, M. S. Fedorova, A. V. Pokrovsky, N. V. Melnikova, A. D. Kaprin, A. A. Moskalev and A. V. Snezhkina, *Oncotarget*, 2016, **7**, 44879-44905.
66. H. Maslah, C. Skarbek, S. Pethe and R. Labruère, *Eur. J. Med. Chem.*, 2020, **207**, 112670.
67. M. Redza-Dutordoir and D. A. Averill-Bates, *Biochim. Biophys. Acta, Mol. Cell Res.*, 2016, **1863**, 2977-2992.
68. H.-Y. Tan, N. Wang, S. Li, M. Hong, X. Wang and Y. Feng, *Oxid. Med. Cell. Longev.*, 2016, **2016**, 2795090.
69. I. S. Young and J. V. Woodside, *J. Clin. Pathol.*, 2001, **54**, 176.
70. D. Farbstein, A. Kozak-Blickstein and A. P. Levy, *Molecules*, 2010, **15**, 8098-8110.
71. S. B. Nimse and D. Pal, *RSC Adv.*, 2015, **5**, 27986-28006.
72. J. Pizzorno, *Integr. Med. (Encinitas)*, 2014, **13**, 8-12.
73. A. Pastore, G. Federici, E. Bertini and F. Piemonte, *Clin. Chim. Acta*, 2003, **333**, 19-39.
74. S. Spaans, R. Weusthuis, J. Van Der Oost and S. Kengen, *Front. Microbiol.*, 2015, **6**.

75. A. M. Metwaly, M. M. Ghoneim, I. H. Eissa, I. A. Elsehemy, A. E. Mostafa, M. M. Hegazy, W. M. Afifi and D. Dou, *Saudi J. Biol. Sci.*, 2021, **28**, 5823-5832.
76. G. M. Cragg and D. J. Newman, *J. Ethnopharmacol.*, 2005, **100**, 72-79.
77. C. Veeresham, *J. Adv. Pharm. Technol. Res.*, 2012, **3**, 200-201.
78. H. Lachance, S. Wetzel, K. Kumar and H. Waldmann, *J. Med. Chem.*, 2012, **55**, 5989-6001.
79. A. D. G. Lawson, M. MacCoss and J. P. Heer, *J. Med. Chem.*, 2018, **61**, 4283-4289.
80. E. C. Barnes, R. Kumar and R. A. Davis, *Nat. Prod. Rep.*, 2016, **33**, 372-381.
81. T. A. Ban, *Dialogues Clin. Neurosci.*, 2006, **8**, 335-344.
82. E. P. Abraham, E. Chain, C. M. Fletcher, A. D. Gardner, N. G. Heatley, M. A. Jennings and H. W. Florey, *Lancet*, 1941, **238**, 177-189.
83. A. Fleming, *Br. J. Exp. Pathol.*, 1929, **10**, 226.
84. S. M. Marcy and J. O. Klein, *Med. Clin. North Am.*, 1970, **54**, 1127-1143.
85. L. Verbist, *Antimicrob Agents Chemother*, 1979, **16**, 115-119.
86. G. W. White, J. B. Malow, V. M. Zimelis, H. Pahlavanzadeh, A. P. Panwalker and G. G. Jackson, *Antimicrobial Agents and Chemotherapy*, 1979, **15**, 540-543.
87. D. Dowell, T. M. Haegerich and R. Chou, *MMWR Recomm. Rep.*, 2016, **65**, 1-49.
88. F. Kroschinsky, F. Stölzel, S. von Bonin, G. Beutel, M. Kochanek, M. Kiehl and P. Schellongowski, *Crit. Care*, 2017, **21**, 89.
89. D. Tila, S. Ghasemi, S. N. Yazdani-Arazi and S. Ghanbarzadeh, *J. Biomater. Appl.*, 2015, **30**, 3-16.
90. G. M. Cragg and D. J. Newman, *J. Ethnopharmacol.*, 2005, **100**, 72-79.
91. A. L. Demain and P. Vaishnav, *Microb. Biotechnol.*, 2011, **4**, 687-699.
92. F. Arcamone, F. Animati, G. Capranico, P. Lombardi, G. Pratesi, S. Manzini, R. Supino and F. Zunino, *Pharmacol. Ther.*, 1997, **76**, 117-124.
93. S. H. Giordano, Y. L. Lin, Y. F. Kuo, G. N. Hortobagyi and J. S. Goodwin, *J. Clin. Oncol.*, 2012, **30**, 2232-2239.
94. T. W. Wang, H. Yuan, W. L. Diao, R. Yang, X. Z. Zhao and H. Q. Guo, *BMC Urol.*, 2019, **19**, 90.
95. C. Nabhan, M. Byrtek, A. Rai, K. Dawson, X. Zhou, B. K. Link, J. W. Friedberg, A. D. Zelenetz, M. J. Maurer, J. R. Cerhan and C. R. Flowers, *Br. J. Haematol.*, 2015, **170**, 85-95.
96. C. R. Hutchinson and A. L. Colombo, *J. Ind. Microbiol. Biotechnol.*, 1999, **23**, 647-652.
97. C. K. Hwang, H. S. Kim, Y. S. Hong, Y. H. Kim, S. K. Hong, S. J. Kim and J. J. Lee, *Antimicrob. Agents Chemother.*, 1995, **39**, 1616-1620.
98. C. F. Thorn, C. Oshiro, S. Marsh, T. Hernandez-Boussard, H. McLeod, T. E. Klein and R. B. Altman, *Pharmacogenet. Genomics*, 2011, **21**, 440-446.
99. X. Wang, X. Tian, Y. Wu, X. Shen, S. Yang and S. Chen, *Prep. Biochem. Biotechnol.*, 2018, **48**, 514-521.
100. S. Malla, N. Prasad Niraula, B. Singh, K. Liou and J. Kyung Sohng, *Microbiol. Res.*, 2010, **165**, 427-435.
101. S. G. Van Lanen and B. Shen, *Curr. Top. Med. Chem.*, 2008, **8**, 448-459.
102. D. Denklau, W. Köhnlein, G. Lüders and J. Stellmach, *Z. Naturforsch., C: Biosci.*, 1983, **38**, 939-942.
103. B. L. Smith, G. B. Bauer and L. F. Povirk, *J. Biol. Chem.*, 1994, **269**, 30587-30594.

104. E. Kraka, T. Tuttle and D. Cremer, *J. Phys. Chem. B*, 2008, **112**, 2661-2670.
105. E. Kraka and D. Cremer, *J. Am. Chem. Soc.*, 2000, **122**, 8245-8264.
106. K. C. Nicolaou, A. L. Smith and E. W. Yue, *Proc. Natl. Acad. Sci. U. S. A.*, 1993, **90**, 5881-5888.
107. K. C. Nicolaou, W.-M. Dai and R. K. Guy, *Angew. Chem. Int. Ed.*, 1994, **33**, 15-44.
108. D. Guenard, F. Gueritte-Voegelein and P. Potier, *Acc. Chem. Res.*, 1993, **26**, 160-167.
109. B. A. Weaver, *Mol. Biol. Cell*, 2014, **25**, 2677-2681.
110. R. A. Holton, C. Somoza, H. B. Kim, F. Liang, R. J. Biediger, P. D. Boatman, M. Shindo, C. C. Smith and S. Kim, *J. Am. Chem. Soc.*, 1994, **116**, 1597-1598.
111. K. C. Nicolaou, Z. Yang, J. J. Liu, H. Ueno, P. G. Nantermet, R. K. Guy, C. F. Claiborne, J. Renaud, E. A. Couladouros, K. Paulvannan and E. J. Sorensen, *Nature*, 1994, **367**, 630-634.
112. J. N. Denis, A. E. Greene, D. Guenard, F. Gueritte-Voegelein, L. Mangatal and P. Potier, *J. Am. Chem. Soc.*, 1988, **110**, 5917-5919.
113. W. C. Liu, T. Gong and P. Zhu, *RSC Adv.*, 2016, **6**, 48800-48809.
114. A. Gilman, *Am. J. Surg.*, 1963, **105**, 574-578.
115. R. K. Singh, S. Kumar, D. N. Prasad and T. R. Bhardwaj, *Eur. J. Med. Chem.*, 2018, **151**, 401-433.
116. A. Sunters, C. J. Springer, K. D. Bagshawe, R. L. Souhami and J. A. Hartley, *Biochem. Pharmacol.*, 1992, **44**, 59-64.
117. A. Polavarapu, J. A. Stillabower, S. G. W. Stubblefield, W. M. Taylor and M.-H. Baik, *J. Org. Chem.*, 2012, **77**, 5914-5921.
118. C. J. O'Connor, W. A. Denny and J.-Y. Fan, *Chem. Biol. Interact.*, 1991, **77**, 223-241.
119. T. Olivier, A. Haslam and V. Prasad, *JAMA Netw Open*, 2021, **4**, e2138793.
120. J. Rueff and A. S. Rodrigues, in *Cancer Drug Resistance: Overviews and Methods*, eds. J. Rueff and A. S. Rodrigues, Springer New York, New York, NY, 2016, DOI: 10.1007/978-1-4939-3347-1_1, pp. 1-18.
121. X. Wang, H. Zhang and X. Chen, *Cancer Drug Resist.*, 2019, **2**, 141-160.
122. T. Conroy, C. Gavoille, E. Samalin, M. Ychou and M. Ducreux, *Curr. Oncol. Rep.*, 2013, **15**, 182-189.
123. R. G. Moran and K. Keyomarsi, *NCI Monogr.*, 1987, 159-163.
124. D. B. Longley, D. P. Harkin and P. G. Johnston, *Nat. Rev. Cancer*, 2003, **3**, 330-338.
125. K.-i. Fujita, Y. Kubota, H. Ishida and Y. Sasaki, *World J. Gastroenterol.*, 2015, **21**, 12234-12248.
126. T. Alcindor and N. Beauger, *Curr. Oncol.*, 2011, **18**, 18-25.
127. X. Li, D. T. Payne, B. Ampolu, N. Bland, J. T. Brown, M. J. Dutton, C. A. Fitton, A. Gulliver, L. Hale, D. Hamza, G. Jones, R. Lane, A. G. Leach, L. Male, E. G. Merisor, M. J. Morton, A. S. Quy, R. Roberts, R. Scarll, T. Schulz-Utermoehl, T. Stankovic, B. Stevenson, J. S. Fossey and A. Agathanggelou, *MedChemComm*, 2019, **10**, 1379-1390.
128. J. J. Murphy, S. Heptinstall and J. R. A. Mitchell, *Lancet*, 1988, **332**, 189-192.
129. M. O'Hara, D. Kiefer, K. Farrell and K. Kemper, *Arch. Fam. Med.*, 1998, **7**, 523-536.
130. A. Pareek, M. Suthar, G. S. Rathore and V. Bansal, *Pharmacogn Rev.*, 2011, **5**, 103-110.
131. N. K. Jain and S. K. Kulkarni, *J. Ethnopharmacol.*, 1999, **68**, 251-259.

132. B. K. Vogler, M. H. Pittler and E. Ernst, *Cephalalgia*, 1998, **18**, 704-708.
133. M. Karin and M. Delhase, *Semin. Immunol.*, 2000, **12**, 85-98.
134. B. H. B. Kwok, B. Koh, M. I. Ndubuisi, M. Elofsson and C. M. Crews, *Chem. Biol.*, 2001, **8**, 759-766.
135. J. N. Kolev, K. M. O'Dwyer, C. T. Jordan and R. Fasan, *ACS Chem. Biol.*, 2014, **9**, 164-173.
136. S. Nasim and P. A. Crooks, *Bioorg. Med. Chem. Lett.*, 2008, **18**, 3870-3873.
137. Z.-J. Yang, W.-Z. Ge, Q.-Y. Li, Y. Lu, J.-M. Gong, B.-J. Kuang, X. Xi, H. Wu, Q. Zhang and Y. Chen, *J. Med. Chem.*, 2015, **58**, 7007-7020.
138. A. R. Gomes, C. L. Varela, E. J. Tavares-da-Silva and F. M. F. Roleira, *Eur. J. Med. Chem.*, 2020, **201**, 112327.
139. K. Fostier, A. De Becker and R. Schots, *Onco Targets Ther.*, 2012, **5**, 237-244.
140. J. Long, Y.-H. Ding, P.-P. Wang, Q. Zhang and Y. Chen, *J. Org. Chem.*, 2013, **78**, 10512-10518.
141. A. Saadane, S. Masters, J. DiDonato, J. Li and M. Berger, *Am. J. Respir. Cell Mol. Biol.*, 2007, **36**, 728-736.
142. A. J. García-Piñeres, V. c. Castro, G. Mora, T. J. Schmidt, E. Strunck, H. L. Pahl and I. Merfort, *J. Biol. Chem.*, 2001, **276**, 39713-39720.
143. C. J. Sweeney, S. Mehrotra, M. R. Sadaria, S. Kumar, N. H. Shortle, Y. Roman, C. Sheridan, R. A. Campbell, D. J. Murry, S. Badve and H. Nakshatri, *Mol. Cancer Ther.*, 2005, **4**, 1004-1012.
144. E. A. Curry, D. J. Murry, C. Yoder, K. Fife, V. Armstrong, H. Nakshatri, M. O'Connell and C. J. Sweeney, *Invest. New Drugs*, 2004, **22**, 299-305.
145. M. L. Guzman, R. M. Rossi, S. Neelakantan, X. Li, C. A. Corbett, D. C. Hassane, M. W. Becker, J. M. Bennett, E. Sullivan, J. L. Lachowicz, A. Vaughan, C. J. Sweeney, W. Matthews, M. Carroll, J. L. Liesveld, P. A. Crooks and C. T. Jordan, *Blood*, 2007, **110**, 4427-4435.
146. D.-R. Hwang, Y.-S. Wu, C.-W. Chang, T.-W. Lien, W.-C. Chen, U.-K. Tan, J. T. A. Hsu and H.-P. Hsieh, *Bioorg. Med. Chem.*, 2006, **14**, 83-91.
147. M. Chadwick, H. Trewin, F. Gawthrop and C. Wagstaff, *Int. J. Mol. Sci.*, 2013, **14**, 12780-12805.
148. S. Neelakantan, S. Nasim, M. L. Guzman, C. T. Jordan and P. A. Crooks, *Bioorg. Med. Chem. Lett.*, 2009, **19**, 4346-4349.
149. A. M. Kempema, J. C. Widen, J. K. Hexum, T. E. Andrews, D. Wang, S. K. Rathe, F. A. Meece, K. E. Noble, Z. Sachs, D. A. Largaespada and D. A. Harki, *Bioorg. Med. Chem.*, 2015, **23**, 4737-4745.
150. V. Tyagi, H. Alwaseem, K. M. O'Dwyer, J. Ponder, Q. Y. Li, C. T. Jordan and R. Fasan, *Bioorg. Med. Chem.*, 2016, **24**, 3876-3886.
151. H. Alwaseem, B. J. Frisch and R. Fasan, *Bioorg. Med. Chem.*, 2018, **26**, 1365-1373.
152. G. T. Prince, M. C. Cameron, R. Fathi and T. Alkousakis, *Int. J. Dermatol.*, 2018, **57**, 1259-1264.
153. S.-L. Kim, S. H. Kim, K. T. T. Trang, I. H. Kim, S.-O. Lee, S. T. Lee, D. G. Kim, S.-B. Kang and S.-W. Kim, *Cancer Lett.*, 2013, **335**, 479-486.
154. Y. Ding, S. Li, W. Ge, Z. Liu, X. Zhang, M. Wang, T. Chen, Y. Chen and Q. Zhang, *Eur. J. Med. Chem.*, 2019, **183**, 111706.
155. M.-A. Légaré, C. Pranckevicius and H. Braunschweig, *Chem. Rev.*, 2019, **119**, 8231-8261.
156. Ł. Charzewski, K. A. Krzyśko and B. Lesyng, *Front. Mol. Biosci.*, 2021, **8**, 633181.

157. F. Yang, M. Zhu, J. Zhang and H. Zhou, *MedChemComm*, 2018, **9**, 201-211.
158. H. S. Ban and H. Nakamura, *Chem. Rec.*, 2015, **15**, 616-635.
159. P. Chellan and P. J. Sadler, *Philos. Trans. R. Soc., A*, 2015, **373**.
160. F. H. Nielsen, *Nutr. Rev.*, 2008, **66**, 183-191.
161. M. Benderdour, T. Van Bui, K. Hess, A. Dicko, F. Belleville and B. Dousset, *J. Trace Elem. Med. Biol.*, 2000, **14**, 168-173.
162. L. Pizzorno, *Integr. Med. (Encinitas)*, 2015, **14**, 35-48.
163. V. N. Charushin, Y. A. Titova and E. R. Milaeva, *Herald Russ. Acad. Sci.*, 2020, **90**, 229-238.
164. G. F. S. Fernandes, W. A. Denny and J. L. Dos Santos, *Eur. J. Med. Chem.*, 2019, **179**, 791-804.
165. P. G. Richardson, T. Hideshima and K. C. Anderson, *Cancer Control*, 2003, **10**, 361-369.
166. D. Chen, M. Frezza, S. Schmitt, J. Kanwar and Q. P. Dou, *Curr. Cancer Drug Targets*, 2011, **11**, 239-253.
167. N. Sharma and D. Sharma, *J. Pharmacol. Pharmacother.*, 2015, **6**, 236-239.
168. T. L. Lincecum, M. Tukalo, A. Yaremchuk, R. S. Mursinna, A. M. Williams, B. S. Sproat, W. Van Den Eynde, A. Link, S. Van Calenbergh, M. Grøtli, S. A. Martinis and S. Cusack, *Mol. Cell*, 2003, **11**, 951-963.
169. F. L. Rock, W. Mao, A. Yaremchuk, M. Tukalo, T. Crépin, H. Zhou, Y. K. Zhang, V. Hernandez, T. Akama, S. J. Baker, J. J. Plattner, L. Shapiro, S. A. Martinis, S. J. Benkovic, S. Cusack and M. R. Alley, *Science*, 2007, **316**, 1759-1761.
170. B. Mansoori, A. Mohammadi, S. Davudian, S. Shirjang and B. Baradaran, *Adv. Pharm. Bull.*, 2017, **7**, 339-348.
171. L. Locher G, *Am. J. Roentgenol.*, 1936, **36**, 1.
172. K. Nedunchezhian, N. Aswath, M. Thiruppathy and S. Thirugnanamurthy, *J. Clin. Diagn. Res.*, 2016, **10**, ZE01-ZE04.
173. T. D. Malouff, D. S. Seneviratne, D. K. Ebner, W. C. Stross, M. R. Waddle, D. M. Trifiletti and S. Krishnan, *Front. Oncol.*, 2021, **11**.
174. T. Jóhannesson, *Laeknabladid*, 2000, **86**, 755-768.
175. F. Kroschinsky, F. Stölzel, S. von Bonin, G. Beutel, M. Kochanek, M. Kiehl and P. Schellongowski, *Crit. Care*, 2017, **21**, 89.
176. S. Chakraborty and T. Rahman, *Ecancermedicalscience*, 2012, **6**, ed16.
177. W. Yin, X. Pan, W. Leng, J. Chen and H. He, *Green Chem.*, 2019, **21**, 4614-4618.
178. Y. Ai, O. N. Obianom, M. Kuser, Y. Li, Y. Shu and F. Xue, *ACS Med. Chem. Lett.*, 2019, **10**, 127-131.
179. B. L. Patenall, G. T. Williams‡, L. Gwynne, L. J. Stephens, E. V. Lampard, H. J. Hathaway, N. T. Thet, A. E. Young, M. J. Sutton, R. D. Short, S. D. Bull, T. D. James, A. C. Sedgwick and A. T. A. Jenkins, *Chem. Commun.*, 2019, **55**, 15129-15132.
180. G. T. Williams, J. L. Kedge and J. S. Fossey, *ACS Sens.*, 2021, **6**, 1508-1528.
181. A. Sikora, J. Zielonka, M. Lopez, J. Joseph and B. Kalyanaraman, *Free Radic. Biol. Med.*, 2009, **47**, 1401-1407.
182. X. Peng and V. Gandhi, *Ther. Deliv.*, 2012, **3**, 823-833.
183. Y. Kuang, K. Balakrishnan, V. Gandhi and X. Peng, *J. Am. Chem. Soc.*, 2011, **133**, 19278-19281.
184. P. S. Danielian, R. White, S. A. Hoare, S. E. Fawell and M. G. Parker, *Mol. Endocrinol.*, 1993, **7**, 232-240.

185. Q. Jiang, Q. Zhong, Q. Zhang, S. Zheng and G. Wang, *ACS Med. Chem. Lett.*, 2012, **3**, 392-396.
186. L. Wang, S. Xie, L. Ma, Y. Chen and W. Lu, *Eur. J. Med. Chem.*, 2016, **116**, 84-89.
187. J. L. Major Jourden and S. M. Cohen, *Angew. Chem. Int. Ed.*, 2010, **49**, 6795-6797.
188. R. Martínez-Máñez, *ChemistryOpen*, 2014, **3**, 232-232.
189. J. P. Lorand and J. O. Edwards, *J. Org. Chem.*, 1959, **24**, 769-774.
190. T. D. James, K. R. A. S. Sandanayake, R. Iguchi and S. Shinkai, *J. Am. Chem. Soc.*, 1995, **117**, 8982-8987.
191. S. Doose, H. Neuweiler and M. Sauer, *ChemPhysChem*, 2009, **10**, 1389-1398.
192. B. E. Collins, S. Sorey, A. E. Hargrove, S. H. Shabbir, V. M. Lynch and E. V. Anslyn, *The Journal of Organic Chemistry*, 2009, **74**, 4055-4060.
193. A. S. Quy, X. Li, L. Male, T. Stankovic, A. Agathanggelou and J. S. Fossey, *Tetrahedron*, 2020, **76**, 131631.
194. J. P. Hughes, S. Rees, S. B. Kalindjian and K. L. Philpott, *Br. J. Pharmacol.*, 2011, **162**, 1239-1249.
195. G. C. Terstappen and A. Reggiani, *Trends Pharmacol. Sci.*, 2001, **22**, 23-26.
196. X.-Y. Meng, H.-X. Zhang, M. Mezei and M. Cui, *Curr. Comput. Aided Drug Des.*, 2011, **7**, 146-157.
197. L. Pinzi and G. Rastelli, *Int. J. Mol. Sci.*, 2019, **20**, 4331.
198. G. W. Price, P. S. Gould and A. Marsh, *J. Chem. Educ.*, 2014, **91**, 602-604.
199. I. Shamovsky, L. Ripa, N. Blomberg, L. A. Eriksson, P. Hansen, C. Mee, C. Tyrchan, M. O'Donovan and P. Sjö, *Chem. Res. Toxicol.*, 2012, **25**, 2236-2252.
200. D. Staveness, T. M. Sodano, K. Li, E. A. Burnham, K. D. Jackson and C. R. J. Stephenson, *Chem.*, 2019, **5**, 215-226.
201. N. Azizi, E. Saki and M. Edrisi, *C. R. Chim.*, 2011, **14**, 973-977.
202. D. Semmingsen, *Tetrahedron Lett.*, 1973, **14**, 807-808.
203. L. F. Tietze, M. Arlt, M. Beller, K.-H. Gl üsenkamp, E. Jähde and M. F. Rajewsky, *Chem. Ber.*, 1991, **124**, 1215-1221.
204. F. R. Wurm and H.-A. Klok, *Chem. Soc. Rev.*, 2013, **42**, 8220-8236.
205. L. M. Schwartz and L. O. Howard, *J. Phys. Chem.*, 1970, **74**, 4374-4377.
206. A. Stacchini, M. Aragno, A. Vallario, A. Alfarano, P. Circosta, D. Gottardi, A. Faldella, G. Rege-Cambrin, U. Thunberg, K. Nilsson and F. Caligaris-Cappio, *Leuk. Res.*, 1999, **23**, 127-136.
207. O. Trott and A. J. Olson, *J. Comput. Chem.*, 2010, **31**, 455-461.
208. D. W. Brooks, L. D. L. Lu and S. Masamune, *Angew. Chem. Int. Ed.*, 1979, **18**, 72-74.
209. M. Vidal, M. García-Arriagada, M. C. Rezende and M. Domínguez, *Synthesis*, 2016, **48**, 4246-4252.
210. P. J. Kocieński, *Protecting Groups*, Georg Thieme Verlag KG, Stuttgart, 3rd Edition edn., 2005.
211. B. J. Graham, I. W. Windsor, B. Gold and R. T. Raines, *Proc. Natl. Acad. Sci. U. S. A.*, 2021, **118**, e2013691118.
212. H. L. D. Hayes, R. Wei, M. Assante, K. J. Geogheghan, N. Jin, S. Tomasi, G. Noonan, A. G. Leach and G. C. Lloyd-Jones, *J. Am. Chem. Soc.*, 2021, **143**, 14814-14826.
213. Sigma-Aldrich, Sigma Aldrich Boronic acid, https://www.sigmaaldrich.com/GB/en/search/boronic-

acids?focus=products&page=1&perpage=30&sort=relevance&term=boronic%20acids&type=product_name, (accessed Jan 2023, 2023).
214. D. M. Knapp, E. P. Gillis and M. D. Burke, *J. Am. Chem. Soc.*, 2009, **131**, 6961-6963.
215. G. J. Lovinger, M. D. Aparece and J. P. Morken, *J. Am. Chem. Soc.*, 2017, **139**, 3153-3160.
216. A. Kilic, A. Savci, Y. Alan and L. Beyazsakal, *J. Organomet. Chem.*, 2020, **917**, 121268.
217. H. Sun, *J. Chem. Inf. Comput. Sci.*, 2004, **44**, 748-757.
218. S. Hitosugi, D. Tanimoto, W. Nakanishi and H. Isobe, *Chem. Lett.*, 2012, **41**, 972-973.
219. G. Vancoillie, W. L. A. Brooks, M. A. Mees, B. S. Sumerlin and R. Hoogenboom, *Polym. Chem.*, 2016, **7**, 6725-6734.
220. W. L. A. Brooks, C. C. Deng and B. S. Sumerlin, *ACS Omega*, 2018, **3**, 17863-17870.
221. G. Springsteen and B. Wang, *Chem. Commun.*, 2001, DOI: 10.1039/B104895N, 1608-1609.
222. G. Springsteen and B. Wang, *Tetrahedron*, 2002, **58**, 5291-5300.
223. T. M. McCollom, F. Klein, P. Solheid and B. Moskowitz, *Philos. Trans. R. Soc., A*, 2020, **378**, 20180428.
224. V. M. Shinde, G. N. Patil, A. Katariya and Y. S. Mahajan, *Chem. Eng. Process.*, 2015, **95**, 241-248.
225. Sigma-Aldrich, Buffer Reference Centre, https://www.sigmaaldrich.com/GB/en/technical-documents/protocol/protein-biology/protein-concentration-and-buffer-exchange/buffer-reference-center, (accessed December 2022, 2022).
226. I. Ahmad, M. A. Sheraz, S. Ahmed, S. H. Kazi, T. Mirza and M. Aminuddin, *Results Pharma Sci.*, 2011, **1**, 11-15.
227. M. Offidani, L. Corvatta, P. Caraffa, S. Gentili, L. Maracci and P. Leoni, *Onco Targets Ther.*, 2014, **7**, 1793-1800.
228. M. D. Liptak, K. C. Gross, P. G. Seybold, S. Feldgus and G. C. Shields, *J. Am. Chem. Soc.*, 2002, **124**, 6421-6427.
229. F.-B. Christa and B. Thomas, *Carbohydr. Polym.*, 2009, **76**, 123-128.
230. D. Toczek, K. Kubas, M. Turek, S. Roszak and R. Gancarz, *J. Mol. Model.*, 2013, **19**, 4209-4214.
231. M. Carnovali, S. Pasqualetti, G. Banfi and M. Mariotti, *J. Anal. Chem.*, 2021, **76**, 267-272.
232. H. Puchtler, S. N. Meloan and M. S. Terry, *J. Histochem. Cytochem.*, 1969, **17**, 110-124.
233. K. Yamakawa, H. Iwasaki, I. Masuda, Y. Ohjimi, I. Honda, K. Saeki, J. Zhang, E. Shono, M. Naito and M. Kikuchi, *J. Rheumatol.*, 2003, **30**, 1032.
234. A. Bensimon-Brito, J. Cardeira, G. Dionísio, A. Huysseune, M. L. Cancela and P. E. Witten, *BMC Dev. Biol.*, 2016, **16**, 2-2.
235. H. Wu and L. Jin, *J. Mater. Chem. C*, 2016, **4**, 3415-3421.
236. M. Prudent and H. H. Girault, *Metallomics*, 2009, **1**, 157-165.
237. F.-Y. Wu, W.-s. Liao, Y.-M. Wu and X.-F. Wan, *Spectrosc. Lett.*, 2008, **41**, 393-398.
238. S. Takahashi, I. Suzuki, T. Sugawara, M. Seno, D. Minaki and J.-I. Anzai, *Materials*, 2017, **10**.

239. S. R. Ali, R. R. Parajuli, Y. Ma, Y. Balogun and H. He, *J. Phys. Chem. B*, 2007, **111**, 12275-12281.
240. J. A. Godbold and M. Solan, *Philos. Trans. R. Soc., B*, 2013, **368**, 20130186-20130186.
241. I. D. Kuntz, F. P. Gasparro, M. D. Johnston and R. P. Taylor, *J. Am. Chem. Soc.*, 1968, **90**, 4778-4781.
242. J. F. Bunnett and R. E. Zahler, *Chem. Rev.*, 1951, **49**, 273-412.
243. S. Rohrbach, A. J. Smith, J. H. Pang, D. L. Poole, T. Tuttle, S. Chiba and J. A. Murphy, *Angew. Chem. Int. Ed.*, 2019, **58**, 16368-16388.
244. C. Hansch, A. Leo and R. W. Taft, *Chem. Rev.*, 1991, **91**, 165-195.
245. Y.-Q. Chen, S. Ghosh and G. Ghosh, *Nat. Struct. Biol.*, 1998, **5**, 67-73.
246. K. Lawrence, S. E. Flower, G. Kociok-Kohn, C. G. Frost and T. D. James, *Anal. Methods*, 2012, **4**, 2215-2217.